NANOCONFINED ALKALI-METAL BOROHYDRIDES FOR REVERSIBLE HYDROGEN STORAGE

NANOBEGRENSDE ALKALIMETAALBOORHYDRIDEN VOOR DE REVERSIBELE OPSLAG VAN WATERSTOF

(met een samenvatting in het Nederlands)

PROEFSCHRIFT

ter verkrijging van de graad van doctor aan de Universiteit Utrecht op gezag van de rector magnificus, prof.dr. G.J. van der Zwaan, ingevolge het besluit van het college voor promoties in het openbaar te verdedigen op maandag 16 januari 2012 des middags te 2.30 uur

door

PETER NGENE

geboren op 28 augustus 1978 te Enugu, Nigeria

Promotor: Prof. dr. ir. K. P. de Jong

Co-promotor: Dr. P. E. de Jongh

This thesis was accomplished with financial support from de Nederlandse Organisatie voor Wetenschappelijk Onderzoek (NWO) under VIDI project number 016.072.316

With God chances are eliminated

Max Lucado

ISBN: 978-90-5335-502-2

Printed by Ridderprint BV

Contents

Chapter 1

General Introduction

1.1 Hydrogen fuel: opportunities and challenges

The development of the industrialized world was accelerated by the use of energy to power steam engines. The economic growth and well- being of modern society is still highly dependent on the availability of low cost energy for the production and transport of goods and services. Presently the vast majority of this energy is obtained from fossil fuels such as coal, oil and natural gas. Over the last two decades, the demand for oil has been increasing rapidly while the world proven oil reserves are declining, a trend which is already causing volatility in oil prices and affecting the world economy[1-5]. The use of oil is also associated with the emission of green house gases like carbon dioxide (CO_2) that contribute to global warming[2-4, 6]. Therefore development of sustainable energy systems is crucial in order to meet the needs of the growing world population and simultaneously reduce pollution associated with the use of hydrocarbons[1, 3, 7-11].

Hydrogen has potential to play a vital role in future sustainable energy scenarios[3, 8-10, 12-15]. Hydrogen can be produced in a sustainable way from water using solar, wind, nuclear and geothermal energy, and also from biomass. Hydrogen has the highest gravimetric energy density and can be used in combination with fuel cells[16] to produce electrical energy for automobiles, stationary applications such as power generators and portable electronics. Burning of hydrogen does not produce pollutant gases or particulates[16]. Currently energy for transportation accounts for more than 62 % of all the crude oil used[17], replacement of gasoline fuelled combustion engines with hydrogen fuel cell vehicles will significantly reduce both oil demand and air pollution. Hydrogen-fuel cell cars are currently the focus of intense research and development activity worldwide and are expected to reach commercial applications in 2015[9]. Hydrogen is also expected to be used for energy storage in future scenarios in which most electricity is generated from renewable sources like wind and solar. These sources depend on weather conditions. If the energy supplies are higher than can be accommodated by the electricity grid, excess energy can be used to produce hydrogen from electrolysis of water. The hydrogen can then be converted to electrical energy in fuel cells when needed.

A typical hydrogen cycle[18] shown in figure 1.1 consists of three major steps which are hydrogen production from renewable energy sources, transportation/storage of the hydrogen, and its use in fuel cell to produce energy. Each of these steps is

associated with significant technical challenges[13] that must be solved before the benefits of using hydrogen as an energy carrier can be fully realized.

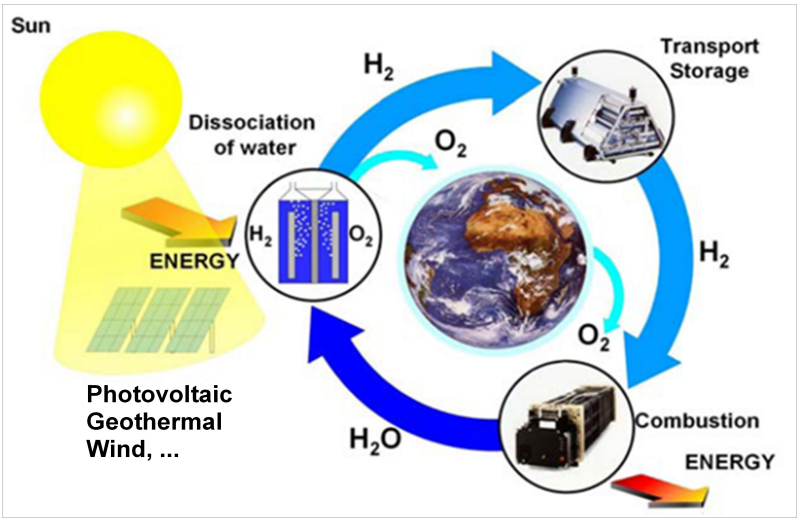

Figure 1.1: The hydrogen cycle. The energy from sunlight is converted into electricity by means of solar cells. The electricity is used to split water into hydrogen and oxygen. The oxygen is released in the atmosphere while the hydrogen is stored, transported and distributed. Finally, hydrogen and oxygen from air are reacted electrochemically in a fuel cell to produce electricity and heat leaving water or steam as the by product (Adapted from [18])

Hydrogen Production: Although hydrogen is the most abundant element on Earth, it is not commonly found as molecular H_2 but rather chemically bound in water, and partially in hydrocarbons and carbohydrates. Therefore hydrogen has to be produced as a synthetic fuel from hydrogen containing–sources. Currently the majority of the hydrogen is produced from natural gas using a process called steam reforming. This process produces CO_2, which implies that the total greenhouse-gas production of a fuel-cell vehicle is not dramatically less than that of a conventional petrol vehicle[9]. For sustainability, the hydrogen should be produced from the electrolysis of water using energy from renewable and non-fossil resources like solar, wind, geothermal, tidal/wind and biomass[19-21]. However the cost of producing hydrogen through such means is currently several times higher than from natural gas[22]. Hence cost reduction is a major challenge.

***Hydrogen utilization- hydrogen-fuel cell*:** The widespread use of hydrogen as an energy carrier depends on the availability of efficient and affordable fuel cells[9, 13,

[14]. Although for vehicular applications hydrogen can also be used directly in internal combustion engines of cars this is not as efficient as using it in fuel cells. Fuel cells are currently very expensive mostly because of the use of Platinum as catalyst. Therefore the major technological challenge for fuel cells is to reduce the precious metal content or find an alternative catalyst.

***Distribution Infrastructure*:** The current distribution system for gasoline cannot easily be adapted for use with hydrogen. Wide spread use of hydrogen especially for cars will require the development of an efficient hydrogen delivery infrastructure.

1.2 Hydrogen Storage

Another crucial challenge facing the wide spread use of hydrogen as a fuel especially for mobile applications is how to store the hydrogen on-board in an efficient, safe and cost effective way[7, 23, 24]. To be comparable to conventional gasoline or diesel based vehicles, hydrogen fuel cell vehicles need to drive about 500 km before refuelling. Typically only about 5 kg of hydrogen is required to cover this distance but due to the low density of hydrogen (0.089 g/l), this will occupy a volume of 56,000 litres at ambient conditions[12]. The challenge is to contain this 5 kg (56,000 l) of hydrogen safely in a system that is light weight and compact enough to be comparable to the gasoline tank of a conventional car (about 30-35 litres)[12]. An ideal hydrogen storage system should contain at least 5.5 wt% H_2 or 40 g/l H_2[25]. Developing such a system or material has been a subject of intense scientific interest during the past decade[23-27]. At present, hydrogen can be stored in two different ways:

Liquefied hydrogen: Hydrogen can be liquefied at -252.9 C (20 K) and stored in cryogenic containers. However, liquefaction consumes more than 30% of the energy content of the hydrogen, and cryogenic liquid containers require costly insulation system [10, 23]. The use of liquid hydrogen is further hampered by continuous loss (about 1% per day)[14] of hydrogen through boil-off and therefore this storage method is not considered viable for application in cars at a large scale.

High-pressure gas cylinders: Hydrogen can be stored at high pressures in gas cylinders. Conventional steel cylinders can hold up to 200 bar H_2 and have a gravimetric density of approximately 1 wt%. Higher hydrogen densities are

achieved using light weight carbon fibre composite cylinders which can store hydrogen at pressures between 700–1000 bar, with gravimetric hydrogen densities up to 10 wt%[10, 14]. However compressing higher than ~ 800 bar is not useful due to non ideality of the gas. High pressure cylinders are currently expensive, and even at these high pressures the volumetric energy density of the system is much less than that of gasoline tank. Other drawbacks of the system are safety concerns and the fact that about 20% of the energy content of the hydrogen is used to compress the gas. Despite these limitations, it is currently the most matured technology for automotive applications[8, 9]

1.3 Solid state hydrogen storage

Some solid state materials have the capacity to reversibly release and take-up hydrogen. The hydrogen is released by heating or decreasing the pressure. The use of solid state materials for hydrogen storage has generated a lot of interest over the last decade due to its advantages in terms of safety and hydrogen contents when compared to liquid and gaseous hydrogen storage[7, 23]. There are two mechanisms in which hydrogen can bind onto materials.

Physisorption: In this process molecular hydrogen (H_2) is weakly adsorbed onto the surface of a material by van der Waals interactions. The amount of hydrogen adsorbed is proportional to the surface area of the material therefore porous materials (sorbents) with high surface areas such as metal organic frameworks (MOFs)[28-33] and carbon based materials such as carbon nanotubes, fibers, fullerenes, and activated carbon[34-39] are been investigated for hydrogen storage. MOFs and carbon based sorbents posses some desirable hydrogen storage properties which includes adequate hydrogen densities (up to 7.5wt% H_2 for MOF)[40] and fast hydrogen sorption kinetics. Furthermore hydrogen release can easily be triggered by relatively small changes in pressure and/or temperature, avoiding large heat flows. However owing to the weak interaction strength (typically 1-10 kJ/mol H_2)[23] significant physisorption occur only at low temperatures (less than 100 K)[10] and hydrogen pressures up to 70 bar. Extensive studies are now focusing on increasing the strength of hydrogen binding through doping and surface modifications, and the combination of sorbents with high pressure gaseous hydrogen storage[32, 33].

Metal hydrides: The second class of solid state hydrogen storage media are materials in which atomic hydrogen (H) is absorbed by metal or metal alloys to form a metal hydride [18, 24, 41-43]. Metal hydrides are often classified according to the nature of the bonding between hydrogen and the metal. Ionic or saline hydrides (e.g. LiH, NaH, MgH_2 and CaH_2) are formed by alkali or alkaline earth metals. They are characterized by strong ionic bonds between the hydrogen and metal atoms and therefore very stable. LiH and MgH_2 have high gravimetric hydrogen densities (12.6 and 7.6 wt% H_2 respectively) but due to their stability, dissociation or hydrogen release only occurs at temperatures (~ 400 °C for MgH_2 and 700 °C for LiH) that are too high for fuel cell applications. Also kinetic limitations make hydrogen absorption by Mg difficult at moderate temperatures and pressures.

Metallic or interstitial hydrides are hydrides like $LaNi_5H_6$, TiH_2, PdH_x and $FeTiH_2$ that originate from metallic bonding between hydrogen and either a transition metal, a rare earth metal or metal alloys. The hydrogen occupies the interstitial sites in the metallic (alloy) matrix such that the crystal structure of the metal (alloy) does not topologically change upon hydrogen absorption. Some metallic alloys like $LaNi_5H_6$, $FeTiH_2$ and PdH_x can release and reabsorb hydrogen repeatedly around ambient temperatures and hydrogen pressure but are limited by low gravimetric hydrogen contents (3 wt% H_2) due to the presence of heavy transition metals in their structure.

Another class is the so-called complex metal hydrides [44-46] which are composed of a light weight metal cation (Li, Na, Ca and Mg) that is ionically bonded to a hydrogen-containing complex anion such as the aluminium tetrahydride AlH_4^-, borohydrides BH_4^- and amides NH_2^-. Examples of complex hydrides are $LiBH_4$, $NaBH_4$, $NaAlH_4$, $Mg(BH_4)_2$ and $LiNH_2$. Most of the current research on metal hydrides focuses on these hydrides due to their very high gravimetric and volumetric hydrogen contents. Although complex hydrides have been known for a very long time [47, 48] they were initially not considered for reversible onboard hydrogen storage because they are expensive and hydrogen release from them involves high-temperature solid-phase transitions which are not readily reversible. However the discovery in 1996 by Bogdanovic et al[49] that $NaAlH_4$ can reversibly store hydrogen at more moderate conditions when doped with titanium based catalysts, sparked off a huge interest in the use of complex metal hydrides for

onboard hydrogen storage. Current research efforts are largely focused on discovering new complex hydrides with favorable hydrogen storage properties and tailoring the thermodynamics and kinetics of the hydrogen sorption in existing ones.

Apart from the above mentioned metal hydrides, other hydrides such as ammonia borane (NH_3BH_3) [50-52] and metal-amidoboranes[53-56] are also currently being investigated for on-board applications. These hydrides are sometimes referred to as chemical or covalent hydrides[23]. Although NH_3BH_3 possesses 19.6 wt% H_2 and releases about 6.5 wt% of the hydrogen at temperatures slightly less than 100 °C, the hydrogen release is associated with the poisonous gas borazine [51, 57, 58]. More importantly, the dehydrogenation is exothermic and hence non reversible under realistic conditions. Covalent hydrides are regarded as single-use fuels, and must be regenerated off board. Unfortunately no energy efficient and cost effective method has been found yet for the regeneration of spent ammonia borane and amidoboranes.

1.4 Requirements for hydrogen storage materials

Thermodynamics: The equilibrium temperature and pressure combination of (de)hydrogenation is a fundamental property of hydrogen storage materials. The equilibrium relationship is described by van't Hoff equation (when neglecting the temperature dependence of the enthalpy and entropy).

$$\ln\left(\frac{P_{eq}}{P_0}\right) = \frac{\Delta H^0}{RT} - \frac{\Delta S^0}{R} \tag{1.1}$$

Where P_{eq} is the equilibrium pressure, P_0 is the normal pressure (1 bar), R is the gas constant, T is the temperature, ΔH^0 and ΔS^0 are the changes in enthalpy and entropy respectively at standard conditions, accompanying the (de)hydrogenation

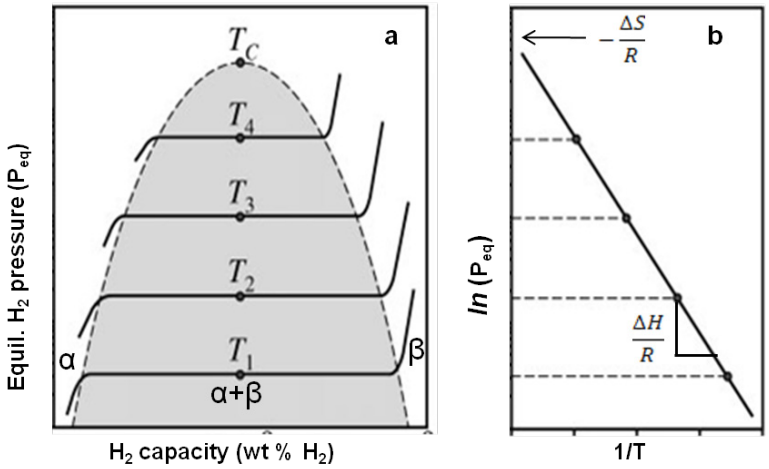

Figure 1.2: (a) Pressure composition isotherms of metal hydride showing plateau pressures corresponding to phase transitions from low H concentration(α phase) to the metal hydride phase (β phase). (b) van't Hoff plot. (Logarithm of the equilibrium pressures versus the inverse temperature). The enthalpy and entropy is evaluated from the slope and intercept of the plot respectively.(adapted from reference [59])

reactions. From equation (1.1) the temperature at which the equilibrium pressure equals 1 bar is

$$T_{dec} = \frac{\Delta H^0}{\Delta S^0} \tag{1.2}$$

ΔH^0 and ΔS^0 are known from literature or can be determined experimentally from pressure-composition-isotherms (PCI) of (de)hydrogenation reactions as shown in figure 1.2.

The entropy change ΔS_r associated with the decomposition of most metal hydrides is mainly due to the entropy of hydrogen gas and then it can be assumed that $\Delta S_r \approx S^0_{H2}$ = 130 J K^{-1}(mol H_2)$^{-1}$. However for some complex hydrides like $LiBH_4$ the entropy change is lower than 130 J K^{-1}(mol H_2)$^{-1}$ due to the relatively large vibrational contribution of the solid state phases to the total dehydrogenation entropy[60]. From equation (1.2) an enthalpy change in the range of 20–50 kJ/(mol H_2)$^{-1}$ is ideal in order to release hydrogen at conditions suitable for optimal fuel cell application (around 100 °C and 3 bar H_2). Materials with enthalpy of decomposition less than these values are generally unstable while those with higher

enthalpy values are relatively too stable and require high temperatures to release the hydrogen.

Kinetics and reversibility: A thermodynamically favourable reaction will only occur very slowly if there is a large kinetic barrier. Poor kinetics is a major reason why most metal hydrides are not reversible at moderate conditions. This is explained in figure 1.3 which shows a sketch of an energy profile for hydrogenation/dehydrogenation reactions of a metal M. The main driving force for any reaction is the Gibbs free energy, and it is negative for the hydrogenation reaction since the initial state (metal M + H_2) is at a higher energy than the final state (MH_2). Therefore the hydrogenation reaction should be spontaneous at ambient conditions. However hydrogen absorption can only occur if an activation (kinetic) barrier is overcome by supplying energy equal to E_A (typically by increase in temperature). This activation energy can be estimated using an Arrhenius rate equation (1.3):

$$K(T) = A_0 \exp(-E_A/RT) \qquad (1.3)$$

In which $K(T)$ is the temperature-dependent reaction rate, A_0 is the pre-exponential

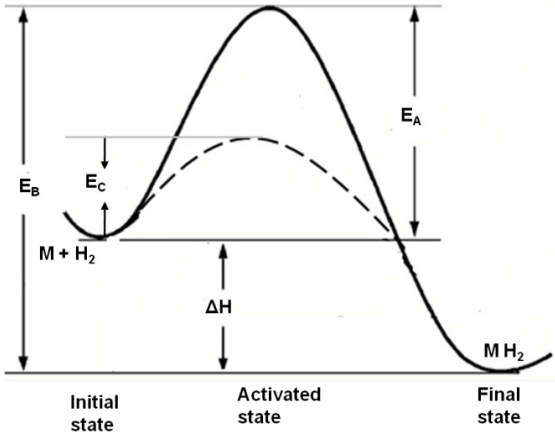

Figure 1.3: Energy-profile of a hydrogen sorption reaction from an initial to final state through an activated state. ΔH is the enthalpy difference between the initial and final states (reaction enthalpy), E_A is the activation energy for hydrogen absorption, E_B is the total energy change for dehydrogenation and the E_C the activation barrier in the presence of a catalyst.

or frequency factor, E_A is the apparent activation energy for hydrogenation, R is the gas constant and T the absolute temperature.

For the dehydrogenation reaction, the change of the standard Gibbs free energy is positive since the metal hydride will go from a low energy state (MH_2) to a higher energy state ($M+H_2$). Therefore in addition to the activation energy, energy equal to ΔH must be supplied for the reaction to proceed. This explains why most metal hydrides desorb hydrogen only at high temperatures. The major factor which determines the activation energy and rate of a reaction is the rate limiting step, and it depends on the particular reaction. For binary hydrides like MgH_2 the dissociation of molecular hydrogen/chemisorptions and diffusion through the hydride layers are typically rate limiting steps for hydrogenation while hydride decomposition and/or diffusion are typically the rate limiting steps for dehydrogenation[61]. For complex metal hydrides, much less is known about the rate-limiting step(s). The de/re-hydrogenation reaction kinetics of metal hydrides can be improved by the addition of catalysts which decreases the activation energy (from E_A to E_C) by speeding up the rate-limiting step(s), by alloying with other metals or by nano-sizing which enhances the diffusion rate by decreasing the diffusion distances.

1.5 Metal Borohydrides:

Hydrogen storage in the borohydrides of the alkali metals Li and Na, $LiBH_4$ and $NaBH_4$, is the focus of this thesis. Metal borohydrides are a class of complex metal hydrides in which a metal cation M^{n+} is ionically bonded to a borohydride anion BH_4^-. The general formula is $M(BH_4)_n$ where n is the valency of the metal. Most metal borohydrides possess high hydrogen densities (Table 1.1) attractive for hydrogen storage [62-68]. The alkali borohydrides $LiBH_4$, $NaBH_4$ and KBH_4 have been known for a long time[47] but the first report of their use for reversible hydrogen storage was in 2003[69]. They can be synthesized by the reaction between the corresponding metal hydride and diborane (B_2H_6) in etheral solvents[47, 48] and by direct reaction of the metal, boron and hydrogen at 550-700 °C and 3-150 bar H_2[70]. Fredrick et al. recently discovered a solvent free method to synthesize borohydrides using the corresponding metal hydride and diborane at 120 °C[71, 72].

Table 1.1: Metal borohydrides and their hydrogen densities

$M(BH_4)_n$	(wt% H_2)	(g H_2/ l)
$LiBH_4$	18.5	122.1
$NaBH_4$	10.8	114.5
KBH_4	7.5	87.8
$Be(BH_4)_2$	20.8	146
$Mg(BH_4)_2$	14.9	147.4
$Ca(BH_4)_2$	11.6	124.1
$Mn(BH_4)_2$	9.5	117.8
$Al(BH_4)_3$	16.9	133.5
$Zr(BH_4)_4$	10.7	126.2
$Zn(BH_4)_2$	8.5	-

Structure: Studies by neutron powder diffraction on the isotropically substituted $^7Li^{11}BD_4$ reveal that in alkali metal borohydrides, four deuterium atoms surrounds a central boron atom to form a regular tetrahedron with a B-D distance of 1.18-1.2 Å, 1.178 Å and 1.196 Å for $LiBD_4$, $NaBD_4$ and KBD_4 respectively[73-75]. The alkali borohydrides crystallize into a cubic NaCl-like structure (with the exception of $LiBH_4$) at ambient conditions although the exact space group symmetry for $NaBH_4$ is still debated[74, 76-79]. The cubic structure transforms into a low temperature ordered tetragonal phase at 190 K (-83 °C) and 76 K(- 197 °C) for $NaBH_4$ and KBH_4 respectively[74, 75, 80].

$LiBH_4$ has the orthorhombic *Pnma* structure at room temperature and undergoes an endothermic structural phase transition to a hexagonal high-temperature phase around 108 °C[73, 81, 82]. Neutron and synchrotron X-ray diffraction studies reveal an anisotropic displacement of the hydrogen atoms in the BH_4 units which increases by almost 2 orders of magnitude from 4 to 400 K[73, 81, 83]. This increase is due to the high disorder in the high temperature phase[84, 85]. Rotation of the BH_4 units has also been observed in $NaBH_4$ and KBH_4[86]. The increase in the cation size in going from Li to K leads to the expansion of the unit cell and an increase in the H-H distances between the neighbouring BH_4 anions resulting in weaker H-H repulsion. The decrease in H-H repulsion upon expansion of the unit cell leads to increased

stability of the structure and therefore a decrease in the phase transition temperatures in going from $LiBH_4$- KBH_4[75].

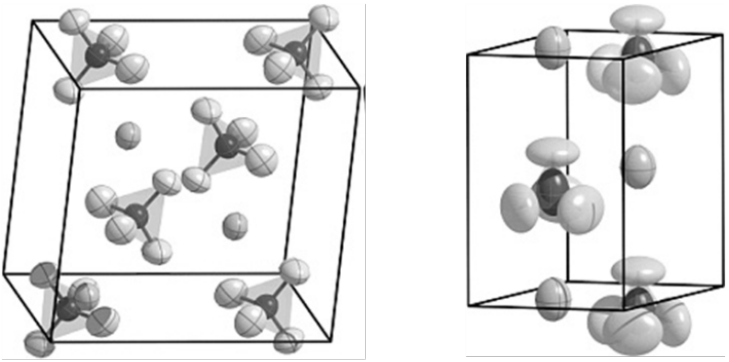

Figure 1.4: Crystal structure of $LiBH_4$ phases: (a) orthorhombic, (b) Hexagonal

***Stability and dehydrogenation*:** The dehydrogenation temperatures and decomposition pathway of metal borohydrides depend on their thermodynamic stability. Experimental results and first principle calculations show that their stability is related to the charge transfer from the metal cation M^{n+} to the borohydride anion BH_4^-. Therefore the stability decreases on going from less to more electronegative metal M[87, 88]. The heat of formation of $M(BH_4)_n$ increases linearly with the Pauling electronegativity χ_p of M while the hydrogen desorption temperatures decreases with increasing χ_p. Borohydrides of metals with ($\chi_p \leq 1.5$) decompose at high temperatures into the corresponding metal hydrides, boron and hydrogen while those with ($\chi_p > 1.5$) such as Mn, Zn and Al are less stable and decompose into the metal, hydrogen and diborane (B_2H_6) at temperatures less than 90 °C. The alkali metals have low electronegativity ($\chi_p < 1$) therefore their borohydrides are thermodynamically very stable, with experimental enthalpy and entropy change of -74 kJ $(mol\ H_2)^{-1}$ and 115 J K^{-1} $(mol\ H_2)^{-1}$ respectively for the dehydrogenation reaction of $LiBH_4$[89]. Similarly for $NaBH_4$, ΔH = -108 kJ$(mol\ H_2)^{-1}$ and ΔS = 133 J K^{-1} $(mol\ H_2)^{-1}$[178]. Therefore they start to release hydrogen only when heated to elevated temperatures (370 °C for $LiBH_4$ and 530 °C for $NaBH_4$)[78, 89] which are not even close to operating temperature ranges required for fuel cell

applications. The following overall decomposition equations can be written for alkali-metal borohydrides[69, 90].

$$2\ MBH_4 \rightarrow 2\ MH + 2\ B + 3\ H_2 \quad (1.4)$$

$$2\ MH \rightarrow 2\ M + H_2 \quad (1.5)$$

Upon heating from room temperature to about 500 °C, $LiBH_4$ decomposes in multiple steps[69] into LiH, B and H_2 via the formation of an intermediate product generally accepted to be $Li_2B_{12}H_{12}$[91-95] (1.6 and 1.7). Although $LiBH_4$ contains 18.5 wt% H_2, it releases only 13.8 wt% H_2 because decomposition of LiH to Li and H_2 occurs at temperatures well above 500 °C and therefore equation 1.7 is not normally considered for $LiBH_4$.

$$12\ LiBH_4 \rightarrow Li_2B_{12}H_{12} + 10\ LiH + 13\ H_2 \quad (1.6)$$

$$Li_2B_{12}H_{12} \rightarrow 2\ LiH + 12\ B + 5\ H_2 \quad (1.7)$$

$NaBH_4$ also contains significant amount of hydrogen (10.8 wt% and 115 kg of H_2 m^{-3}) but unlike $LiBH_4$ that is well studied for solid state reversible hydrogen sorption, much less is known about the thermal decomposition of $NaBH_4$ though it was recently suggested that $NaBH_4$ also decomposes into Na/NaH, B and hydrogen when heated to temperatures above 500 °C[78, 90, 96].

Kinetics and reversibility: The alkali borohydrides also have sluggish dehydrogenation kinetics with an activation energy of about 146 kJ/(mol $LiBH_4$) found for bulk $LiBH_4$ mixed with graphite[97]. Furthermore, the reversibility of the hydrogen release is limited due to slow rehydrogenation kinetics which is mostly attributed to solid state diffusion barriers. The dehydrogenation product contains at least two solid phases, (the metal hydride and B phase) that have to recombine to form the metal borohydride under hydrogen pressure. However due to the low mobility of both LiH and B, recombination is only possible at high hydrogen pressures and temperatures close to the melting point of the hydride phase. For example partial reversibility (8.3 wt% H_2) was achieved for dehydrogenated $LiBH_4$ at severe conditions (600 °C, 155 bar H_2, 12 h)[89] while no reversibility has been demonstrated yet for $NaBH_4$. Major focus of research activities on these materials which is also the focus of this thesis is on fundamental understanding of

the hydrogen uptake and release mechanisms and how the hydrogen desorption/absorption properties could be improved. The next section describes the major strategies that have been developed to tailor the thermodynamics and improve the kinetics and reversibility of the hydrogen desorption from metal borohydrides.

Changing Equilibrium: Two major approaches are been explored to alter the equilibrium temperature and pressure of hydrogen sorption in metal borohydrides. The first strategy is called product stabilization as the goal is to stabilize the dehydrogenation products[98-104]. In this method the borohydride is mixed with elements or compounds (especially hydrides) that could form dehydrogenation products that are more stable than the decomposition products of pure alkali borohydride, thereby reducing the overall dehydrogenation enthalpy of the system from (ΔH) to (ΔH_b) as shown in figure 1.5. For instance the addition of MgH_2 to $LiBH_4$ led to the formation of MgB_2 and LiH upon dehydrogenation, resulting to a dehydrogenation enthalpy which is 25 kJ/(mol H_2) lower than for the decomposition of pure $LiBH_4$ to LiH and B[99].

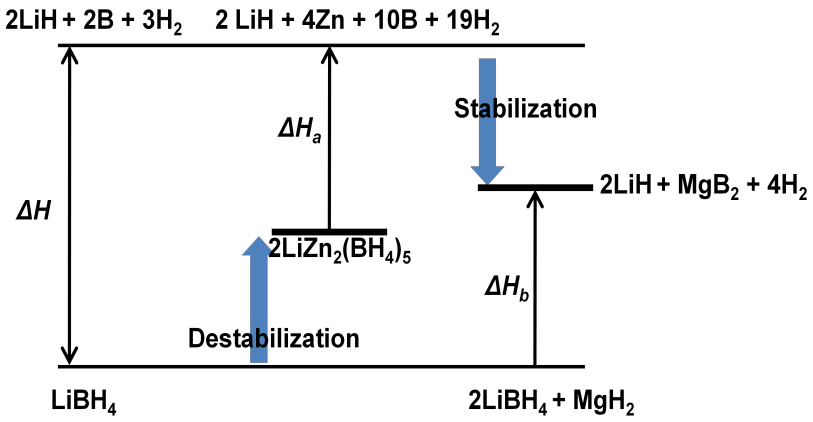

Figure1.5: Generalized enthalpy diagram illustrating destabilization and stabilization.

The second approach is reactant destabilization which focuses on the use of atomic substitution or alloying to create new phase borohydrides such as $LiZr(BH4)_5$, $NaZn_2(BH_4)_5$, $LiZn_2(BH_4)_5$ and $LiSc(BH4)_4$ [105-109]. These borohydrides are known

as mixed or double cation borohydrides and generally have dehydrogenation enthalpies (ΔH_a) lower than that of pure $LiBH_4$ (ΔH) as illustrated in figure 1.5. This strategy is based on the principle that the stability of borohydrides can be tuned by the electronegativity of the cation [87, 88]. For example the electronegativity of Zn (1.63) is higher than that of Li (0.98) and Na (0.93), hence $Zn(BH_4)_2$ is less stable than $LiBH_4$ and $NaBH_4$ and decomposes below 100°C[90, 110] while $LiBH_4$ and $NaBH_4$ decomposes ~370 °C and 530 °C respectively. It is expected that double cation borohydrides such as $NaZn_2(BH_4)_5$, and $LiZn_2(BH_4)_5$ will have dehydrogenation enthalpies that are less than those of pure $NaBH_4$ and $LiBH_4$. Using this approach, many new double cation borohydrides with lower decomposition temperatures than those of pure mono-cation borohydrides have been synthesized[66]. However a major drawback in this strategy is the non reversibility of the systems and the release of B_2H_6 during hydrogen desorption.

Improving Kinetics: Most light weight metal hydrides like MgH_2 consist of atoms without a d- orbital therefore hydrogen splitting/recombination are often rate-limiting. Thus elements with d- electrons like Pt, Pd, and Ni are often used as catalysts to speed up their (de)hydrogen kinetics. However for the complex hydrides like $LiBH_4$, no efficient catalyst is known yet. The search for a catalyst for hydrogen release and uptake reactions of metal borohydrides was pioneered by Züttel et al. who first reported that SiO_2 acted as a catalyst for the dehydrogenation of $LiBH_4$[69]. However later investigations showed that SiO_2 reacts with $LiBH_4$ to form stable silicates [111, 112] while irreversibly releasing hydrogen, as is the case with most metal oxide additives [113, 114]. A large range of materials, including metal halides[99, 115, 116], Al, Pt, carbon nanotubes, fullerene and Ni[117-121], has been investigated in an effort to identify an effective catalyst for the de/rehydrogenation reactions of metal borohydrides especially $LiBH_4$. Addition of these materials generally led to a decrease in the dehydrogenation temperatures but without a significant impact on reversibility as most of the systems still require temperatures above 450 °C and hydrogen pressures above 50 bar to achieve only partial rehydrogenation of the desorbed material. For example 600 °C, 100 bar H_2 and 30 h were required for partial (12 wt% H_2) reversibility in $LiBH_4$ ball milled with Ni[121] (600 °C and 350 bar hydrogen for bulk $LiBH_4$).

The failure of classical hydrogen dissociation catalysts like Ni, Pd and Pt to have a tangible impact on especially the hydrogen uptake kinetics in desorbed $LiBH_4$ suggests that hydrogen dissociation is not rate- limiting in the rehydrogenation reactions of metal borohydrides but solid state diffusion barriers as mentioned in previous section. Thus limiting the phase segregation of the dehydrogenation product could be highly beneficial to reversible hydrogen uptake in alkali borohydrides. This is the approach adopted in this thesis and is described in detail in the next section.

1.6 Nanosizing and Nanoconfinement

Recently increasing attention has been paid to taking advantage of the unique chemical and physical properties exhibited by materials at the nanoscale to improve the hydrogen sorption properties of metal hydrides[59, 122-127]. Kirchheim et al [123] showed that the solubility of hydrogen in nanocrystalline Pd (8- 12 nm) produced by condensation of Pd-vapor in a helium atmosphere, increased by a factor of 10-30 in comparison with polycrystalline samples (10-20 μm). Improved hydrogen sorption kinetics was reported for MgH_2 nanostructures produced through high-energy ball milling and gas phase deposition [122]. These observations were attributed to the high surface area to volume ratios, increased number of grain boundaries and reduced diffusion (nano-scales) distances exhibited by these nanostructured metal hydrides. Since then, several experimental and computational results have shown that the kinetics and also the thermodynamics of hydrogen sorption in metal hydrides can significantly be enhanced by nano-sizing [59, 124-127].
The most common and convenient method to produce nanosized metal hydride is high-energy ball-milling. However this method is not suitable to prepare metal hydrides with crystallites sizes less than 10 nm. Additionally, nanostructured metal hydrides produced through ball-milling easily loose the benefits of nano-sizing upon cycling due to sintering and agglomeration of the nanoparticles. Alternatively, Baldé et al.[128, 129] synthesized carbon nanofibre-supported $NaAlH_4$ nanoparticles in the size range 3-1000 nm via wet- chemical synthesis. Although favourable nanosizing effects were reported the loadings were low (< 12 wt % $NaAlH_4$). A new approach to overcome these limitations is nanoconfinement in which the metal hydride nanoparticles are confined into a nanoporous scaffold

material such as carbon, silica or MOF[130-133]. These nanoporous materials normally contain micropores (≤ 2 nm) and/or mesopores (2- 50 nm) and sometimes macropores (> 50 nm). The first report on the beneficial effects of nanoconfinement came from Autrey *et al.*[130] who successfully incorporated ammonia borane (NH_3BH_3) into ordered mesoporous silica (SBA-15) with a pore diameter of 7-8 nm and showed that the inclusion of the ammonia borane in this nanoporous silica resulted in a significant improvement on its hydrogen release properties. The onset of hydrogen release decreased by 15 °C compared to the bulk sample and the apparent activation energy for hydrogen release decreased from 184 kJ/mol in the bulk to 67 kJ/mol in the NH_3BH_3/SBA-15 nanocomposite. Furthermore, the decomposition pathway of NH_3BH_3 changed upon confinement in the nanoporous silica, leading to a significant suppression of the borazine ($B_3H_6N_3$) formation which is normally associated with hydrogen release from NH_3BH_3. Similar observations were reported for NH_3BH_3 confined in nanoporous carbon cryogels[134]. Extending this to metal borohydrides, Gross et al.[97] confined $LiBH_4$ in nanoporous carbon aerogel by melt infiltration and showed that both the dehydrogenation kinetics, reversibility and the stability of the $LiBH_4$ upon cycling were greatly enhanced in comparison to the bulk $LiBH_4$. Furthermore, unlike with bulk $LiBH_4$, no diborane was associated with the hydrogen release.

These findings clearly showed that nanoconfinement can drastically change the properties of hydrogen storage materials, and therefore ignited a lot of interest in investigating the effects of nanoconfinement in different nanoporous materials on the hydrogen sorption properties of $LiBH_4$ (and other metal borohydrides as well). To this end $LiBH_4$ has been successfully confined into different carbon based nanoporous materials[135-137], silica[138] and most recently in Cu-MOF[139]. A significant decrease in the hydrogen release temperatures were observed in these nanocomposites although for Cu-MOF and silica, interaction between $LiBH_4$ and oxygen in their frame works led to irreversibility of the systems and the release of B_2H_6 as will be discussed in chapter 2. Improved reversibility was reported for some of the carbon based materials. Unlike for the bulk $LiBH_4$, only a single hydrogen desorption step was observed, suggesting that nanoconfinement in carbon based materials could also alter the decomposition pathway and/or enthalpy of

$LiBH_4$[135-137] as in the case of nanoconfined NH_3BH_3[130, 134] and $NaAlH_4$ confined in nanoporous carbon materials[140, 141].
Nanoconfinement continues to generate a lot of interest as it offers a relatively easy route to synthesize and stabilize nanostructured metal hydrides using nanoporous hosts as a template. Additionally, the average size of the metal hydride nanoparticles can be tuned by changing the pore sizes of the scaffold.

Preparation methods and nanoporous host: Nanoconfined hydrides are commonly prepared in two ways. In the first method, the nanoporous host is impregnated with a solution of the metal hydride and subsequently the solvent is dried leaving the metal hydride inside the pores of the host[130, 134]. A second method is to melt the metal hydride (sometimes under hydrogen pressure to avoid decomposition) and infiltrate the nanoporous host with the molten metal hydride via capillary suction[97]. Sometimes the metal or metal precursor is impregnated or melt infiltrated into the nanoporous host and subsequently hydrogenated to form the metal hydride[142]. Ideally the nanoporous host should be light (to avoid loosing much hydrogen capacity), inert towards the metal hydride (to avoid irreversible reactions), and highly porous so as to achieve high loadings of the metal hydride. Furthermore the nanoporous material should be easily available and low cost. High purity nanoporous carbon materials seem to satisfy most of these requirements and are therefore the preferred material for nanoconfinement especially for reactive metal hydrides like $LiBH_4$, MgH_2 and $NaAlH_4$.

1.61 Effects of Nanoconfinement on Kinetics and thermodynamics

The effects of nanoconfinement on the dehydrogenation/rehydrogenation kinetics and thermodynamics of metal hydrides (and especially metal borohydrides) are not well understood, but can be related to particle size, physical confinement and interface effects. However it is difficult to separate one effect from another especially for complex materials like metal borohydrides.

***Size effects*:** Zaluska et al. showed that decreasing the particle size of MgH_2 from micrometer to ~ 30 nm resulted in an increase in the hydrogen release and uptake kinetics[122]. It was also shown that both the desorption temperatures and activation

energy of $NaAlH_4$ nanoparticles supported on carbon nanofibre decreased as their particle size decreased[129]. The increased surface-to-volume ratio and the presence of defects at nanoscale could enhance nucleation and improve (de)hydrogenation kinetics[59]. Furthermore, mass transport distances required for recombination of dehydrogenation products are significantly reduced. This explains the huge impact of nanosizing on especially the reversible kinetics in complex hydrides like $LiBH_4$. The change in the equilibrium of hydrogen uptake and release reported for nanoconfined complex hydrides might be related to significant increase in the surface energy when reduced to sizes ≤ 10 nm. For metal hydrides nanoparticles (≤ 10 nm) or clusters such as MgH_2 it is has been predicted that its standard enthalpy of formation could be significantly higher than that of the bulk due the strong increase of the surface energy and the nature of the bond [59, 125, 143]. Nanosizing can stabilize or destabilize metal hydrides[127, 143]. Computational studies based on density functional theory and the cluster expansion method predicted that the stability of $NaAlH_4$ is increased when reduced to sizes less than 10 nm. The two step decomposition into NaH, Al and H_2 is changed to single step due to instability of the intermediate decomposition phase (Na_3AlH_6) at this size range[144, 145]. These predictions are in line with experimental results[140, 141]. Predictions based on first principle calculations showed that the instability of Na_3AlH_6 nanoclusters is due to a Jahn-Teller distortion that destabilizes the $[AlH_6]^{3-}$ anions and causes them to split into two H^- ions and $[AlH_4]^-$, thereby stabilizing the $NaAlH_4$ with respect to the Na_3AlH_6[145]. Although very little is known for other complex-metal hydrides like the borohydrides, it is possible that such effects could also be important in nanoconfined $LiBH_4$. Another important thermodynamic parameter that could alter the thermodynamic equilibrium in nanoconfined complex hydrides like $LiBH_4$ is the entropy (equation 1.2). $LiBH_4$ has a relatively high entropy change (-115 J K^{-1} (mol H_2)$^{-1}$) compared to ionic metal hydrides due to the vibrational contribution of the complex anion in the structure[60]. The high disorder, increased vibration or rotation, lack of long-range order and change in physical properties such as melting and phase transition temperatures exhibited by nanoconfined complex hydrides [97, 135-137, 146, 147] could affect their stability.

***Confinement effects*:** Physical confinement of metal hydrides could lead to both kinetic and thermodynamic effects. For complex hydrides, the dehydrogenated

products are often macroscopically segregated immobile solid phases. Physical confinements will restrict this phase segregation of the dehydrogenation products as both phases are expected to be contained within the nanopores. Therefore it is logical to expect improved reversible kinetics for nanoconfined complex hydrides. However this might not be the case if one of the desorbed components is in liquid or gaseous state during desorption as this phase might easily be redistributed or even lost through evaporation.

Physical confinement could also lead to thermodynamic effects in metal hydrides. Significant volume expansion normally occurs upon hydrogen absorption in most metals, although the reverse is the case for Na. Physical confinement could restrict the volume change upon hydrogen uptake and release. This restriction can change the energetics of the hydrogen sorption. For example it has been theoretically predicted that the enthalpy change for dehydrogenation reaction of MgH_2 could be reduced by up to 50 % if confined in three dimensions such as in carbon nanotubes[148]. Physical confinement can induce stress or pressure on a metal hydride, and also lead to a significant change in its interfacial energy (surface tension), thereby changing the stability of the metal hydride.

***Support effects*:** Nanoconfined metal hydrides could have physical, chemical, or electronic interactions with the nanoporous host material which can lead to a change in the kinetics and/or thermodynamics of the hydrogen sorption in the metal hydride. This is very obvious in some systems while for others it difficult to observe especially due to lack of long-range crystallinity in most nanoconfined metal hydrides. For example, it was recently shown that the use of oxygen-containing nanoporous hosts like silica, porous alumina or MOF leads to irreversible formation of stable silicates, aluminates or oxides [138, 139](except for covalent hydrides like NH_3BH_3) which changed the kinetics and thermodynamics of hydrogen desorption. However reversible hydrogen sorption cannot be realised in such systems. Carbon based nanoporous materials are assumed to be inert, however they may be far from inert as they often contain significant amounts of, e.g surface oxygen groups. These surface groups could lead to side reactions such as oxidation, or catalyse the decomposition reactions as reported for ammonia borane confined in carbon[149]. Electronic interaction[120] and irreversible formation of B-C bonds[135] and LiC_2[150] have been reported for $LiBH_4$ confined in nanoporous

carbon materials. Nanoporous host materials could also improve hydrogen sorption by providing extra nucleation sites for phase transitions and enhancing heat and mass transport during de/rehydrogenation.
In conclusion several explanations are possible for the change in kinetics and thermodynamics observed in nanoconfined metal hydrides. Nanoconfinement is relatively new and at the moment most of these effects are not well understood. However it is clear that nanosizing, physical confinement and support effects are important factors that influence the kinetics and thermodynamics of hydrogen sorption in nanoconfined metal hydrides.

1.7 Scope and outline of this thesis

The aim of the study described in this thesis was to investigate the effect of nanosizing/nanoconfinement and possible interaction with the nanoporous hosts on the hydrogen sorption properties of alkali borohydrides. To this end nanoporous carbon and ordered mesoporous silica (SBA-15) were used as templates to synthesize $LiBH_4/SiO_2$, $LiBH_4/C$, $LiBH_4(Ni)/C$ and $NaBH_4/C$ nanocomposites via melt infiltration and solution impregnation. Their structure and hydrogen sorption properties were studied using techniques such as X-ray diffraction (XRD), nitrogen physisorption, Extended X-ray absorption fine edge structures (EXAFS), transmission electron microscopy (TEM), solid- state nuclear magnetic resonance (NMR) spectroscopy, high pressure differential scanning calorimetry (HPDSC) and hydrogen release /uptake measurement techniques.
Initially it was claimed that SiO_2 acted as a catalyst for the dehydrogenation of $LiBH_4$ and we were interested in studying the combined effects of nanoconfinement in, and catalysis by ordered mesoporous SiO_2 (SBA-15) on the hydrogen sorption properties of $LiBH_4$. This study is presented in chapter 2 which describes the synthesis, structural characterization and hydrogen sorption properties of $LiBH_4$ confined in SBA-15. The relevance of hydrogen pressure to successful synthesis of $LiBH_4/SiO_2$ nanocomposites is discussed. However reactions between decomposition product(s) of $LiBH_4$ and SiO_2 during hydrogen desorption led to irreversible formation of lithium silicates.
In chapter 3 the dehydrogenation and rehydrogenation behaviour of $LiBH_4$ confined in nanoporous carbon is discussed. The melt infiltration process for the

preparation of $LiBH_4$/C nanocomposites is studied and the impact of carbon impurities is reported. A detailed discussion of the influence of the $LiBH_4$ loading on the microstructure, hydrogen sorption kinetics, thermodynamics and reversibility of the nanocomposites is presented. Chapter 4 presents the impact of adding Ni to the $LiBH_4$/C nanocomposite. The synergetic effects of Ni addition and nanoconfinement in carbon on the hydrogen sorption properties of $LiBH_4$ are demonstrated. The role of Ni in enhancing especially the reversibility of the hydrogen release from the nanoconfined $LiBH_4$ is discussed using results from EXAFS and NMR measurements. It was interesting to investigate if the effects observed in nanoconfined $LiBH_4$ could be applicable to other alkali borohydrides; therefore chapter 5 describes a study on $NaBH_4$/C nanocomposites. The preparation methods, structural characterisation, decomposition pathways and reversible hydrogen sorption are presented. The influence of preparation methods on the hydrogen release kinetics, thermodynamics and decomposition reactions are discussed. Additionally, the limiting factor for full reversibility is highlighted and a strategy to overcome this demonstrated and discussed.

References

1. J. A. Turner, *Science*, 1999, **285**, 687-689.
2. *Key World Energy Statistics, International Energy Agency, 2009. Available from http://www.iea.org (accessed July 2011).*
3. *Internal Energy Agency, World Energy Outlook 2010 http://www.iea.org/Textbase/nptoc/weo2010toc.pdf (accessed July 2011).*
4. *Mobility 2030: Meeting the Challenges to Sustainability, World Business Council for Sustainable Development, (2004). ISBN: 2-940240-57-4, Geneva, Switzerland. Available on-line at: http://www.wbcsd.org/web/publications/mobility/mobility-full.pdf. (accessed August 2011.*
5. *Fourth Assessment Report of the Intergovernmental Panel on Climate Change, Cambridge University Press, Cambridge 2007. Available from http://www.ipch.ch (accessed July 2011)*

6. T. J. Wallington, J. L. Sullivan and M. D. Hurley, *Meteorologische Zeitschrift*, 2008, **17**, 109-116.
7. L. Schlapbach and A. Züttel, *Nature*, 2001, **414**, 353-358.
8. K. Hirose, *Philosophical Transactions of the Royal Society A: Mathematical, Physical and Engineering Sciences*, 2010, **368**, 3365-3377.
9. J. Tollefson, *Nature*, 2010, **464**, 1262-1264.
10. A. Züttel, A. Remhof, A. Borgschulte and O. Friedrichs, *Philosophical Transactions of the Royal Society A: Mathematical, Physical and Engineering Sciences*, 2010, **368**, 3329-3342.
11. M. Z. Jacobson, W. G. Colella and D. M. Golden, *Science*, 2005, **308**, 1901-1905.
12. L. Schlapbach, *Nature*, 2009, **460**, 809-811.
13. *The Hydrogen Economy: Opportunities, Costs, Barriers and R&D Needs, Committee on Alternatives and Strategies for Future Hydrogen Production and Use, The National Academies Press, Washington, D.C., 2004.*
14. P. P. Edwards, V. L. Kuznetsov and W. I. F. David, *Philosophical Transactions of the Royal Society A: Mathematical, Physical and Engineering Sciences*, 2007, **365**, 1043-1056.
15. T. I. Sigfusson, *Philosophical Transactions of the Royal Society A: Mathematical, Physical and Engineering Sciences*, 2007, **365**, 1025-1042.
16. B. C. H. Steele and A. Heinzel, *Nature*, 2001, **414**, 345-352.
17. J.-P. Rodrigue, C. Comtois and B. Slack, *The Geography of Transport Systems, Second Edition, New York: Routledge*, 2009.
18. A. Züttel, A. Borgschulte and L. Schlapbach, *Hydrogen as a future energy carrier. Wiley-VCH, Weinheim*, 2008.
19. S. S. Penner, *Energy*, 2006, **31**, 33-43.
20. S. A. Sherif, F. Barbir and T. N. Veziroglu, *Solar Energy*, 2005, **78**, 647-660.
21. J. A. Turner, *Science*, 2004, **305**, 972-974.
22. B. C. R. Ewan and R. W. K. Allen, *International Journal of Hydrogen Energy*, 2005, **30**, 809-819.
23. J. Yang, A. Sudik, C. Wolverton and D. J. Siegel, *Chem. Soc. Rev.*, 2010, **39**, 656-675.

24. A. Züttel, *Materials Today*, 2003, **6**, 24-33.
25. *US Department of Energy, http://www1.eere.energy.gov/hydrogenandfuelcells/storage/pdfs/targets_onboard_hydro_storage.pdf (accessed June 2011)*.
26. M. Felderhoff, C. Weidenthaler, R. Von Helmolt and U. Eberle, *Phys. Chem. Chem. Phys.*, 2007, **9**, 2643-2653.
27. A. W. C. Van Den Berg and C. O. Areán, *Chem. Commun.*, 2008, 668-681.
28. M. G. Nijkamp, J. E. M. J. Raaymakers, A. J. van Dillen and K. P. de Jong, *Appl. Phys. A: Mater. Sci. Process.*, 2001, **72**, 619.
29. H. Li, M. Eddaoudi, M. O'Keeffe and O. M. Yaghi, *Nature*, 1999, **402**, 276-279.
30. N. L. Rosi, J. Eckert, M. Eddaoudi, D. T. Vodak, J. Kim, M. O'Keeffe and O. M. Yaghi, *Science*, 2003, **300**, 1127-1129.
31. E. Poirier, R. Chahine, P. BÃ©nard, L. Lafi, G. Dorval-Douville and P. A. Chandonia, *Langmuir*, 2006, **22**, 8784-8789.
32. L. J. Murray, M. Dinca and J. R. Long, *Chem. Soc. Rev.*, 2009, **38**, 1294-1314.
33. J. L. C. Rowsell and O. M. Yaghi, *Angew. Chem., Int. Ed.*, 2005, **44**, 4670-4679.
34. C. Carpetis and W. Peschka, *Int. J. Hydrogen Energy*, 1980, **5**, 539-554.
35. R. Chahine and T. K. Bose, *Int. J. Hydrogen Energy*, 1994, **19**, 161-164.
36. R. Dagani, *Chemical and Engineering News*, 2002, **80**, 25-28.
37. A. C. Dillon and M. J. Heben, *Appl. Phys. A: Mater. Sci. Process.*, 2001, **72**, 133-142.
38. G. E. Froudakis, *Journal of Physics Condensed Matter*, 2002, **14**, R453-R465.
39. R. Ströbel, J. Garche, P. T. Moseley, L. Jörissen and G. Wolf, *J. Power Sources*, 2006, **159**, 781-801.
40. H. Furukawa, M. A. Miller and O. M. Yaghi, *J. Mater. Chem.*, 2007, **17**, 3197-3204.
41. G. D. Sandrock and E. L. Huston, *CHEMTECH*, 1981, **11**, 754-762.
42. G. D. Sandrock and E. Snape, *ACS Symp. Ser.*, 1980, 293-322.

43. T. Graham, *Proceedings of the Royal Society of London*, 1867, **16**, 422-427.
44. B. Bogdanovic, M. Felderhoff and G. Streukens, *J. Serb. Chem. Soc.*, 2009, **74**, 183-196.
45. S. I. Orimo, Y. Nakamori, J. R. Eliseo, A. Züttel and C. M. Jensen, *Chem. Rev*, 2007, **107**, 4111-4132.
46. J. Wang, A. D. Ebner and J. A. Ritter, *J. Phys. Chem. C*, 2007, **111**, 14917-14924.
47. H. I. Schlesinger and H. C. Brown, *J. Am. Chem. Soc.*, 1940, **62**, 3429-3435.
48. H. I. Schlesinger, H. C. Brown, A. E. Finholt, J. R. Gilbreath, H. R. Hoekstra and E. K. Hyde, *J. Am. Chem. Soc.*, 1953, **75**, 215-219.
49. B. Bogdanovic and M. Schwickardi, *J. Alloys Compd.*, 1997, **253**, 1-9.
50. A. Gutowska, L. Li, Y. Shin, C. M. Wang, X. S. Li, J. C. Linehan, R. S. Smith, B. D. Kay, B. Schmid, W. Shaw, M. Gutowski and T. Autrey, *Angew. Chem., Int. Ed.*, 2005, **44**, 3578-3582.
51. F. H. Stephens, V. Pons and R. Tom Baker, *Dalton Trans.*, 2007, 2613-2626.
52. G. Wolf, J. Baumann, F. Baitalow and F. P. Hoffmann, *Thermochim. Acta*, 2000, **343**, 19-25.
53. Z. Xiong, C. K. Yong, G. Wu, P. Chen, W. Shaw, A. Karkamkar, T. Autrey, M. O. Jones, S. R. Johnson, P. P. Edwards and W. I. F. David, *Nat. Mater.*, 2008, **7**, 138-141.
54. X. Kang, Z. Fang, L. Kong, H. Cheng, X. Yao, G. Lu and P. Wang, *Adv. Mater*, 2008, **20**, 2756-2759.
55. H. V. K. Diyabalanage, R. P. Shrestha, T. A. Semelsberger, B. L. Scott, M. E. Bowden, B. L. Davis and A. K. Burrell, *Angew. Chem., Int. Ed.*, 2007, **46**, 8995-8997.
56. Y. S. Chua, P. Chen, G. Wu and Z. Xiong, *Chem. Commun.*, **47**, 5116-5129.
57. F. Baitalow, J. Baumann, G. Wolf, K. Jaenicke-Rößler and G. Leitner, *Thermochim. Acta*, 2002, **391**, 159-168.

58. V. Sit, R. A. Geanangel and W. W. Wendlandt, *Thermochim. Acta*, 1987, **113**, 379-382.
59. V. Bérubé, G. Radtke, M. Dresselhaus and G. Chen, *International Journal of Energy Research*, 2007, **31**, 637-663.
60. D. J. Siegel, C. Wolverton and V. Ozolins, *Physical Review B*, 2007, **76**.
61. M. Martin, C. Gommel, C. Borkhart and E. Fromm, *J. Alloys Compd.*, 1996, **238**, 193-201.
62. A. Züttel, A. Borgschulte and S.-I. Orimo, *Scr. Mater.*, 2007, **56**, 823-828.
63. Y. Nakamori, H. W. Li, K. Miwa, S. Towata and S. Orimo, *Mater. Trans.*, 2006, **47**, 1898-1901.
64. R. Cerny, Y. Filinchuk, H. Hagemann and K. Yvon, *Angewandte Chemie, International Edition* 2007, **46**, 5765-5767.
65. K. Miwa, M. Aoki, T. Noritake, N. Ohba, Y. Nakamori, S. Towata, A. Zuttel and S. Orimo, *Physical Review B*, 2006, **74**.
66. H. W. Li, Y. G. Yan, S. Orimo, A. Zuttel and C. M. Jensen, *Energies*, 2011, **4**, 185-214.
67. W. Grochala and P. P. Edwards, *Chem. Rev*, 2004, **104**, 1283-1315.
68. H. Hagemann and R. Cerny, *Dalton Trans.*, 2010, **39**, 6006-6012.
69. A. Züttel, P. Wenger, S. Rentsch, P. Sudan, P. Mauron and C. Emmenegger, *J. Power Sources*, 2003, **118**, 1-7.
70. D. Goerrig, *German Patent 1077644, 1958, F27373 IVa/12i.*
71. O. Friedrichs, A. Borgschulte, S. Kato, F. Buchter, R. Gremaud, A. Remhof and A. Züttel, *Chemistry – A European Journal*, 2009, **15**, 5531-5534.
72. O. Friedrichs, A. Remhof, A. Borgschulte, F. Buchter, S. I. Orimo and A. Zuttel, *Phys. Chem. Chem. Phys.*, 2010, **12**, 10919-10922.
73. F. Buchter, Z. Łodziana, P. Mauron, A. Remhof, O. Friedrichs, A. Borgschulte, A. Züttel, D. Sheptyakov, T. Strässle and A. J. Ramirez-Cuesta, *Physical Review B*, 2008, **78**, 094302.
74. P. Fischer and A. Züttel, *Mater. Sci. Forum 443-444, 287 (2004).*
75. G. Renaudin, S. Gomes, H. Hagemann, L. Keller and K. Yvon, *J. Alloys Compd.*, 2004, **375**, 98-106.

76. W. H. Stockmayer and C. C. Stephenson, *The Nature of the Gradual Transition in Sodium Borohydride*, AIP, 1953.
77. Y. Filinchuk and H. Hagemann, *Eur. J. Inorg. Chem.*, 2008, **2008**, 3127-3133.
78. P. Martelli, R. Caputo, A. Remhof, P. Mauron, A. Borgschulte and A. Züttel, *J. Phys. Chem. C*, 2010, **114**, 7173-7177.
79. O. A. Babanova, A. V. Soloninin, A. P. Stepanov, A. V. Skripov and Y. Filinchuk, *J. Phys. Chem. C*, 2010, **114**, 3712-3718.
80. C. C. Stephenson, D. W. Rice and W. H. Stockmayer, *Order?Disorder Transitions in the Alkali Borohydrides*, AIP, 1955.
81. M. R. Hartman, J. J. Rush, T. J. Udovic, R. C. Bowman Jr and S.-J. Hwang, *J. Solid State Chem.*, 2007, **180**, 1298-1305.
82. J. P. Soulié, G. Renaudin, R. Erný and K. Yvon, *J. Alloys Compd.*, 2002, **346**, 200-205.
83. Y. Filinchuk, D. Chernyshov and R. Cerny, *J. Phys. Chem. C*, 2008, **112**, 10579-10584.
84. H. Hagemann, S. Gomes, G. Renaudin and K. Yvon, *J. Alloys Compd.*, 2004, **363**, 129-132.
85. I. Tamio, T. Eiji, I. Kazutaka, M. Motoaki, L. Hai-Wen, K. Yoshiyuki and O. Shin-ichi, *Diffuse and doubly split atom occupation in hexagonal LiBH4*, AIP, 2009.
86. O. A. Babanova, A. V. Soloninin, A. P. Stepanov, A. V. Skripov and Y. Filinchuk, *The Journal of Physical Chemistry C*, **114**, 3712-3718.
87. Y. Nakamori, H. W. Li, K. Kikuchi, M. Aoki, K. Miwa, S. Towata and S. Orimo, *J. Alloys Compd.*, 2007, **446**, 296-300.
88. Y. Nakamori, K. Miwa, A. Ninomiya, H. W. Li, N. Ohba, S. I. Towata, A. Zuttel and S. I. Orimo, *Physical Review B*, 2006, **74**.
89. P. Mauron, F. Buchter, O. Friedrichs, A. Remhof, M. Bielmann, C. N. Zwicky and A. Zuttel, *J. Phys. Chem. B*, 2008, **112**, 906-910.
90. W. Grochala and P. P. Edwards, *Chem. Rev*, 2004, **104**, 1283-1316.
91. N. Ohba, K. Miwa, M. Aoki, T. Noritake, S. I. Towata, Y. Nakamori, S. I. Orimo and A. Züttel, *Phys. Rev. B: Condens. Matter Mater. Phys.*, 2006, **74**.

92. S. I. Orimo, Y. Nakamori, N. Ohba, K. Miwa, M. Aoki, S. I. Towata and A. Züttel, *Appl. Phys. Lett.*, 2006, **89**.
93. S. J. Hwang, R. C. Bowman, J. W. Reiter, J. Rijssenbeek, G. L. Soloveichik, J. C. Zhao, H. Kabbour and C. C. Ahn, *J. Phys. Chem. C*, 2008, **112**, 3164-3169.
94. O. Friedrichs, A. Remhof, S. J. Hwang and A. Züttel, *Chem. Mater.*, 2010, **22**, 3265-3268.
95. V. Ozolins, E. H. Majzoub and C. Wolverton, *J. Am. Chem. Soc.*, 2008, **131**, 230-237.
96. J. Urgnani, F. J. Torres, M. Palumbo and M. Baricco, *Int. J. Hydrogen Energy*, 2008, **33**, 3111-3115.
97. A. F. Gross, J. J. Vajo, S. L. Van Atta and G. L. Olson, *J. Phys. Chem. C*, 2008, **112**, 5651-5657.
98. J. J. Vajo and G. L. Olson, *Scr. Mater.*, 2007, **56**, 829-834.
99. J. J. Vajo, S. L. Skeith and F. Mertens, *J. Phys. Chem. B*, 2005, **109**, 3719-3722.
100. M. Aoki, K. Miwa, T. Noritake, G. Kitahara, Y. Nakamori, S. Orimo and S. Towata, *Applied Physics A*, 2005, **80**, 1409-1412.
101. G. Barkhordarian, T. Klassen, M. Dornheim and R. Bormann, *J. Alloys Compd.*, 2007, **440**, L18-L21.
102. U. Bösenberg, S. Doppiu, L. Mosegaard, G. Barkhordarian, N. Eigen, A. Borgschulte, T. R. Jensen, Y. Cerenius, O. Gutfleisch, T. Klassen, M. Dornheim and R. Bormann, *Acta Mater.*, 2007, **55**, 3951-3958.
103. S. Garroni, C. Pistidda, M. Brunelli, G. B. M. Vaughan, S. Surinach and M. D. Baro, *Scr. Mater.*, 2009, **60**, 1129-1132.
104. J. F. Mao, X. B. Yu, Z. P. Guo, H. K. Liu, Z. Wu and J. Ni, *J. Alloys Compd.*, 2009, **479**, 619-623.
105. H. W. Li, S. Orimo, Y. Nakamori, K. Miwa, N. Ohba, S. Towata and A. Züttel, *J. Alloys Compd.*, 2007, **446-447**, 315-318.
106. H. Hagemann, M. Longhini, J. W. Kaminski, T. A. Wesolowski, R. Černy, N. Penin, M. H. Sørby, B. C. Hauback, G. Severa and C. M. Jensen, *J. Phys. Chem. A*, 2008, **112**, 7551-7555.

107. C. Kim, S. J. Hwang, R. C. Bowman Jr, J. W. Reiter, J. A. Zan, J. G. Kulleck, H. Kabbour, E. H. Majzoub and V. Ozolins, *J. Phys. Chem. C*, 2009, **113**, 9956-9968.
108. D. Ravnsbæk, Y. Filinchuk, Y. Cerenius, H. J. Jakobsen, F. Besenbacher, J. Skibsted and T. R. Jensen, *Angew. Chem., Int. Ed.*, 2009, **48**, 6659-6663.
109. E. A. Nickels, M. O. Jones, W. I. F. David, S. R. Johnson, R. L. Lowton, M. Sommariva and P. P. Edwards, *Angew. Chem., Int. Ed.*, 2008, **47**, 2817-2819.
110. S. Srinivasan, D. Escobar, M. Jurczyk, Y. Goswami and E. Stefanakos, *J. Alloys Compd.*, 2008, **462**, 294-302.
111. Y. Zhang, W.-S. Zhang, M.-Q. Fan, S.-S. Liu, H.-L. Chu, Y.-H. Zhang, X.-Y. Gao and L.-X. Sun, *J. Phys. Chem. C*, 2008, **112**, 4005-4010.
112. L. Mosegaard, B. Moller, J. E. Jorgensen, Y. Filinchuk, Y. Cerenius, J. C. Hanson, E. Dimasi, F. Besenbacher and T. R. Jensen, *J. Phys. Chem. C*, 2008, **112**, 1299-1303.
113. X. B. Yu, D. A. Grant and G. S. Walker, *J. Phys. Chem. C*, 2008, **112**, 11059-11062.
114. S. M. Opalka, X. Tang, B. L. Laube and T. H. Vanderspurt, *Nanotechnology*, 2009, **20**.
115. M. An and A. Jurgensen, *J. Phys. Chem. B*, 2006, **110**, 7062-7067.
116. M. Au, A. R. Jurgensen, W. A. Spencer, D. L. Anton, F. E. Pinkerton, S. J. Hwang, C. Kim and R. C. Bowman, *J. Phys. Chem. C*, 2008, **112**, 18661-18671.
117. X. D. Kang, P. Wang, L. P. Ma and H. M. Cheng, *Applied Physics A*, 2007, **89**, 963-966.
118. J. Xu, X. B. Yu, Z. Q. Zou, Z. L. Li, Z. Wu, D. L. Akins and H. Yang, *Chem. Commun.*, 2008, 5740-5742.
119. Z. Z. Fang, X. D. Kang, P. Wang and H. M. Cheng, *J. Phys. Chem. C*, 2008, **112**, 17023-17029.
120. M. S. Wellons, P. A. Berseth and R. Zidan, *Nanotechnology*, 2009, **20**.
121. G. L. Xia, Y. H. Guo, Z. Wu and X. B. Yu, *J. Alloys Compd.*, 2009, **479**, 545-548.

122. L. Zaluski, A. Zaluska and J. O. Ström-Olsen, *J. Alloys Compd.*, 1997, **253-254**, 70-79.
123. R. Kirchheim, T. Mütschele, W. Kieninger, H. Gleiter, R. Birringer and T. D. Koblé, *Materials Science and Engineering*, 1988, **99**, 457-462.
124. A. Zaluska, L. Zaluski and J. O. Ström-Olsen, *Applied Physics A: Materials Science and Processing*, 2001, **72**, 157-165.
125. R. W. P. Wagemans, J. H. Van Lenthe, P. E. de Jongh, A. J. Van Dillen and K. P. de Jong, *J. Am. Chem. Soc.*, 2005, **127**, 16675-16680.
126. C. P. Balde, B. P. C. Hereijgers, J. H. Bitter and K. P. de Jong, *Angewandte Chemie - International Edition*, 2006, **45**, 3501-3503.
127. M. Fichtner, *Nanotechnology*, 2009, **20**, 4.
128. C. P. Baldé, B. P. C. Hereijgers, J. H. Bitter and K. P. de Jong, *Angew. Chem., Int. Ed.*, 2006, **45**, 3501-3503.
129. C. P. Baldé, B. P. C. Hereijgers, J. H. Bitter and K. P. De Jong, *J. Am. Chem. Soc.*, 2008, **130**, 6761-6765.
130. A. Gutowska, L. Y. Li, Y. S. Shin, C. M. M. Wang, X. H. S. Li, J. C. Linehan, R. S. Smith, B. D. Kay, B. Schmid, W. Shaw, M. Gutowski and T. Autrey, *Angew. Chem., Int. Ed.*, 2005, **44**, 3578-3582.
131. P. E. de Jongh and P. Adelhelm, *Chemsuschem*, 2010, **3**, 1332-1348.
132. T. K. Nielsen, F. Besenbacher and T. R. Jensen, *Nanoscale*, 2011, **3**, 2086-2098.
133. J. J. Vajo, *CURR OPIN SOLID ST M*, 2011, **15**, 52-61.
134. A. Feaver, S. Sepehri, P. Shamberger, A. Stowe, T. Autrey and G. Cao, *J. Phys. Chem. B*, 2007, **111**, 7469-7472.
135. N. Brun, R. Janot, C. Sanchez, H. Deleuze, C. Gervais, M. Morcrette and R. Backov, *Energy Environ. Sci*, 2010, **3**, 824-830.
136. S. Cahen, J. B. Eymery, R. Janot and J. M. Tarascon, *J. Power Sources*, 2009, **189**, 902-908.
137. Z. Z. Fang, P. Wang, T. E. Rufford, X. D. Kang, G. Q. Lu and H. M. Cheng, *Acta Mater.*, 2008, **56**, 6257-6263.
138. P. Ngene, P. Adelhelm, A. M. Beale, K. P. de Jong and P. E. de Jongh, *J. Phys. Chem. C*, 2010, **114**, 6163-6168.

139. W. Sun, S. Li, J. Mao, Z. Guo, H. Liu, S. Dou and X. Yu, *Dalton Trans.*, 2011, **40**, 5673-5676.
140. J. Gao, P. Adelhelm, M. H. W. Verkuijlen, C. Rongeat, M. Herrich, P. J. M. Van Bentum, O. Gutfleisch, A. P. M. Kentgens, K. P. de Jong and P. E. de Jongh, *J. Phys. Chem. C*, 2010, **114**, 4675-4682.
141. W. Lohstroh, A. Roth, H. Hahn and M. Fichtner, *ChemPhysChem*, 2010, **11**, 789-792.
142. P. E. de Jongh, R. W. P. Wagemans, T. M. Eggenhuisen, B. S. Dauvillier, P. B. Radstake, J. D. Meeldijk, J. W. Geus and K. P. de Jong, *Chem. Mater.*, 2007, **19**, 6052-6057.
143. V. Berube, G. Chen and M. S. Dresselhaus, *Int. J. Hydrogen Energy*, 2008, **33**, 4122-4131.
144. T. Mueller and G. Ceder, *ACS Nano*, 2010, **4**, 5647-5656.
145. E. H. Majzoub, F. Zhou and V. Ozoliņš, *J. Phys. Chem. C*, **115**, 2636-2643.
146. P. Adelhelm, J. B. Gao, M. H. W. Verkuijlen, C. Rongeat, M. Herrich, P. J. M. van Bentum, O. Gutfleisch, A. P. M. Kentgens, K. P. de Jong and P. E. de Jongh, *Chem. Mater.*, 2010, **22**, 2233-2238.
147. X. Liu, D. Peaslee, C. Z. Jost, T. F. Baumann and E. H. Majzoub, *Chem. Mater.*, 2011, **23**, 1331-1336.
148. J. J. Liang, *Appl. Phys. A: Mater. Sci. Process.*, 2005, **80**, 173-178.
149. S. Sepehri, A. Feaver, W. J. Shaw, C. J. Howard, Q. Zhang, T. Autrey and Cao, *J. Phys. Chem. B*, 2007, **111**, 14285-14289.
150. Y. Zhang, W.-S. Zhang, A.-Q. Wang, S. Li-Xian, M.-Q. Fan, H.-L. Chu, J.-C. Sun and T. Zhang, *Int. J. Hydrogen Energy*, 2007, **32**, 3976-3980.

Chapter 2

$LiBH_4$ in Ordered Mesoporous Silica: Synthesis and Hydrogen Sorption Properties

Abstract

Lithium borohydride ($LiBH_4$) is a promising material for hydrogen storage, with a gravimetric hydrogen content of 18.5%. However, the thermodynamics and kinetics of its hydrogen release and uptake need to be improved before it can meet the requirements for mobile applications. In this study, we investigate the nanoconfinement of $LiBH_4$ in ordered mesoporous SiO_2 and its effect on the hydrogen sorption properties. We demonstrate that melt infiltration is an effective method for the synthesis of $LiBH_4$/SBA-15 nanocomposites only if performed under hydrogen pressure. Our work clearly shows that under hydrogen pressure, $LiBH_4$ can fully fill the mesopores of SBA-15 while the long-range order of the mesopores is maintained. The confined $LiBH_4$ has enhanced hydrogen desorption properties, with desorption starting at 150 °C. However, upon dehydrogenation under Ar, SiO_2 and decomposition products of $LiBH_4$ reacts to form Li_2SiO_3 and Li_4SiO_4, leading to irreversible hydrogen loss.

This chapter is based on the following manuscript: P. Ngene, P. Adelhelm, A. M. Beale, K.P. de Jong, and P. E. de Jongh, *$LiBH_4$/SBA-15 Nanocomposites Prepared by Melt Infiltration under Hydrogen Pressure: Synthesis and Hydrogen Sorption Properties.* J. Phys. Chem. C **2010,** 114, 6163–6168.

2.1 Introduction

For an efficient use of hydrogen as an energy carrier for automobile applications, its compact, safe and efficient storage is an important issue[1]. Storage in the form of a solid hydride is attractive from a safety, gravimetric and volumetric density point of view. A promising class of materials is the light weight metal hydrides due to their high hydrogen contents. For instance $LiBH_4$ has a gravimetric hydrogen content of 18.5%. However the compound is thermodynamically very stable, releasing H_2 only at elevated temperatures (equilibrium typically 370 °C under 1 bar H_2). Moreover, it suffers from poor hydrogen uptake kinetics with limited rehydrogenation shown at 150 bar and 600 °C[2].

Approaches such as reactant destabilization and product stabilization have been proposed to improve the thermodynamic of hydrogen sorption in $LiBH_4$[3-11]. These approaches are based on mixing $LiBH_4$ with other elements or compound which can either weaken the strong ionic bond between the Li and BH_4 or result in the formation of more stable dehydrogenation products, and thereby decrease the enthalpy change for dehydrogenation. For example, Vajo *et al.* [3, 4] obtained enhanced hydrogen sorption properties when MgH_2 was added to $LiBH_4$. Formation of MgB_2, LiH and H_2 (instead of LiH, B and H_2) upon dehydrogenation reduced the enthalpy change for dehydrogenation/rehydrogenation by 25 kJ/(mol of H_2) compared with pure $LiBH_4$. The reversibility was also improved.

The use of suitable additives (catalysts) has been shown to be beneficial to the hydrogen release kinetics of metal hydrides such as $NaAlH_4$ [11-13] and MgH_2 [14, 15]. This approach has been extended to $LiBH_4$[3,6-8, 16] but no suitable catalyst or additive has been found yet for the hydrogen release and uptake from $LiBH_4$. Therefore despite these efforts, hydrogen release and uptake in $LiBH_4$ still occur only at temperatures and pressures that are too high for practical applications.

Nanosizing/nanoconfinement of metal hydrides in porous scaffolds is another approach which is promising in terms of altering the kinetics and potentially also thermodynamics of hydrogen storage materials[17-24]. Baldé *et al.*[21, 22] showed that the hydrogen desorption from $NaAlH_4$ was greatly enhanced upon nanosizing using a carbon nanofiber support. Recent work by Vajo *et al.*[23] demonstrates that $LiBH_4$ incorporated into a carbon scaffold shows faster hydrogen release kinetic,

improved reversibility and stability upon cycling than bulk $LiBH_4$. Although the effects were not well understood, they are believed to be related to physical confinement, support effects, shorter diffusion distances and particle size effects which come into play at the nanoscale.

In this study we investigate the possibility to confine $LiBH_4$ in ordered mesoporous silica and the effect of such confinement and close contact/interaction between $LiBH_4$ and porous SiO_2 on the hydrogen sorption properties of the compound. The feasibility of melt infiltration as a preparation route for nanocomposites has been shown previously for the Mg/C[25] and $LiBH_4$/C under Ar pressure.[23] In this work, we prove that this synthesis procedure is also effective for $LiBH_4/SiO_2$ but only if the melt-infiltration is performed under hydrogen pressure high enough to prevent the decomposition of $LiBH_4$ during melting. The interest of using ordered mesoporous silica in this study is the possibility to vary its structural properties such as pore size, specific pore volume and surface area and hence study the effects of these properties on the hydrogen desorption properties of the composite material. Furthermore, the integrity of the pore order of SBA-15 provides an extra tool to monitor possible reactions with the $LiBH_4$.

2.2 Experimental

SBA-15 (amorphous SiO_2 with hexagonally ordered, uniform mesopores for which the diameter can be varied from 5 to 9 nm) was prepared following the procedure of Zhao et al.[28] while $LiBH_4$ (95% pure) was purchased from Acros-organics and used without further purification. Sample handling and storage was conducted under N_2 atmosphere in a glove-box (contamination typically 1 ppm of O_2 and H_2O respectively). The required amounts of dried SBA-15 and $LiBH_4$ were mixed in a graphite sample holder and placed into a stainless steel autoclave. An initial pressure of 100 bar H_2 was applied and the sample was heated at 3 °C/min to 295 °C ($LiBH_4$ melting point = 268 °C) and allowed to stay for 25 min at 295 °C at a final pressure of 180 bar H_2. The sample was then allowed to cool down to room temperature, the hydrogen gas was released and the samples were stored in the glove box. Nanocomposites with $LiBH_4$ of 10, 25, 50 and 65 nominal weight percentage loading were prepared and the samples labeled according to the weight percentage $LiBH_4$ in the mixture (% mass of $LiBH_4$/total mass of the mixture).

Physical mixtures were prepared by mixing $LiBH_4$ with dried SBA-15 in a mortar using a pestle.

Structural characterization was done using N_2-physisorption and X-ray diffraction measurements in air tight sample holders. N_2-physisorption measurements were performed at -196 °C, using a Micromeritics Tristar 3000 apparatus. Prior to analysis, the samples were dried under vacuum for 14 hours at 120 °C. The pore size distributions of the samples were calculated from the desorption branch using BJH theory with the Harkins and Jura thickness equation. XRD patterns were obtained at room temperature from 0.5 to 90° 2θ with a Bruker-AXS D-8 Advance X-ray diffractometer setup using $Co_{K\alpha 1,2}$ radiation with λ = 1.79026Å. The crystalline phases were quantified and the amount of amorphous material estimated using a crystalline Si reference powder (nr 640 supplied by NIST formerly known as NBS (USA), purity 99.9%, average particle size 10 μm). Quantitative phase analysis was performed by Rietveld profile fitting using the Powdercell program.

Hydrogen release properties were measured by temperature programmed desorption (TPD) using a Micromeritics AutoChem II 2920 apparatus. 30 to 100 mg of sample was heated at 5 °C/min from room temperature to 500 °C in 25 ml/min Ar flow. Cycling under H_2 pressure was performed in a magnetic suspension balance from Rubotherm. 50-100 mg of the sample was loaded in a graphite sample holder and inserted into the stainless steel sample holder. The sample was heated under 1.3 bar H_2 pressure (99.999 % purity) to 450 °C. Rehydrogenation was performed at 450 °C by increasing the pressure from 1.3 bar to 100 bar in 1 hr and remaining at 450 °C for 2 hrs. Hydrogen uptake and release were determined from the weight changes while correcting for buoyancy. Hydrogenation of desorbed samples was also performed in an autoclave under 100 bar H_2 at 300 °C for 3 h after which the samples were analyzed with XRD and TPD.

Results

2.3 Synthesis of $LiBH_4$/SBA-15 nanocomposites

Figure 2.1 shows the XRD patterns of SBA-15 and melt infiltrated $LiBH_4$/SBA-15 nanocomposites with different $LiBH_4$ weight loadings. SBA-15 shows a broad peak between 20-40° 2θ due to the scattering of amorphous silica. A Comparison

of the 50 wt% samples prepared under hydrogen (figure 2.1 d) and argon pressure (figure 2.1 f) shows that in both cases a large part of $LiBH_4$ crystallinity is lost. However for the sample prepared under argon pressure the broad peak due to silica has completely disappeared while the silica broad peak is retained in the samples synthesized under hydrogen pressure. Furthermore, only diffraction lines due to $LiBH_4$ were observed, indicating that there is no formation of new crystalline phases. At weight loadings of $LiBH_4$ less than 25 wt %, no $LiBH_4$ diffraction lines were visible. This is in contrast with physical mixtures (not shown here) for which $LiBH_4$ diffraction lines were clearly seen even at 5 wt% loading. It suggests that for the lower loadings the $LiBH_4$ is confined in the pores, hence not X-ray visible. For loadings of 25 wt% and above crystalline $LiBH_4$ (probably located outside the pores) is detected.

For pure SBA-15, the order of the mesopores leads to diffraction lines at low angles as illustrated in Figure 2.2. The major peak at about 1.1° and two additional ones at higher angles due to the (100), (110) and (200) diffractions indicate well ordered SBA-15 with a hexagonal unit cell parameter of 10.8 nm. Small angle XRD patterns of the nanocomposite samples heated to 295 °C under Ar pressure gave no diffraction lines indicating that the long range order of the SBA-15 had

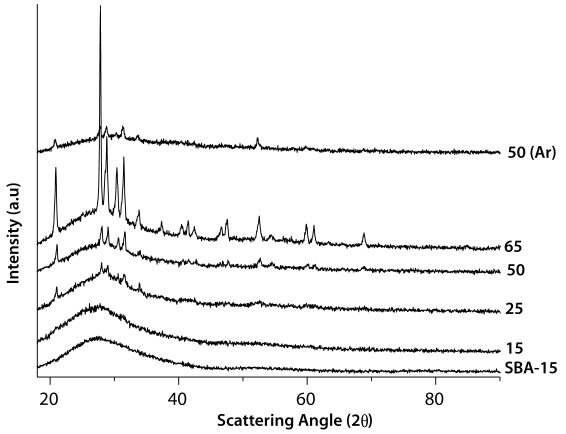

Figure 2.1: XRD patterns pure SBA-15, $LiBH_4$/SBA-15 nanocomposites containing different weight fractions of $LiBH_4$ (as indicated) melt infiltrated under H_2 pressure, and 50 wt% $LiBH_4$/SBA-15 synthesized under 50 bar Ar.

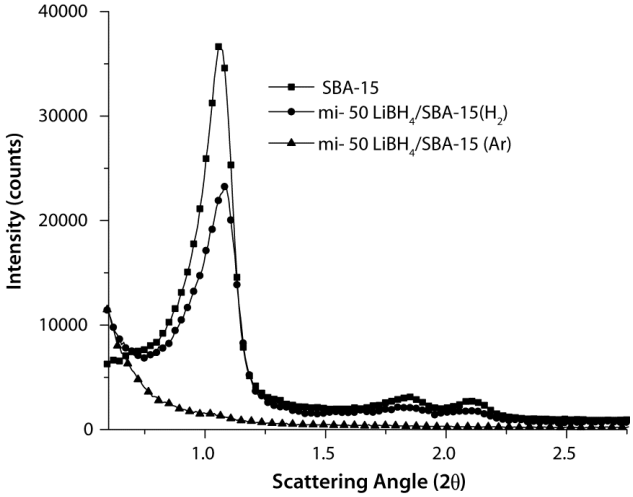

Figure 2.2: Small angle XRD of pure SBA-15 and melt infiltrated $LiBH_4$/SBA-15 composites prepared under 50 bar Ar and 50 bar H_2.

been destroyed during heating under Ar. It was demonstrated earlier that $LiBH_4$ can be melt infiltrated into carbon aerogel under Ar pressure[23]. The results from XRD and SAXS clearly indicate that this is not true for $LiBH_4$/SBA-15 composites as the SiO_2 ordered pore structure is destroyed. However, well-resolved diffraction lines are present in the composites prepared under 180 bar hydrogen. The decrease in the intensity of the diffraction lines is expected due to change in the electron density differences between an empty pore and a filled pore. Clearly, the SBA-15 porous structure has been well retained after melt-infiltrating with $LiBH_4$ under hydrogen atmosphere. Also at lower hydrogen pressures (50 bar) the structure of the SBA-15 scaffold was maintained.Nitrogen adsorption/desorption isotherms (normalized to 1g SBA-15) and the corresponding structural parameters of the pristine SBA-15, a physical mixture and $LiBH_4$/SBA-15 composites prepared under hydrogen pressure are presented in figure 2.3 and table 2.1 respectively. The isotherms of the pristine material (Fig. 2.3a) show a steep capillary condensation step and a hysteresis loop at a high relative pressure (above 0.6), typical of well ordered mesoporous SBA-15. After the melt infiltration, the BET surface area and the pore volume of SBA-15 had decreased. However, this is not the case with the physically mixed sample (figure 2.3b). Therefore the decrease in pore volume after melt infiltration indicates that the SBA-15 pores have been destroyed, blocked or

filled due to interaction with the molten $LiBH_4$. XRD and SAXS proved that the SBA-15 was not damaged upon heating.

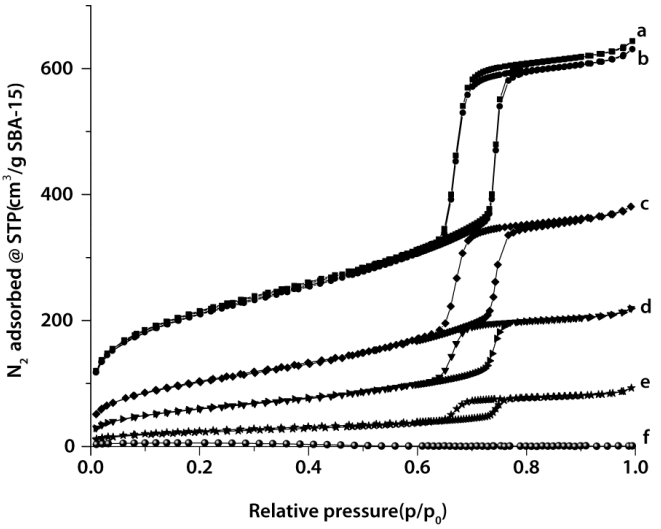

Figure 2.3: Nitrogen physisorption isotherms for (a) pure SBA-15, (b) physical mixture-50wt%, and (c) 10 wt%, (d) 25 wt%, (e) 50 wt% and (f) 65 wt% melt infiltrated $LiBH_4$/SBA-15 nanocomposites.

Table 2.1: N_2-physisorption data for pure SBA-15 and melt infiltrated $LiBH_4$/SBA-15 nanocomposites. (Data are normalized to the weight of the SBA-15)

Sample	V_{tot} (cm^3/g)	V_{meso} (cm^3/g)	A_{BET} (m^2/g)	V_{loss} (%)	Calculated V_{loss} (%)
SBA-15	1.10	0.98	760	-	-
pm-50wt%	1.10	0.98	760	-	-
mi-10wt%	0.73	0.47	381	34	24
mi-25wt%	0.42	0.24	221	62	58
mi-50wt%	0.10	0.10	46	98	100
mi-65wt%	-	-	-	-	>100

V_{tot}: total pore volume, V_{meso}: mesopore volume, A_{BET}: BET surface area, V_{loss}: measured pore volume loss, Calculated V_{loss}: Calculated pore volume loss assuming complete melt infiltration, pm: physical mixture, mi: melt infiltrated

Furthermore, table 2.1 shows that the decrease in pore volume with increasing loading of $LiBH_4$ corresponds roughly to the expected volume of the added $LiBH_4$. Hence the pore volume loss can be ascribed to filling and possibly some blocking of the pores. Most likely the capillary suction force enables the transport of the molten $LiBH_4$ into the pores of SBA-15, and on cooling the molten $LiBH_4$ re-solidifies. As no diffraction pattern was observed at low $LiBH_4$ loadings, the $LiBH_4$ in the pores shows no long-range crystallinity. The $LiBH_4$ diffraction lines observed at higher loading are most likely due to unconfined $LiBH_4$. Above 50 wt% (corresponding to > 100% pore filling) the pore volume is negligible, indicating that all the pores are filled. We can thus conclude that melt infiltration is an effective preparation technique for $LiBH_4$/SBA-15 if and only if performed under hydrogen pressure.

2.4 Hydrogen desorption properties

Figure 2.4 compares the TPD profiles of pure $LiBH_4$ and melt infiltrated nanocomposites with 10, 50 and 65 wt% loadings of $LiBH_4$. During the TPD runs, heat effects were observed (data not shown here) which can be ascribed to respectively the transition from the orthorhombic to the hexagonal phase of $LiBH_4$ (around 100 ^oC), and the melting transition (around 270 ^oC), hence at temperatures slightly lower than those reported for bulk $LiBH_4$. The onset of dehydrogenation for bulk $LiBH_4$ is around 280 °C, close to its melting point and shows multiple desorption peaks as also reported in literature. The majority of the hydrogen is only released well above 400 °C. For the melt infiltrated samples, H_2 desorption started at about 150 °C, which is more than 100 °C reduction of the onset temperature compared to the bulk material. The 10 and 50 wt% $LiBH_4$/SBA-15 nanocomposites display a single broad desorption peak with a maximum between 280-300 °C, and a shoulder at 300-350 ^oC. The 65 wt% sample has in addition a hydrogen release peak around 380 ^oC. Above 50 wt%, all the SBA-15 pores are filled and some bulk $LiBH_4$ is expected to be outside the pores. Indeed for the extra peak in the hydrogen desorption from the 65 wt% nanocomposites the release temperature is similar to that of the first and second minor release peaks for bulk $LiBH_4$. However, remarkably no second bulk-like release peak is observed in the

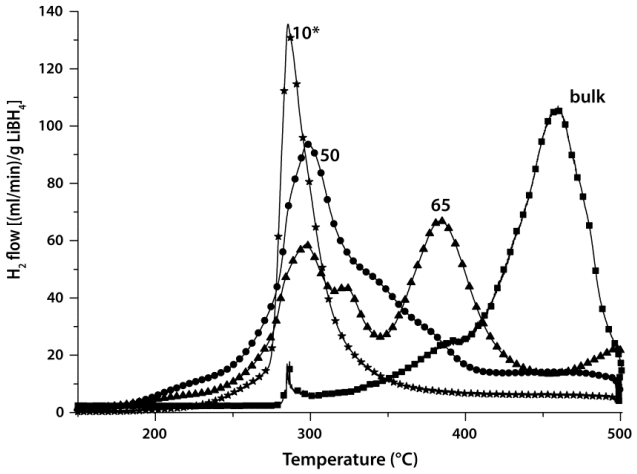

Figure 2.4. TPD profiles (while heating with 5 °C/min in Ar flow) of bulk $LiBH_4$ and melt infiltrated $LiBH_4$/SBA-15 nanocomposites with different loadings of $LiBH_4$ (as indicated). * the 10 wt% ample has twice the H_2 flow shown in the graph.

temperature range of 450-500 ^oC. This indicates that although for the 65 wt% nanocomposite sample part of the $LiBH_4$ is outside the pores, the release of hydrogen is still influenced by the presence of the SiO_2, modifying the multiple step release normally observed for pure $LiBH_4$.

Clearly, confining $LiBH_4$ in the pores of SBA-15 leads to lower hydrogen desorption temperatures. This can have several reasons. Firstly, it might be that reducing the size of the $LiBH_4$ to nanoscale alters its dehydrogenation properties as demonstrated for $LiBH_4$/C nanocomposites.[23] Secondly, it might be due to catalytic effects of SiO_2 (as originally claimed by Züttel *et al*).[16] A third reason for the change in desorption could be due to reaction with SiO_2 during heating as recently reported in literature.[26, 27] To investigate for possible reaction with SiO_2, XRD patterns of the 65 wt% $LiBH_4$ nanocomposite was obtained after heating to different temperatures (Figure 2.5). Prior to heating diffraction lines due to $LiBH_4$ and a broad peak due to amorphous silica were seen (figure 2.5 a). After thermal desorption at 300 °C (after the first desorption peak), Li_2SiO_3 and $LiBH_4$ diffraction lines were observed while the diffraction lines due to SiO_2 had disappeared. Quantitative phase analysis suggests that the majority of the SiO_2 had reacted with $LiBH_4$ to form Li_2SiO_3, while also a part of the remaining $LiBH_4$ had

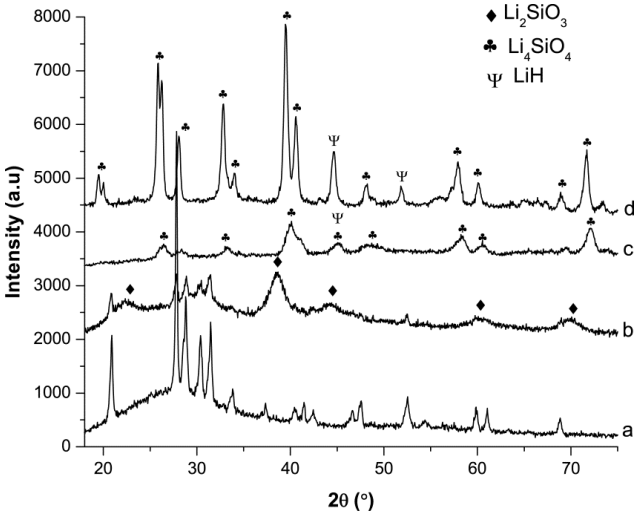

Figure 2.5: XRD patterns of the nanocomposites at different desorption stages showing the formation of lithium silicates (a) $LiBH_4$/SBA-15 nanocomposite after synthesis (b) after TPD at 300 °C, (c) after TPD at 500 °C, (d) after hydrogenation at 450 °C and 100 bar H_2 for 2h.

decomposed. After heating to 500 °C (Fig. 2.5d), the Li_2SiO_3 and $LiBH_4$ diffraction lines had disappeared, while Li_4SiO_4 and LiH diffraction lines were observed. Quantitative analysis showed that the majority of the $LiBH_4$ that was still present in the sample had reacted with the Li_2SiO_3 to form crystalline Li_4SiO_4. These observations indicate that a major part of the gas desorption at lower temperatures is due to reaction of $LiBH_4$ with SiO_2 and later with Li_2SiO_3.

Another possibility to distinguish whether gas release is either due to reaction forming silicates or due to reversible decomposition of $LiBH_4$ is by studying the rehydrogenation and further cycling. Reactions to form silicates would exclude reversibility of the reaction. We tried to rehydrogenate the nanocomposites at 450 °C and 100 bar H_2 for 2 h. At lower weight loadings (≤ 45 wt% $LiBH_4$), no hydrogen uptake was observed. These findings suggest that for samples with a low loading the hydrogen release at low temperatures during the first cycle can indeed be predominantly ascribed to reaction with SiO_2. However, we could partially rehydrogenate our nanocomposites at 450 °C and 100 bar (figure 2.6) and cycle it several times, if the $LiBH_4$ loading was 45 wt% or above. Visual inspection reveals that the composites changes from a white to black powder after thermal desorption, whereas after hydrogenation it turned brown. However, the XRD data (Fig. 2.5d)

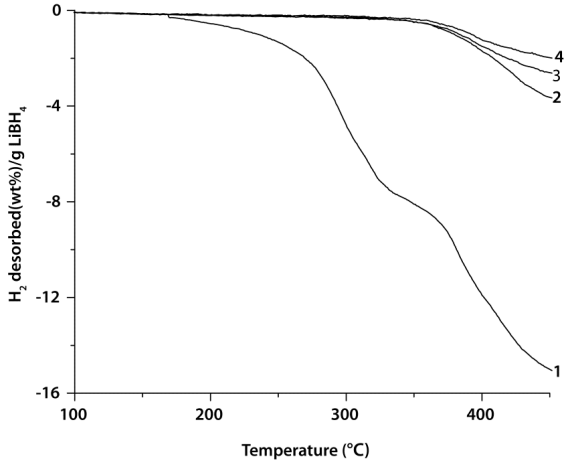

Figure 2.6: Cycling measurements in magnetic suspension balance for 65 wt% $LiBH_4$/SBA-15 composite. Desorption at 3 °C/min, 1.3 bar H_2 and 30 ml/min H_2 flow. Rehydrogenation was done at 450 °C by increasing the H_2 pressure from 1.3 to 100 bar in 1 h with a dwell time of 2 h at 450 °C.

did not indicate the formation of crystalline $LiBH_4$ after hydrogenation. This suggests that the $LiBH_4$ might be in an amorphous state after rehydrogenation or the formation of another intermediate hydride has occurred. Similar cycling performance was obtained by charging the dehydrogenated sample in an autoclave at 170 bar and 300 °C for 3 h, indicating that rehydrogenation is possible under relatively mild conditions. However, the recyclable capacity is highly reduced after the first cycle while the desorption temperature increased to about 370 °C. Furthermore, the capacity decreases with increasing cycling possibly due to boron loss [6, 8].

To study the effects of the structural properties of SBA-15 on the desorption properties of the nanocomposites in more detail, experiments using SBA-15 with different pore sizes and volumes were performed for nanocomposites with 50 wt% $LiBH_4$ loading. Figure 2.7 shows that the structural properties of the porous silica have two remarkable effects on the hydrogen release properties of the nanocomposites. Firstly the hydrogen desorption profile is changed, with lower hydrogen release temperatures favored by high surface areas/pore volumes for the same given $LiBH_4$ wt% loading. Secondly the onset of hydrogen desorption shows a clear contribution at temperatures far below the bulk $LiBH_4$ melting temperature,

especially for the SiO_2 with the highest surface area and pore volume. These effects will be discussed in more detail in the following section.

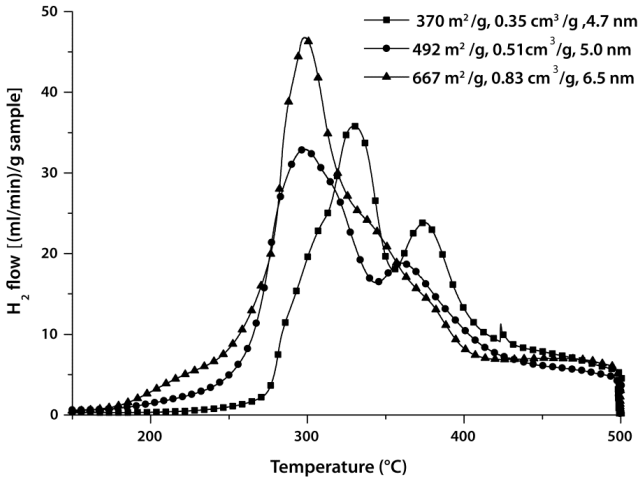

Figure 2.7: TPD profiles of 50wt% $LiBH_4$ confined in SBA-15 of different BET specific surface areas and pore volumes. Both the onset of hydrogen release and desorption profile are affected by the surface area and pore volume of the SBA-15

2.5 Discussion

Originally it was proposed in the papers by Züttel *et al.* that SiO_2 acted as catalyst for the hydrogen release from $LiBH_4$.[16] Hydrogen dissociation and recombination catalysts are typically d-electron metals such as Ni or Co. However, for hydrogen storage materials, especially those prepared by ball milling, several non-classical (de)hydrogenation catalysts seem very effective [29], although the mechanism or exact action of the catalyst is often not clear yet. Nevertheless in these cases the dehydrogenation reaction is reversible, and high rates require only a small amount of additives. In the case of $LiBH_4$ and SiO_2 thermodynamics calculations show that the combination is not stable, not even at room temperature, as silicates and boron are the most stable species as shown in figure 2.8. This does not exclude that for kinetic reasons the reversible release of hydrogen from $LiBH_4$ might be possible even in the presence of SiO_2. For the $LiBH_4$/SBA-15 nanocomposites, hydrogen is released at low temperatures. It is difficult to determine from simple desorption experiments whether this is due to catalysis, nano effects or reaction since

comparable amounts of hydrogen can be evolved in the reaction with SiO_2 as well as in the dissociation of $LiBH_4$ (reaction (2.1) versus (2.2))

$$6LiBH_4 + 3SiO_2 \rightarrow 2Li_2SiO_3 + Si + 4B + 2LiBH_4 + 8H_2 \quad (2.1)$$
$$\rightarrow \tfrac{3}{2} Li_4SiO_4 + \tfrac{1}{2} Si + 2B + 4H_2$$

$$6LiBH_4 \rightarrow 6LiH + 6B + 9H_2 \rightarrow 6Li + 6B + 3H_2 \quad (2.2)$$

Since the first papers, several authors have discussed that $LiBH_4$ might actually react with the SiO_2 upon heating, forming silicates. Evidence for the formation of silicates was demonstrated by means of XRD and in situ synchrotron radiation powder X-ray diffraction.[26, 27] Also experiments in which TiO_2 was added to $LiBH_4$ show that lithium titanate was formed after heating the sample.[30] Hence, at the moment, it is generally assumed that reaction between $LiBH_4$ and SiO_2 is kinetically hindered at room temperature, but upon heating takes place, especially when the $LiBH_4$ starts melting leading to irreversible reaction to lithium silicates.[26]

In this paper, we use the XRD signature of the pore order in mesoporous SBA-15 as a clear fingerprint whether reaction involving SiO_2 has taken place or not. This means that it is possible to detect the reaction, even if no crystalline silicates are

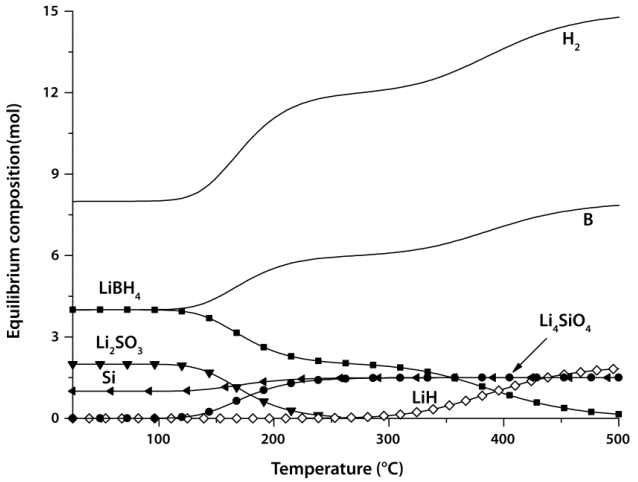

Figure 2.8: Thermodynamic equilibrium compositions for reactions between $LiBH_4$-SiO_2 at 1 bar H_2. Calculations were done using HSC CHEMISTRY version 4.1. The tabulated enthalpy of formation for $LiBH_4$ was 190.464 kJ/mol and the corresponding entropy = 75.818 J/(mol K). The input was 50 wt% $LiBH_4$ and 50 wt% SiO_2 (≈8 kmol of $LiBH_4$, and 3 kmol SiO_2)

formed. The results presented in this paper show that indeed melt infiltration of SBA-15 (a high surface area and amorphous hence reactive form of SiO_2) under Ar is not possible. The SBA-15 structure was destroyed after heating to 295 °C in the presence of $LiBH_4$. This would be in line with the assumption that as soon as the kinetic barriers have been overcome (because the $LiBH_4$ starts melting) fast reaction is possible. However, if we use hydrogen pressures well above the calculated equilibrium pressure at 300 °C (using data from ref. [2]), the reaction with the SiO_2 was effectively suppressed. Hence the presence of molten $LiBH_4$ alone is not enough for reaction with the SiO_2. Apparently molten $LiBH_4$ does not react directly with SiO_2, but most likely its decomposition products. In literature, intermediate phases are suggested that can be formed during thermal dehydrogenation of $LiBH_4$. [16, 31-36] Most likely one of these intermediate products might be the reactive species. Under hydrogen pressure, the decomposition is hindered and thus melt infiltration can be performed even above 300 °C without any silicate formation.

Unfortunately, upon decomposition of the $LiBH_4$ in the nanocomposites, reaction takes place with the SiO_2. The multiple hydrogen desorption peaks observed at higher $LiBH_4$ loadings (figure 2.4) can be ascribed to reactions first to form Li_2SiO_3 around 300 °C and subsequent reaction with the Li_2SiO_3 to form Li_4SiO_4.[8,26-27] As this leads to very stable lithium silicates, this reaction is irreversible. The partial reversibility observed in the composite with 65 wt% $LiBH_4$ loading is probably due to partial rehydrogenation of $LiBH_4$ in excess of the stoichiometric amount required for complete reaction with SiO_2. The further decrease in capacity on cycling might be due to boron loss as reported in literature.[6, 8-37] For the 65 wt%, it is expected that the $LiBH_4$ in excess of the stoichiometric amount required to completely react with SiO_2 will exhibit bulk dehydrogenation behavior. However the desorption profile (figure 2.4) shows a clear departure from bulk behavior, with only one clearly defined hydrogen release peak instead of the multiple peak desorption profile observed for bulk $LiBH_4$. To test whether this was due to interaction with the lithium silicates in the sample, we made a physical mixture of $LiBH_4$ and Li_4SiO_4. In this case a similar desorption profile was obtained, showing that departure from bulk behavior is due to the interaction of the $LiBH_4$ with Li_4SiO_4.

Figure 2.7 shows the effects for a given molar ratio ($LiBH_4$:SiO_2=8:3) which roughly corresponds to the stoichiometry needed to fully form Li_4SiO_4. However, SiO_2 with different pore sizes is used, which enabled us to distinguish between the impact of nanoconfinement in the pores (which will be more pronounced for the smaller pore sizes), and the kinetics of the reaction to form lithium silicates (which will be more pronounced for the higher pore volumes/surface areas, hence the samples with the largest pores). As seen in figure 2. 6, both the onset of dehydrogenation and the TPD profile for the 50 wt% sample change as the structural properties of the SBA-15 are changed. Interestingly, for the 50 wt% nanocomposite with the highest specific surface area and pore volume of SBA-15, the two steps in reaction 1 occurs almost simultaneously. This is probably due to the fact that all the $LiBH_4$ is confined in the pores of SBA-15 and more intimate contact and shorter diffusion distance increase the rate of the reaction. For the nanocomposites with lower pore volumes a large part of the $LiBH_4$ is outside the porous SiO_2, hence leading to slower reaction due to diffusion limitations. The reaction to form lithium silicates might be prevented by using a less reactive matrix such as carbon. Another possibility is to passivate the SBA-15 for instance by silanation as shown effectively in the case of impregnation with sodium alanates.[38]

2.6 Conclusions

Melt infiltration as a preparation method for $LiBH_4$/SBA-15 nanocomposites has been investigated and the hydrogen sorption properties of the nanocomposites determined. It was shown that melt infiltration is effective only if performed under hydrogen pressure to avoid the decomposition of $LiBH_4$. Surprisingly, molten $LiBH_4$ can fill the pores of SBA-15, forming $LiBH_4$/SBA-15 nanocomposites while the ordered porous structure of SBA-15 remains intact. Only upon decomposition of the nanostructured $LiBH_4$ reaction with the SiO_2 takes place, leading to irreversible hydrogen loss. Monitoring the pore order in SBA-15 is a simple and sensitive probe to follow the reaction between the $LiBH_4$ and SiO_2, even if no crystalline products are formed. Varying the structural properties of the ordered mesoporous SiO_2 allowed further understanding of the reaction, and the different products formed.

Acknowledgement

We acknowledge A. van der Eerden, A. Mens, V. Koot, and M. Versluijs-Helder for their technical support, and NWO-Vidi 016.072.316 for financial support.

References

[1] Schlapbach, L.; Züttel, A. *Nature* 2001, **414**, 353.

[2] Mauron, ph.; Buchter, F.; Friedrichs, O.; Remhof, A.; Bielmann, M.; Zwicky, C. N.; Züttel, A. *J. Phys. Chem. B* 2008, 112, 906

[3] Vajo, J.J.; Skeith, S.L. *J. Phys. Chem. B* 2005, 109, 3719.

[4] Vajo J.J.; Olson, G. L. *Scr. Mater.* 2007, 56, 829.

[5] Bösenberg, U.; Doppiu, S.; Mosegaard, L.; Barkhordarian, G., Eigen, N.; Borgschulte, A.; Jensen, T. R., Cerenius, Y.; Gutfleisch, O.; Klassen, T.; Dornheim, M.; Bormann, R. *Acta Mater.* 2007, 55, 3951

[6] Au, M.; Jurgensen, A. *J. Phys. Chem. B* 2006, 110, 7062.

[7] Au, M.; Jurgensen, A.; Zeigler, K. *J. Phys. Chem. B* 2006, 110, 26482.

[8] Au, M.; Jurgensen, A. R.; Spencer,A.W.; Anton, D.L.; Pinkerton, E.P.; Hwang, S. J.; Kim, C.; Bowman Jr. R, C. *J. Phys. Chem. C*, 2008, 112, 18661

[9] Aoki, M.; Miwa, K.; Noritake, T.; Kitahara, G.; Nakamori, Y.; Orimo, S.; Towata, S. *Appl. Phys. A* 2005, 80, 1409.

[10] Meisner, G. P.; Scullin, M. L.; Balogh, M. P.; Pinkerton, F. E.; Meyer, M. L. *J. Phys. Chem. B* 2006, 110, 4186.

[11] Pinkerton, F. E.; Meisner, G. P.; Meyer, M. S.; Balogh, M. P.; Kundrat, M. D. *J. Phys. Chem. B* ***2005***, 109, 6

[12] Bogdanović, B.; Schwickardi, M. *J. Alloys Compd*. 1997, 253–254, 1.

[13] Bogdanović, B.; Schwickardi, M.; Brand, R.; Marjanovic, A.; Schwickardi, M.;. Tölle, J. *J. Alloys Compd.* 2000, 302, 36.

[14] Jensen, C. M.; Gross, K. J. *Appl. Phys. A* 2001, 72, 213.

[15] Barkhordarian, G.; Klassen, T.; Bormann, R. *J. Phys. Chem. B* 2006, 110, 11020.

[16] Züttel, A.; Rentsch, S.; Fischer, P. Wenger, P.; Sudan, P.; Mauron, Ph.; Emmenegger, Ch. *J. Alloys Compd*. 2003, 356-357, **515**

[17] Zaluska, A.; Zaluski, L,; Ström-Olsen, J. O. *J. Alloys Compd.* 1997, 253-254, **70**

[18] Bérubé, V.; Radtke, G.; Dresselhaus, M.; Chen, Int. J. Energy Res. 2007, 31, 637

[19] Wagemans, R.W.P.; van Lenthe, J.H.;, de Jongh, P.E.; van Dillen, A.J.; de Jong, K.P. *J. Am. Chem. Soc.* 2005, 127, 16675

[20] Gutowska, A.; Li, L.; Shin, Y.; Wang, C. M.; Li, X. S.; Linehan, J. C.; Smith, R. S.; Kay, B. D.; Schmid, B.; Shaw, W.; Gutowski, M.; Autrey, T. *Angew. Chem. Int. Ed.* 2005, 44, 3578.

[21] Baldé, C. P.; Hereijgers, B.P.C.; Bitter, J.H.; de Jong, K.P. *Angew. Chem. Int. Ed*. 2006**,** 45, 3501.

[22] Baldé,C. P.; Hereijgers, B.P.C.; Bitter, J.H.; de Jong, K.P *J. Am. Chem. Soc.* 2008, 130, **21**, 6761.

[23] Gross, A. F.; Vajo, J. J.; Van Atta, S. L.; Olson, G. L. *J. Phys. Chem. C* 2008, 112, 5651.

[24] Cahen, S.; Eymery, J. B.; Janot, R.; Tarascon, J. M. *J. Power Sources* 2009, 189, **902**

[25] de Jongh, P. E.; Wagemans, R. W. P.; Eggenhuisen, T.M.; Dauvillier, B.S.; Radstake, P.B.; Meeldijk, D.; Geus, J.W.; de Jong, K.P *Chem. Mater*. 2007, 19, 6052.

[26] Zhang, Y.; Zhang, W.Z.; Fan, M.Q.; Liu, S.S.; Chu, H.L.; Zhang, Y.H.; Gao, X.Y.; Sun, L.X. *J. Phys. Chem. C* 2008, 112, 4005.

[27] Mosegaard, L.; Møller, B.; Jørgensen, J.; Filinchuk,Y.; Cerenius, Y.; Hanson, J. C. Dimasi, E.; Besenbacher, F.; Jensen, T.R. *J. Phys. Chem. C* 2008, 112, 1299.

[28] Zhao, D.; Feng, J., Huo, Q.; Melosh, N.; Fredrickson, G. H.; Chmelka, B. F.; Stucky, G. D. *Science* 1998, 279, 548

[29] Oelerich, W.; Klassen, T.; Bormann, R. *J Alloys Compd*. 2001, 315, 237

[30] Yu, X. B.; Grant, D.M.; Walker, G.S. *J. Phys. Chem. C* 2008, 112, 11059

[31] Her, J, H.; Yousufuddin, M.; Zhou, W.; Jalisatgi, S. S.; Kulleck, J. G.; | Zan, J. A.; Hwang, S. J.;. Bowman, R. C. J.; Udovic, T. J. *Inorg. Chem.* 2008, 47, 9757

[32] Orimo, S. I.; Nakamori, Y.; Ohba, N.; Miwa, K.; Masakazu Aoki, M.; Towata, S. I.; Züttel, A. *Appl. Phys. Lett* 2006, 89, 021920

[33 Lodziana, Z.; Vegge, T. *Phys. Rev. Lett*. 2004, 93, 145501

[34] Kang, J. K.; Kim, S. Y.; Han, Y. S.; Muller, R. P.; Goddard, W. A. *Appl. Phys.Lett.* 2005, 87, 111904

[35] Ohba, N.; Miwa, K.; Aoki, M.; Noritake, T.; Towata, S. *Phys. Rev. B* 2006, 74, 075110
[36] Mosegaard, L.; Møller, B.; Jørgensen, J. E.; Bösenberg, U.; Dornheim, M.; Hanson, J. C.; Cerenius, Y.; Walker, G.; Jakobsen, H. J.; Besenbacher, F.; Jensen, T.R. *J. Alloys Comp.* 2007, 446–447, 301
[37] Kostka, L.; Lohstroh, W.; Fichtner, M.; Hahn, H. *J. Phys. Chem. C* 2007, 111, 14026
[38] Shiyou, Z.; Fang, F.; Guangyou, Z.; Guorong, C.; Liuzhang, O.; Min Z.; Dalin, S. *Chem. Mater*. 2008, 20, 3954

Chapter 3

$LiBH_4$ in Nanoporous Carbon Materials

Abstract

$LiBH_4$/carbon nanocomposites were prepared by melt infiltration, and the influence of $LiBH_4$ loading on the structure and hydrogen sorption properties studied. Melt infiltration clearly led to confinement of $LiBH_4$ in the nanopores of the carbon material: N_2 physisorption showed that the pore volume of the carbon dropped, and XRD measurements indicated that the long-range crystallinity of $LiBH_4$ vanished upon melt infiltration. The melting point of the nanoconfined $LiBH_4$ as detected by DSC measurements was 10-50 ^oC lower than the bulk melting point (280 ^oC), and the phase transition at 110 °C (orthorhombic $\leftrightarrow$ hexagonal structure) had shifted to ~90 ^oC. If less than 50% of the pores was filled (corresponding to <15 wt %) the phase transitions could not even be detected. The nanocomposite with 5 wt% $LiBH_4$ had the highest decomposition rate at 400 ^oC, ~5 times higher than that for a loading corresponding to full pore filling (35 wt%) and two orders of magnitude faster than for bulk $LiBH_4$. Though the activation energy for dehydrogenation obtained from TPD measurements was generally lower for nanocomposites (110-140 kJ/mol) than for bulk $LiBH_4$ (169 ± 5 kJ/mol), also the pre-exponential factor played an important role. Nanocomposites with nearly full pores (35 and 25 wt%) released ~14 wt% H_2/$LiBH_4$ upon heating to 400 °C, while for lower loadings ~18.5 wt% H_2 was detected, corresponding to full decomposition to B, H_2 and either LiH or Li respectively. The equilibrium decomposition (to LiH and B) temperature for bulk $LiBH_4$ at 1 bar H_2 is ~370 °C. However, decomposition of nanoconfined $LiBH_4$ started already around 255 °C under 1 bar H_2, while reloading was observed under relatively mild rehydrogenation conditions. Factors that could contribute to $LiBH_4$ decomposition at temperatures lower than bulk equilibrium might be a change in stability due to the confinement, intercalation of part of the Li formed or formation of stable intermediate phases in the decomposition.

3.1 Introduction

In chapter 2, we showed that the temperatures of hydrogen release from $LiBH_4$ were significantly lowered when the $LiBH_4$ was confined in ordered mesoporous silica. However this was at least partially related to irreversible reactions between the decomposition product(s) of $LiBH_4$ and SiO_2 to form lithium silicates with concomitant hydrogen release. To evaluate the intrinsic effect of nanoconfinement on the hydrogen sorption behaviour of $LiBH_4$ we need to avoid (or limit) such irreversible reactions. Carbon based nanoporous materials have high stability and are light weight, and hence attractive for nanoconfinement of $LiBH_4$. Recent literature suggests that at least some carbon based nanoporous materials are inert to $LiBH_4$ while others react[1-4]. Gross et al. reported reversible hydrogen uptake for $LiBH_4$ confined in nanoporous carbon aerogels by melt infiltration[1]. Similar enhancement in reversibility was demonstrated for $LiBH_4$ nanoconfined in activated carbon (AC) via impregnation with $LiBH_4$-THF solution[2]. However reversibility was not reported for $LiBH_4$/ordered mesoporous carbon nanocomposites[3, 4]. These carbon materials have low crystallinity and contain more oxygen; hence they are more likely to react with $LiBH_4$ to form B-C[4] and Li-C[5] bonds or oxides of lithium and/or boron. In addition, different hydrogen release temperatures and capacities have been reported for $LiBH_4$/C nanocomposites.[1-4, 6-8] These findings suggests that the nature of the nanoporous carbon material, its purity and physical properties influences hydrogen sorption of confined $LiBH_4$. Therefore a first aim of this study is to evaluate the possibility to melt infiltrate mesoporous turbostratic graphitic carbon material with $LiBH_4$, using calorimetry to track possible reactions.

The degree to which the nanopores are filled could significantly influence the dehydrogenation and rehydrogenation of nanoconfined $LiBH_4$ because the morphology of $LiBH_4$ and its interface with carbon could vary with the loading of $LiBH_4$ in the nanocomposite. An indication is that Christian et al [8] reported the release of all the hydrogen contained in $LiBH_4$ (18.5 wt% H_2) at 250 °C when only 1.5 wt% $LiBH_4$ was confined in carbon nanofibre while a 25-30 wt% $LiBH_4$ confined in carbon aerogel released only 12.6 wt% upon heating to temperatures above 300 °C[1]. Baldé et al varied the sizes of $NaAlH_4$ nanoporticles supported on carbon nanofibres by varying the loading of the $NaAlH_4$ and showed that this had

significant effect on the activation energy for hydrogen desorption from $NaAlH_4$[9, 10]. Therefore a second focus of the present study is to gain more understanding on how $LiBH_4$ loading influences the structure of the nanoconfined $LiBH_4$ and its hydrogen sorption.

3.2 Experimental Details

High surface area turbostratic graphite (HSAG-500,Timcal Switzerland) was used as the nanoporous carbon material for this study. It has a pore volume of 0.66 cm^3/g, BET surface area 500 m^2/g, and a broad pore size distribution dominated by 2-3 nm pores. Prior to use, the carbon was dried at 500 °C for 5 h under nitrogen flow and cooled down under nitrogen flow. $LiBH_4$ (Acros-organics 95% pure) was incorporated into the dried carbon by melt infiltration. The required amounts of carbon and $LiBH_4$ were mixed and placed in a graphite sample holder and inserted into a stainless steel autoclave. An initial pressure of 50 bar H_2 was applied and the sample was heated at 3 °C min^{-1} to 295 °C and allowed to stay for 30 min at 295 °C at a final pressure of ≈ 100 bar H_2. The sample was then allowed to cool down to room temperature, the hydrogen gas was released and the samples were stored in a glove box. All sample handling and storage was under Ar atmosphere in a glove-box (contamination typically less than 0.1 ppm of O_2 and H_2O) to avoid exposure and contamination. $LiBH_4$/C nanocomposites containing 5-35 wt% $LiBH_4$ were synthesized and labeled according to the weight percentage of $LiBH_4$ in the nanocomposites.

Structural characterization was performed using High Pressure Differential Scanning Calorimetry(DSC), X-ray diffraction (XRD), N_2- physisorption and both ^{11}B and ^{7}Li solid-state Nuclear Magnetic Resonance (NMR) spectroscopy. All measurements were done in air tight sample holders. DSC measurements were performed with an apparatus from Metler Toledo (HP DSC1). The equipment was caliberated for temperature and heat flow under 1 bar H_2 using standard Zn, In and Al. The samples were measured while ramping at 5 K/min with an initial pressure of 15 bar H_2. XRD patterns were obtained at room temperature from 18 to 75° 2θ with a Bruker-AXS D-8 Advance X-ray diffractometer setup using $CoK\alpha_{1,2}$ radiation with λ= 1.79026 Å. N_2-

physisorption measurements were performed at -196 °C, using a Micromeritics Tristar 3000 apparatus. The pore size distributions of the samples were calculated from the desorption branch using BJH theory with the Harkins and Jura thickness equation.

Solid-state NMR experiments were performed (at Radboud University, Nijmegen) on a 600 MHz Varian spectrometer using a 2.5 mm HX MAS probe. ^{11}B and ^{7}Li single pulse excitation spectra were obtained using a short hard pulse of 0.20 μs at an effective rf-field strength of 140 kHz after taking pulse rise and decay times into account. Spectra were acquired without proton decoupling. The ^{7}Li spectra were referenced with respect to an aqueous solution of LiCl (δ = 0 ppm). All NMR data processing was done using matNMR[11].

Hydrogen release from the samples was measured by temperature programmed desorption (TPD) using a caliberated Micromeritics AutoChem II 2920 apparatus. 60 to 100 mg of sample was heated at 5 °C/min from room temperature to 400-500 °C in 25 ml/min Ar (99.99 % purity) flow with a dwell time of 25 min at the maximum temperature. The amounts of hydrogen released were determined by integrating the plots of hydrogen flow (ml/min) versus time (min) using the peak editor software of the AutoChem II 2920. Rehydrogenation of desorbed samples was performed in an autoclave at 50 bar H_2 and 325 °C for 3 h after which the amount of H_2 absorbed by the sample was determined by a second TPD run. Isothermal manometric hydrogen release and uptake measurements were done using a Sievert type apparatus (PCTPro-2000, Hy-Energy & Setaram, pressure measurement accuracy: 1% of reading). For desorption, about 100 mg of the sample was placed in a stainless steel sample holder (~ 5 ml) and heated to 400 °C under 22 bar H_2 after which the hydrogen is expanded into a 166 ml reservoir that had been properly evacuated. On opening the reservoir valve, the pressure drops to approximately 0.2 bar and then increases gradually due to hydrogen release from the sample (final pressure typically < 0.55 bar). The dehydrogenated samples were evacuated for 1 h at 400 °C and cooled down to 330 °C. Subsequently, hydrogen uptake was measured by charging the dehydrogenated sample with an intial pressure of approximately 27 bar H_2 at 330 °C and the pressure drop due to hydrogen absorption by the nanocomposites recorded (final pressure typically 24 bar).

Determination of the effective sample holder volume was done at the temperature of measurement using helium. Gravimetric hydrogen measurements were performed in a magnetic suspension balance from Rubotherm. About 100 mg of the sample was loaded in a graphite cup (stainless steel for bulk $LiBH_4$) and inserted into a stainless steel sample holder. The sample was heated at 5 °C/min to 400 °C under 1.05 bar H_2 or 1 bar Ar at a flow rate of 25 ml/min. The amount of hydrogen released was determined from the weight changes after having corrected for buoyancy effects.

Results and discussion

3.3 Melt infiltration process studied by DSC

The wetting and melt infiltration process of $LiBH_4$ into nanoporous carbon material was studied in-situ using high pressure DSC. $LiBH_4$ mixed with graphite (BET surface area 7 m^2/g) was used as a reference. Figure 3.1A and B show the heat flow while the enthalpy values are tabulated in table 3.1. During heating, the bulk $LiBH_4$ and the 25 wt% $LiBH_4$-graphite shows two endothermic peaks around 107±2 °C and 275 °C which are ascribed to the phase transition from orthorhombic to hexagonal structure and melting of $LiBH_4$ respectively[12-14]. The measured enthalpy values for the structural transition and melting of bulk $LiBH_4$ are 2.45 kJ/mol and 3.76 kJ/mol respectively, and the corresponding values for $LiBH_4$ supported on graphite are 1.92 and 3.16 kJ/(mol $LiBH_4$). These values are less than those reported for $LiBH_4$ (4.18 kJ/mol and 7.56 kJ/mol) [12]. This is most likely due to heat losses during measurements via the highly conductive hydrogen gas especially at high pressures. Therefore the measured enthalpies are taken as relative values. During cooling, two exothermic heat flows were observed around 270 °C and 96 °C which are ascribed to the solidification of molten $LiBH_4$ and transition from hexagonal (high temperature) phase to the orthorhombic (low temperature) phase. The absolute values of the measured enthalpy of the exothermic process is very close to the corresponding endothermic process during heating, showing that the phase transition is reversible in these samples.

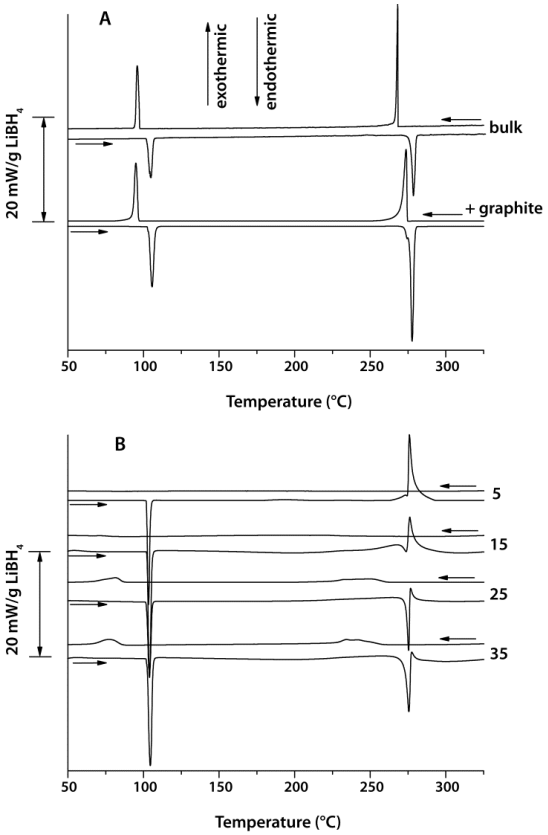

Figure 3.1: High pressure DSC measurements showing heat flow under 15 bar H_2 while heating and cooling with 5 °C/min. **A**: Bulk $LiBH_4$ and a physical mixture of 25wt% $LiBH_4$ and graphite, B: Physical mixtures of nanoporous carbon material and different loading of $LiBH_4$ (wt% indicated)

Next to the endothermic signal due to melting, an additional exothermic event was recorded around 280 °C for $LiBH_4$-nanoporous carbon mixtures (figure 3.1B). The measured enthalpy values due to the exothermic event increased with decreasing $LiBH_4$ loading and for samples with ≤ 15 wt% $LiBH_4$, the endothermic melting was overshadowed by this exothermic event. During cooling (after melt infiltration) two minor broad exothermic signals ascribed to solidification of molten $LiBH_4$ and transition from high to low temperature phase were recorded at ~ 263 °C - 220 °C and 86 - 67 °C respectively, hence lower than for the bulk and graphite supported $LiBH_4$ by about 10-50 °C. In contrast to the bulk and graphite supported $LiBH_4$, the absolute values of the measured enthalpy for these exothermic events during cooling were about 85 % lower than for the

corresponding endothermic events during heating and the exothermic signals were not even detected in samples with ≤ 15 wt% $LiBH_4$. These observations suggest that the physical properties of $LiBH_4$ such as the melting/solidification and structural transition temperatures are changed upon confinement in nanoporous carbon materials and that this change in properties is highly influenced by the loading of $LiBH_4$ in the nanocomposite.

Table 3.1: Measured enthalpy changes ΔH (normalized per gram $LiBH_4$) for bulk $LiBH_4$ and $LiBH_4$ mixed with graphite (G), porous carbon(C) and purified porous carbon(PC). $\Delta H_{S,}h$ and $\Delta H_{S,}c$ are enthalpy changes associated with structural transition to hexagonal (heating curve) and from hexagonal back to orthorhombic (cooling curve) respectively. ΔH_M, ΔH_r and ΔH_{SLD} are enthalpy change for melting (assumed constant), surface reactions/wetting and solidification respectively. Negative sign stands for exothermic while positive number implies the process is endothermic

Sample	Structural transition		Melting, reaction & solidification		
	$\Delta H_{S,}h$ (kJ/mol)	$\Delta H_{S,}c$ (kJ/mol)	ΔH_M (kJ/mol)	ΔH_r (kJ/mol)	ΔH_{SLD} (kJ/mo l)
bulk $LiBH_4$	2.45	-2.25	3.76	-	-3.76
25$LiBH_4$-G	1.92	-1.90	3.16	-0.6	-2.9
35$LiBH_4$-C	1.82	-0.53	3.76	-2.58	-0.56
25$LiBH_4$-C	1.80	-0.34	3.76	-3.64	-0.50
15$LiBH_4$-C	1.80	-	3.76	-3.72	-
5$LiBH_4$-C	1.44	-	3.76	-5.68	-
25$LiBH_4$-PC	1.71	-0.42	3.76	-0.96	-0.43
15$LiBH_4$-PC	1.71	-0.31	3.76	-1.19	-0.31
5$LiBH_4$-PC	1.78	-	3.76	-2.10	-

The exothermic signal observed in the $LiBH_4$-nanoporous carbon samples around the melting temperature of $LiBH_4$ might be due to wetting of the carbon material with molten $LiBH_4$ but could also be due to reaction with impurities in the nanoporous carbon material.[15] To investigate the possibility of the latter, the porous carbon was purified prior to mixing with $LiBH_4$ by heating to 600 °C under H_2 and dwelling for 2 h at 600 °C with a flow of 100 ml/min H_2. This process is known to remove oxygen-containing surface groups, stabilize some of the reactive sites by forming stable C-H bonds and gasify the most reactive unsaturated carbon atoms[16]. The carbon pore volume had decreased by about 0.08 cm^3/g (12 %) after the purification.

Figure 3.2A shows the DSC curves for the experiments conducted with the purified carbon material. In this case the entire exothermic signal around the melting point of $LiBH_4$ has almost disappeared. This suggests that the exothermic event associated was mostly due to reaction of molten $LiBH_4$ with terminating oxygen groups (or other impurities) in the carbon and that treatment of the carbon material with hydrogen reduced these impurities significantly. The cooling curves of the composites prepared with the purified carbon also exhibits similar features as those prepared with the non-purified carbon. The absolute enthalpy values of the exothermic heat flows corresponding to the solidification and structural transition of $LiBH_4$ are significantly lower than the corresponding events during heating and also vanished in nanocomposites with < 15 wt% $LiBH_4$.

Since both endothermic (melting) and exothermic (surface oxidation reactions, wetting) events occur simultaneously during heating, the measured DSC signal is a combination of both processes. As melting of $LiBH_4$ occurs before nanoconfinement and reactions with the impurities[17] we can assume that the melting enthalpy signal (normalized per g $LiBH_4$) is the same (ΔH_m in table 3.1) in all the samples and therefore estimate the exothermic contribution due to reaction/wetting of the carbon (ΔH_r in table 3.1) by deconvoluting the peak around the melting of $LiBH_4$. The magnitude of the exothermic event (ΔH_r in table 3.1) generally increased with decreasing $LiBH_4$ loading. It is logical that decreasing the loading will lead to increase in the exothermic contribution since the fraction of carbon (hence surface contamination per gram carbon) increases with decreasing loading of $LiBH_4$. Similarly it is expected that the enthalpy associated with wetting

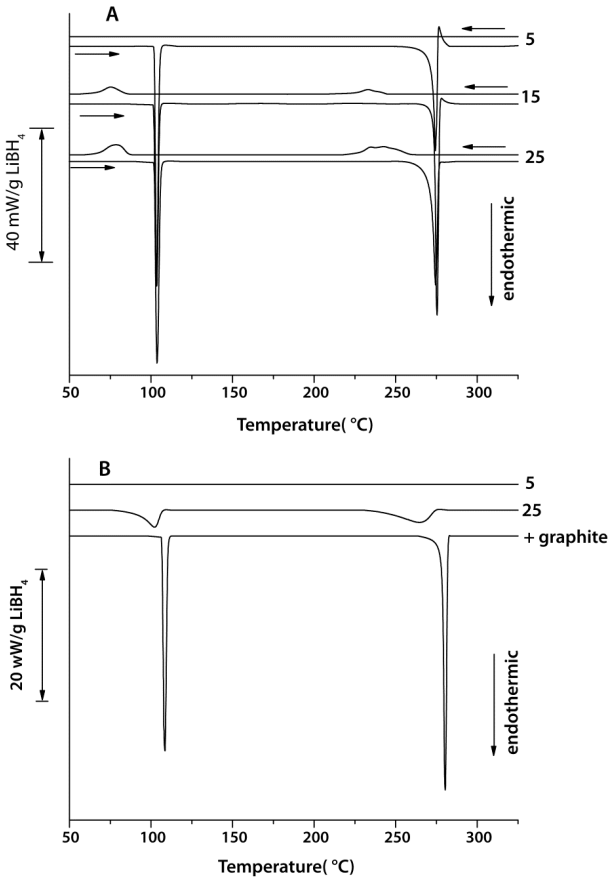

Figure 3.2: Heat flow (while heating and cooling under 15 bar H_2 and 5 °C/min) for A: Physical mixtures of purified nanoporous carbon and $LiBH_4$ with different weight loading as indicated. B: Heat flow during the second cycle DSC heating measurement (samples already heated and cooled to room temperature) on 25 wt% $LiBH_4$-graphite and 5 and 25 wt% $LiBH_4$ /PC

of the carbon surface would increase as the loading decreases due to increased carbon surface area in contact with the molten $LiBH_4$. Therefore it is non-trivial to accurately differentiate between contributions from wetting and surface reactions. The measured enthalpy values due to solidification of $LiBH_4$ (ΔH_{SLD} in table 3.1) also decreased as the loading decreases, and is not observed for $LiBH_4$ loadings less than 15 wt%.

To further investigate the observed changes in structural transition and solidification temperatures during cooling, a second cycle heating DSC measurements was done on the cooled samples (Figure 3.2B). The endothermic

heat flows corresponding to both the structural transitions and the melting of $LiBH_4$ were not detected in the 5 wt% nanocomposites while for the 25 wt%, broadened endothermic peaks due to these events were observed at temperatures (75-102 °C and 224-265 °C respectively) lower than for $LiBH_4$-graphite and in agreement with the first cooling curves. Generally, the heating curve of the nanocomposites in the second run is almost a mirror image of its first cooling curve. Further experiments reveal that the structural transitions and melting were not detected once the loading was less than 15 wt%.

From these results, it is clear that the physical and/or structural properties of $LiBH_4$ are indeed changed when confined in nanoporous carbon material and that these changes in properties are also influenced by the $LiBH_4$ loading. It has been shown that liquids or solutions confined in porous media have melting and solidification temperatures that are considerably lower than the bulk material, and decreases as the diameter of the pores is decreased[18-20]. Also the absolute values of the heat effects associated with melting/ solidification are lower for confined phases as has been shown for metal nitrate hydrates[20, 21]. Hence the observed low enthalpy values, and the depression and broadening of the melting/solidification temperatures could be explained by the presence of $LiBH_4$ in pores with different diameters due to the broad pore size distribution of the nanoporous carbon material used in this study. This explanation might be applicable to the structural transition and also explains why the enthalpy for solidification and structural change (on cooling) increased slightly with increased loading since more $LiBH_4$ is in the larger (or even outside) pores and displays more bulk- like behaviour.

3.4 Structural characterisation

After cooling to room temperature, XRD measurements were done to check the crystallinity of the nanocomposites. Figure 3.3 shows that the nanoconfined $LiBH_4$ lacks long- range crystallinity especially at low $LiBH_4$ loadings. Above 25 wt% loading, crystalline $LiBH_4$ is observed which is in line with the fact that about 30 wt% $LiBH_4$ is required to completely fill the pores, assuming the density of the $LiBH_4$ is not changed when nanoconfined.

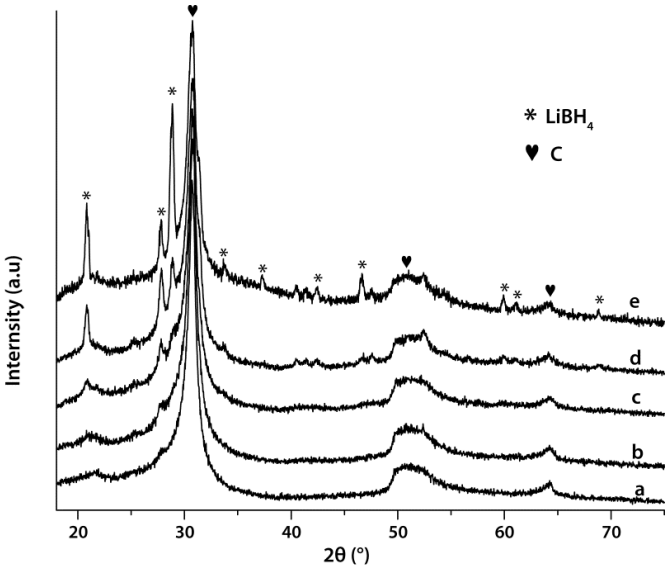

Figure 3.3: XRD patterns for (a) 5wt%, (b) 15 wt%, (c) 25wt% and (d) 35wt% $LiBH_4$/C nanocomposites (e) physical mixture of 25wt% $LiBH_4$ and carbon

To investigate the influence of $LiBH_4$ loadings on the filling of the carbon pores, nitrogen physisorption measurements were used to probe the porosity of the carbon in the synthesized $LiBH_4$/C nanocomposites. Figure 3.4 shows the differential pore volume loss by the carbon as a function of the pore sizes of the carbon. The total pore volume loss by the carbon is almost equal to the volume of $LiBH_4$ added to the mixture (table 3.2). This is explained by the fact that the $LiBH_4$ occupies the pores of the carbon as shown for $LiBH_4/SiO_2$ nanocomposites[22]. The difference between the volume of $LiBH_4$ added and pore volume loss (especially the 5 wt% $LiBH_4$/C) is probably due to partial pore blockage. Above 25 wt% $LiBH_4$, no nitrogen was adsorbed, in line with the fact that all the pores were filled above this loading. From figure 3.4 it can be seen that about 99 % of $LiBH_4$ in the 5 wt% nanocomposite were confined in pores < 10 nm. About 95 % of the $LiBH_4$ in the 15 wt% nanocomposites were confined in pores ≤ 10 nm while the rest are in pores up to 25 nm. Similarly for 25$LiBH_4$/C, about 12 % of the $LiBH_4$ were in pores between 10-60 nm while the rest were confined in carbon pores ≤ 10 nm. This implies that increasing the loading of $LiBH_4$ leads to increase in the average domain sizes of $LiBH_4$ in the nanocomposites, in line with the melting point

depression trend as obtained from the DSC measurements. This also indicates favourable wetting of the carbon by molten $LiBH_4$.

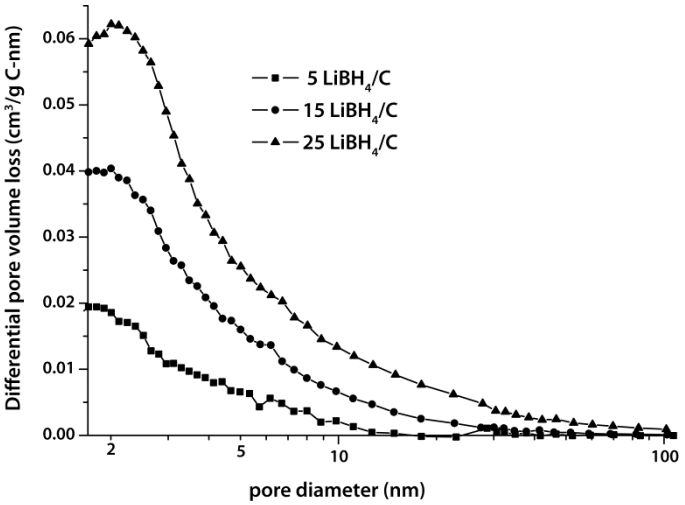

Figure 3.4: Nitrogen physisorption measurements showing differential pore volume loss versus pore diameter (pore size distribution) for nanoporous carbon after melt infiltrating with varying $LiBH_4$ wt% loading.

Table 3.2: Nitrogen physisorption data for porous carbon and melt infiltrated $LiBH_4$/C nanocomposites: V_T = total pore volume, V_{loss} = carbon pore volume loss (total pore volume lost and percentage of these pores less than 10 nm), and V_{LiBH4} = volume of $LiBH_4$ added in 1 g carbon)

	V_T	V_{loss} (cm^3/g C)		V_{LiBH4}
Sample	(cm^3/g C)	total	< 10 nm (%)	(cm^3/g C)
Dried porous C	0.65	-	-	-
5 $LiBH_4$/C	0.53	0.120	99	0.079
15 $LiBH_4$/C	0.38	0.270	95	0.265
25 $LiBH_4$/C	0.10	0.552	88	0.501

3.5 Hydrogen Release

Figure 3.5 shows hydrogen release profiles (heating at 5 °C/min under Ar flow) from bulk $LiBH_4$, 25 wt% $LiBH_4$ melted with non-porous graphite and $LiBH_4$/porous carbon nanocomposites with varying $LiBH_4$ loading. The bulk $LiBH_4$ releases hydrogen in three steps; two minor hydrogen release peaks around 280 °C (melting point of $LiBH_4$) and 390 °C, and a major hydrogen release starting at 400 °C. Similarly the 25 wt% $LiBH_4$/G exhibits multiple hydrogen release peaks as the bulk $LiBH_4$ but the second and the third desorption peaks occurred at temperatures 30-40 °C lower than for the bulk. Interestingly, for all the nanocomposites with porous carbon hydrogen desorption occurred in a single step and at significantly lower temperatures than for the other samples. The 35 and 25 wt% $LiBH_4$ nanocomposites releases hydrogen starting from ~ 230 °C while hydrogen release started ~ 200 °C in the 15 and 5 wt% $LiBH_4$/C nanocomposites. Hence the hydrogen release temperatures of $LiBH_4$ nanoconfined in carbon decrease with decreasing $LiBH_4$ loading.

Table 3.3 shows the amount of hydrogen released from the bulk and 25 wt%

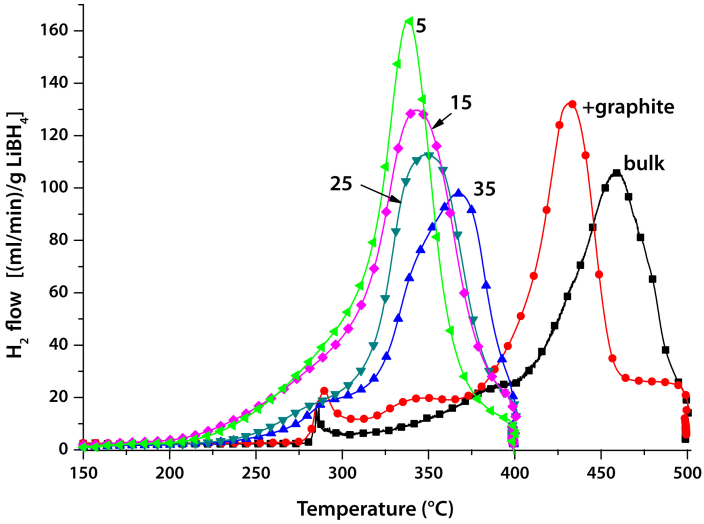

Figure 3.5: Temperature programmed desorption (TPD) while heating at 5 °C/min under 25 ml/min Ar flow for bulk $LiBH_4$, 25 wt% $LiBH_4$/graphite and $LiBH_4$/C nanocomposites with different wt% loading as indicated.

Table 3.3: Normalized hydrogen release (wt% based on $LiBH_4$) obtained from TPD measurements of the bulk, graphite supported (G) and $LiBH_4$/C nanocomposites synthesized with porous carbon and purified porous carbon. The wt% loadings of $LiBH_4$ are indicated

Sample	Bulk	25%/G	35%/C	25%/C	15%/C	5%/C
Dried C (wt% H_2)	11.2	13.4	12.7	14	16.7	16.1
Purified C (wt% H_2)	-	-	13.4	14.8	18.0	18.0

$LiBH_4$/G (after dwelling for 25 min at 500 °C), and the $LiBH_4$/C and $LiBH_4$/PC nanocomposites (25 min dwell at 400 °C). The bulk and 35$LiBH_4$/porous carbon samples released less than 13.8 wt% H_2 suggesting that decomposition into LiH, B and H_2 according to equation 3.1 was not yet completed while the 25 $LiBH_4$/C released about 14 wt% H_2 which would mean complete decomposition according to equation 3.1. The 15 and 5 wt% $LiBH_4$/C nanocomposites released ~ 16 wt% H_2 which suggests that decomposition of the $LiBH_4$ into Li and B in a single step (equation 3.2) has proceeded to some extent. This is surprising as LiH is very stable and requires temperatures up to 700 °C for dehydrogenation.

$$2\ LiBH_4 \leftrightarrow 2\ LiH + 2\ B + 3\ H_2 \qquad (3.1)\ 13.8\ wt\%\ H_2$$
$$2\ LiBH_4 \leftrightarrow 2\ Li + 2\ B + 4\ H_2 \qquad (3.2)\ 18.5\ wt\%\ H_2$$

The nanocomposites synthesized with purified nanoporous carbon material generally released higher amount of hydrogen than the other nanocomposites, most likely because more hydrogen was lost in the latter during synthesis due to reactions with impurities of the support.

Since proper quantitative measure of hydrogen release is not trivial, for validation the hydrogen release from the samples was additionally measured using volumetric (Sievert) method. Figure 3.6 shows hydrogen released from samples that had been heated under 22 bar H_2 and allowed to dehydrogenate at constant temperature of 400 °C (by expanding the hydrogen to higher reservoir volume). Clearly both the amount of hydrogen released and the release rates are influenced by the $LiBH_4$ loading, in line with the TPD results. The $LiBH_4$/G sample has the lowest desorption rate while the 5 wt% $LiBH_4$/C nanocomposites has the highest hydrogen

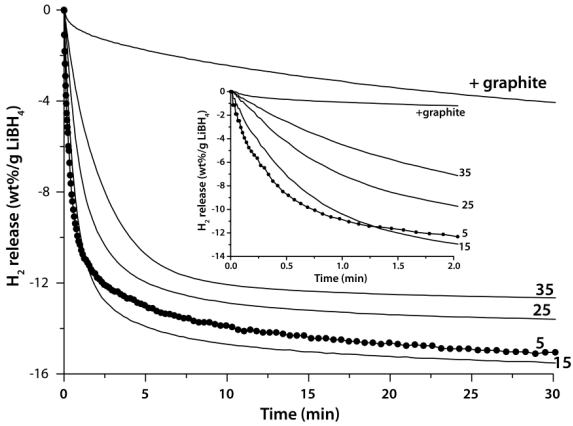

Figure 3.6: Volumetric hydrogen release measurements at 400 °C for 25 wt% $LiBH_4$/graphite and $LiBH_4$/C nanocomposites with different $LiBH_4$ wt % loading (as indicated). Insert shows the variation in dehydrogenation rate as a function of loading in the first 2 min

release rate especially at the first 1 min of desorption (see insert in figure 3.6). Similarly more than 15 wt% hydrogen was released from the 5 and 15wt% nanocomposites. Additional hydrogen release measurements conducted in a magnetic suspension balance (data not shown) further confirmed the release of about 18 wt% H_2 from the 15 wt% $LiBH_4$ nanocomposites even at temperatures as low as 375 °C. This shows that $LiBH_4$ can decompose directly to Li, B and H_2 at relatively lower temperatures if it is confined and in close contact with nanoporous carbon materials. These findings show that the hydrogen release rates and capacity of nanoconfined $LiBH_4$ can significantly be influenced by the $LiBH_4$ loading. The purity of the nanoporous carbon material also affects the H_2 release capacities of the nanocomposites.

3.6 Dehydrogenation Kinetics

To learn how the dehydrogenation rates are influenced by $LiBH_4$ loading, kinetic parameters were estimated from the TPD profiles using the Kissinger method[23]. Kissinger showed that by varying the heating rate of a non-isothermal process (such as the TPD experiments), the kinetic parameters can be determined using the following equation.

$$\ln(\beta/T_p^2) = -(E_a/R) * 1/T_p - \ln(A_0 R/E_a) \qquad (3.3)$$

Where β is the heating rate, T_p is the temperature of maximum (peak) dehydrogenation, E_a is the apparent activation energy, R the gas constant and A_0 is the frequency factor. A graph of ln (β/T_p^2) versus $1/T_p$ gives a straight line from which the apparent activation energy and the frequency factor can be determined from the slope and intercept of the graph respectively. Equation 3.3 has been shown to be valid for many constant rate solid state transformations irrespective of the reaction order[24, 25], and has been used to evaluate the kinetics for $NaAlH_4$ dehydrogenation[10]. For this analysis, the freshly prepared $LiBH_4$/C samples were desorbed under Ar at different heating rates (1, 2.5, 5, 10 and 15 °C/min). Each measurement was repeated at least once and the average peak hydrogen release temperature was used. The Kissinger plots for the samples are shown in figure 3.7 while the kinetic parameters obtained from the analysis are summarized in table 3.4. The apparent activation energy for dehydrogenation decreased from 169 ± 5 kJ/(mol $LiBH_4$) in the bulk $LiBH_4$ to 156 ± 3kJ/(mol $LiBH_4$) in the 25 $LiBH_4$/G sample. The nanocomposites generally have significantly lower activation energy than the bulk and graphite supported $LiBH_4$.

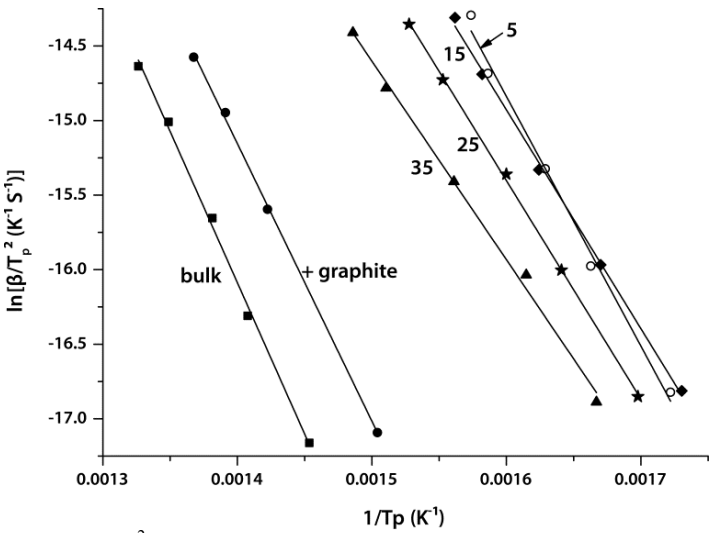

Figure 3.7: plots of ln (β/T_p^2) versus $1/T_p$ and straight regression lines for bulk $LiBH_4$, $LiBH_4$/G and $LiBH_4$/C nanocomposites with varying $LiBH_4$ loadings as indicated.

Table 3.4: Dehydrogenation rate parameters for bulk $LiBH_4$, $LiBH_4$ supported on graphite and $LiBH_4$/C nanocomposites with different wt% $LiBH_4$

Sample	T_p (°C) @ 5 °C/min	E_a (kJ/mol)	A_0 (s^{-1})	K @ 400 °C (s^{-1})
Bulk $LiBH_4$	460	169 ± 5	$(4.5 \pm 0.1)x10^9$	3.44×10^{-4}
25 $LiBH_4$/G	430	156 ± 3	$(1 \pm 0.02)x10^9$	7.80×10^{-4}
35 $LiBH_4$/C	368	111 ± 4	$(2.9 \pm 0.1)x10^6$	7.04×10^{-3}
25 $LiBH_4$/C	350	122 ± 2	$(4.5 \pm 0.06)x10^7$	1.53×10^{-2}
15 $LiBH_4$/C	343	122 ± 3	$(7.6 \pm 0.2)x 10^7$	2.58×10^{-2}
5 $LiBH_4$/C	335	139±7	$(2.3 \pm 0.1)x10^9$	3.75×10^{-2}

The pre-exponential factor for the nanocomposites increased as the loading decreased. Hydrogen release rates of the samples were compared by calculating the dehydrogenation rate constant *K* (per sec) of each sample at one fixed temperature (400 °C) using equation 3.4.

$$K(T) = A_0 \exp(-E_a/RT) \quad (3.4)$$

The 5 wt% nanocomposite has the highest dehydrogenation rate constant at 400 °C (3.75×10^{-2} /s) which is about 1.5, 2.5, 5.3 and 108 times higher than that of nanocomposite with 15 wt% 25 wt%, 35 wt% and bulk $LiBH_4$ respectively.
Clearly, the loading of $LiBH_4$ influences hydrogen release kinetics of $LiBH_4$ in the nanocomposites. Most likely, this is due to change in the morphology, nanostructure and/domain sizes of $LiBH_4$ and its interface with carbon with $LiBH_4$ loading as seen in the Nitrogen physisorption measurements. Baldé et al[10] demonstrated that the activation energy of $NaAlH_4$ supported on carbon nanofiber decreased as the particle size decreased, resulting in faster kinetics. However for

nanoconfined $LiBH_4$, although the activation energy decreased significantly upon nanoconfinement, decreasing the loading (decrease in average size of $LiBH_4$) did not lead to a further decrease in the activation energy but rather to an increase in the pre-exponential factor. Most studies on the dehydrogenation kinetics of complex hydrides focused on the apparent activation energy while often neglecting the pre-exponential factor. However the results from the kinetic measurements clearly show that the pre-exponential factor is also crucial in the accurate evaluation of dehydrogenation rates.

3.7 Reversibility

The reversibility of the hydrogen desorption from the nanocomposites at mild conditions was evaluated by rehydrogenating the dehydrogenated nanocomposites ex-situ in an autoclave at 325 °C and 50 bar H_2 for 3 h. Subsequently the amount of hydrogen absorbed was determined by running a second hydrogen release measurements (figure 3.8). The 25 wt% $LiBH_4$/G sample released negligible amount of hydrogen in line with the fact that desorbed bulk $LiBH_4$ requires 600 °C and 350 bar H_2 for partial reversibility[26]. The rehydrogenated 35 wt% $LiBH_4$/PC released the lowest amount of hydrogen (4.8 wt% H_2/g $LiBH_4$) followed by the

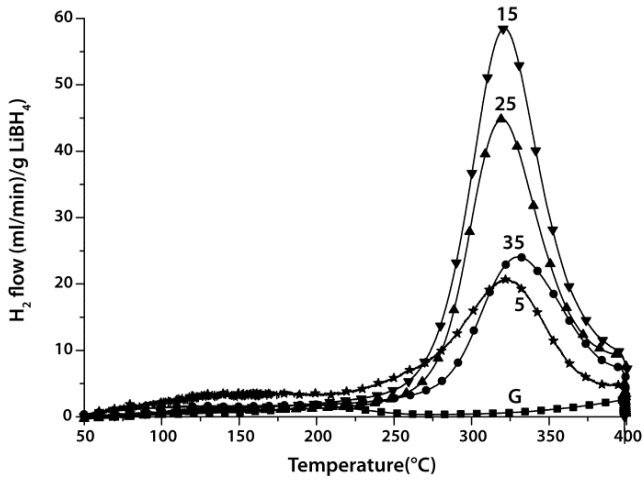

Figure 3.8: TPD measurements showing hydrogen release (5 °C/min, 25 ml/min Ar flow) from rehydrogenated (in autoclave at 325 °C and 50 bar H_2 for 3 hr) $LiBH_4$ supported on graphite(G) and $LiBH_4$/PC nanocomposites with wt% $LiBH_4$ loading as indicated in each curve.

5 wt% $LiBH_4$ /PC which released 5.8 wt% H_2. The 25 $LiBH_4$/PC nanocomposite released 6.6 wt% H_2 while the maximum amount of H_2 (8.1 wt %) was released by the 15 $LiBH_4$/PC. This result shows that only partial reversibility is achieved at this rehydrogenation conditions and that the reversibility of hydrogen desorption from nanoconfined $LiBH_4$ increases with decreasing $LiBH_4$ loading. The low reversibility in the 5 wt% nanocomposites is most likely due to oxidation during sample handling since the $LiBH_4$ in this sample is highly dispersed on the carbon and therefore more prone to oxidation, as will be shown in next section.

The hydrogen uptake kinetics of the nanocomposites was compared by in-situ manometric measurements at 330 °C and an initial hydrogen pressure of ~27 bar. Figure 3.9 shows the hydrogen uptake by the samples during 1 h measurement. The 25 wt% $LiBH_4$/G sample has the slowest absorption rate while the rate of hydrogen uptake in the nanocomposites increases with decreasing $LiBH_4$ loading except for the 5 wt% sample which have slightly lower hydrogen uptake rate than the 15 wt% nanocomposite. A fast hydrogen uptake in the first few (1-2) minutes is followed by a more gradual hydrogen uptake. The amounts of hydrogen absorbed in this initial few minutes increased with decreasing loading (except for 5 wt% sample).

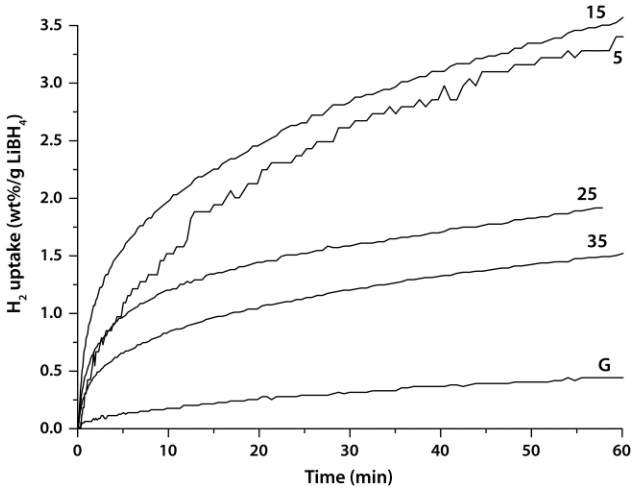

Figure 3.9: Volumetric (Sievert) hydrogen uptake (at 330 °C and initial of about 27 bar H_2) by $LiBH_4$ supported on graphite (G) and $LiBH_4$/PC nanocomposites with wt% $LiBH_4$ loading as indicated in the curves.

Although at the moment the rate limiting step for the rehydrogenation reactions of $LiBH_4$ is not well understood, it is generally believed that the reversibility is mainly limited by the phase segregation of the solid state dehydrogenation products. LiH and B are immobile and if formed after dehydrogenation, it would be a very slow process to recombine. In the case of confined $LiBH_4$ keeping them close to each other (nanoscale) could improve their recombination and the more so at low loadings of $LiBH_4$ if the materials remain inside the pores after dehydrogenation. This explains why hydrogen uptake rate increases with decreasing $LiBH_4$. It was also seen that a substantial fraction of $LiBH_4$ decomposes into elemental Li and B at low loadings. If the Li is not oxidised nor reacted with the nanoporous carbon material, more hydrogen will be absorbed in these samples than in the nanocomposites with higher loadings since more hydrogen is required to form $LiBH_4$ from Li and B than from LiH and B. Li has a lower melting point and higher mobility than LiH, hence it would be expected that the recombination of Li and B to form $LiBH_4$ under hydrogen pressure will be faster than for LiH and B. Furthermore the presence of an initial fast absorption rates might be due to the formation of LiH first followed by the formation of $LiBH_4$ from LiH, B and H_2. This explanation is supported by the fact that this initial fast hydrogen uptake is not observed in the dehydrogenated $25LiBH_4$/G as no elemental Li is expected to be present in this sample.

3.8 Structural changes during de/re-hydrogenation

To investigate the effects of loading on structural changes occurring in the sample during hydrogen sorption, XRD data of the desorbed and rehydrogenated samples were acquired. In figure 3.10A, diffraction lines due to LiH and a broad peak (30°-40° 2θ) are clearly seen in the dehydrogenated bulk $LiBH_4$. The broad peak is possibly due to amorphous B or $Li_2B_{12}H_{12}$. The $35LiBH_4$/C shows weak diffraction due to LiH while no diffraction lines other than that due to the turbostratic carbon are seen in the other nanocomposites, suggesting that the decomposition products of these nanocomposites are confined in the carbon pores and/or lack long-range crystallinity. After rehydrogenation (Figure 3.10B) LiH diffraction lines are clearly seen in the 35 wt% nanocomposite and slightly in the 25 wt% nanocomposite.

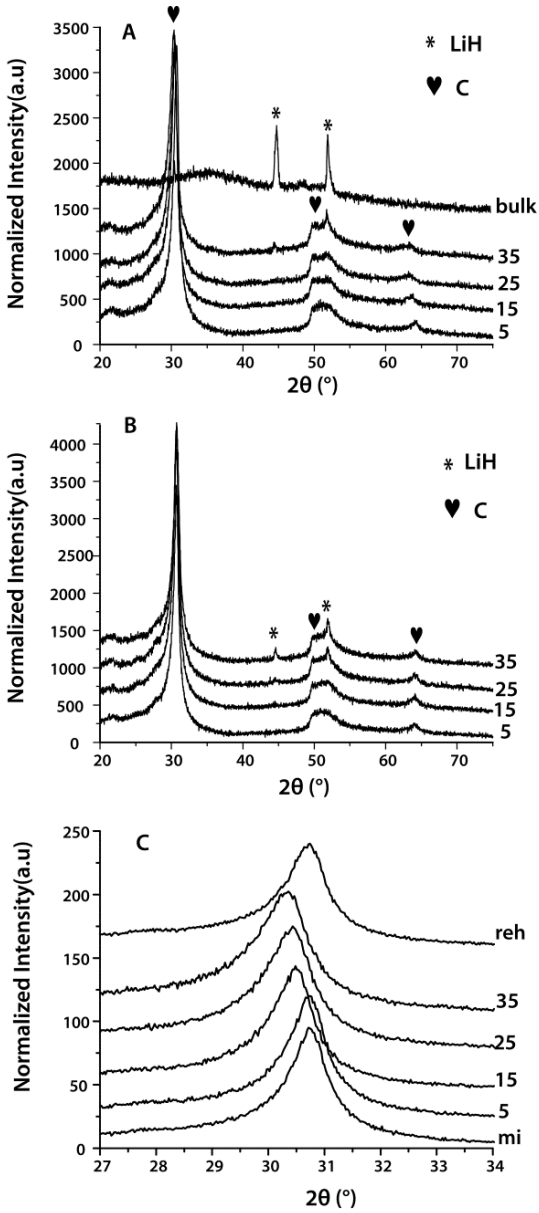

Figure 3.10: XRD pattern of bulk $LiBH_4$ and $LiBH_4$/C nanocomposites with different $LiBH_4$ loading (A) after dehydrogenation and (B) after rehydrogenation in autoclave at 325 °C, 50 bar H_2, 3 h. (C): Comparing the carbon(002) diffraction peak of the as-synthesized 25 wt% $LiBH_4$/C (mi) to those of desorbed nanocomposites with different loadings (wt% as indicated), and that of the rehydrogenated 25 wt% $LiBH_4$/C (reh). Note that the carbon (002) diffraction peak is at the same 2θ position in all the as-prepared and rehydrogenated samples.

For the 5 and 15 wt% nanocomposites, no crystalline product was seen after rehydrogenation (just as in the as-prepared and dehydrogenated samples). Figure 3.10C compares the carbon (002) diffraction line after synthesis, dehydrogenation and rehydrogenation of the nanocomposites. After dehydrogenation the C (002) diffraction line which was originally at 31.10° 2θ in all the nanocomposites shifted to 30.28°, 30.22° and 30.16° 2θ in the 15, 25 and 35 wt% $LiBH_4$/C nanocomposites respectively, and shifted back to its original position upon rehydrogenation. Such a peak shift corresponds to a change in the average graphene interlayer spacing by ~ 0.06-0.08 Å. As it reversible,and occurs upon dehydrogenation (forming metallic Li), it is logical to ascribe it to Li intercalation in the graphitic carbon[27-29]. Previously it has been reported that Na could be reversibly intercalated into this graphitic carbon upon dehydrogenation of NaH[30]. As far as we are aware, this is the first report of reversible Li intercalation in carbon during the dehydrogenation of $LiBH_4$. For full intercalation of Li to form LiC_6, a change in lattice spacing of 0.35 Å would be expected[29, 31]. Hence, in this case intercalation was limited (on the average forming $Li_{0.21}C_6$). It might be of great importance if this effect could be enhanced, as it stabilizes the metallic phase and hence decreases the enthalpy difference between hydrided and dehydrided phase. These results show that the degree of intercalation is only slightly influenced by the $LiBH_4$ loading in the range 15-35 wt%. For the 5 wt% $LiBH_4$/C, no significant shift (intercalation) in the carbon peak was observed probably due to the limited amount of Li in this sample and /or high chance of oxidation during handling of the sample as stated earlier.

The nanostructure of the $LiBH_4$ upon cycling was additionally characterized using solid state magic angle spinning NMR. Figure 3.11 shows ^{11}B and ^{7}Li NMR spectra of bulk $LiBH_4$, $LiBH_4$/C nanocomposites, and the measurement for physical mixture of 25 wt% $LiBH_4$ with dried nanoporous carbon (as reference). The peak due to $LiBH_4$ (-42.9 ppm for ^{11}B and 5 ppm for ^{7}Li) is clearly broadened after melt infiltration of the $LiBH_4$ into the nanoporous carbon material, and the broadening increased with decreasing $LiBH_4$ loading. The line broadening can be ascribed to susceptibility effects because of the close contact between $LiBH_4$ and the conductive carbon material and/or to a high structural disorder in the nanoconfined $LiBH_4$[32, 33]. This suggests a close proximity of $LiBH_4$ and carbon with decreasing

loading, supporting the morphological model arising from N_2 physisorption in which $LiBH_4$ preferentially fills the smaller pores and readily wets the carbon surface. After dehydrogenation, the $LiBH_4$ resonance in the ^{11}B NMR disappeared completely in the 5 and 15 wt% samples while a minor contribution was present especially in the bulk and 35 wt% samples, which indicates incomplete decomposition to LiH, B and H_2, in line with the TPD results. A broad peak (-10-50 ppm) which is most likely due to boron [4] and/or intermediate boron phases (e.g. $Li_2B_{12}H_{12}$) was seen in all the samples. The peak broadening increased with decreasing $LiBH_4$ loading. ^7Li NMR of the dehydrogenated bulk $LiBH_4$ shows a resonance around 5 ppm chemical shift which corresponds to that of pure LiH,

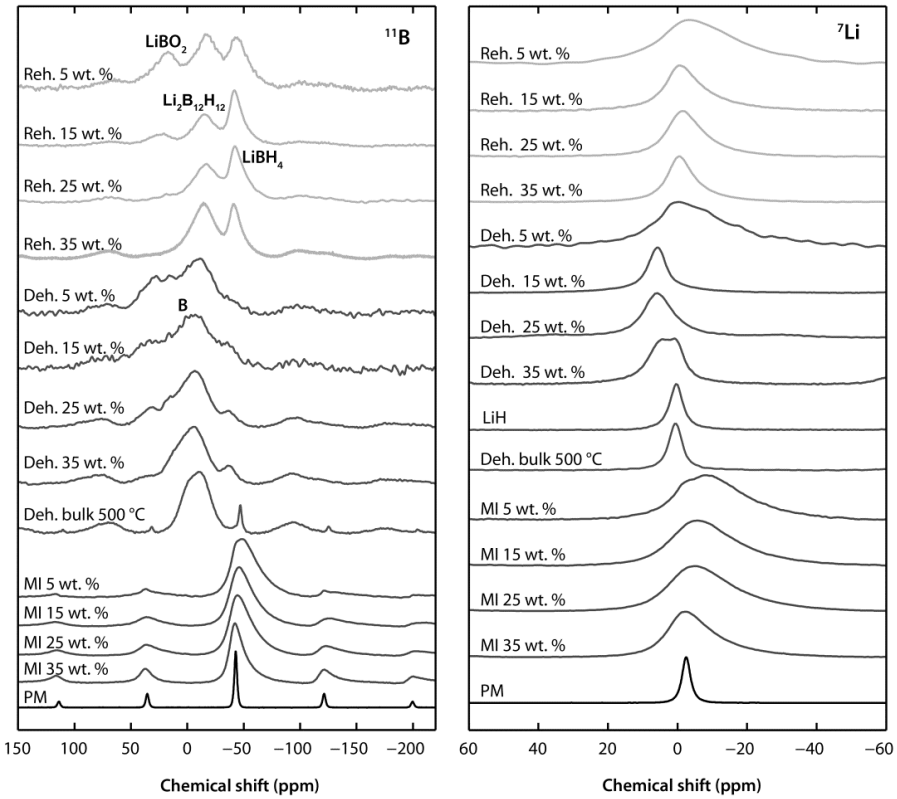

Figure 3.11 ^{11}B and ^7Li MAS-NMR of a physical mixture (PM) of 25wt% $LiBH_4$ and C, and $LiBH_4$/C nanocomposites after melt infiltration (MI), dehydrogenation under Ar (deh) and rehydrogenation at 325 °C, 50 bar H_2, 3h. Included are the NMR spectra of bulk $LiBH_4$ dehydrogenated at 500 °C, and pure LiH as a reference.

while the 35 wt% $LiBH_4$/C nanocomposite shows a broad peak which is a combination of resonance from LiH and a new resonance around 8 ppm which is most likely due to intercalated Li (LiC_x with $x > 12$)[34]. This is in line with the XRD results. The dehydrogenated 25 and 15 wt% nanocomposites also display a resonance around 8 ppm chemical shift but much broader for the 25 wt% likely due to contribution from LiH. However such shift in resonance was not observed in the dehydrogenated 5 wt% sample, which is also in accord with the XRD measurements. After rehydrogenation, both the ^{11}B and ^{7}Li NMR shows a peak due $LiBH_4$ in the nanocomposites, confirming the reversibility of these materials. However in addition, ^{11}B NMR shows resonance due to $Li_2B_{12}H_{12}$[35, 36] in all the nanocomposites, and also a resonance due to $LiBO_2$[37-39] in the 5wt% nanocomposites, which proves that this sample is prone to oxidation. (Note that $LiBH_4$, $Li_2B_{12}H_{12}$, LiH and lithium oxides have close ^{7}Li chemical shifts and therefore not easy to differentiate in samples with broad peaks). This result suggests that the incomplete reversibility of the system might be due to the formation of $Li_2B_{12}H_{12}$ during rehydrogenation as speculated in literature[40].

3.9 Thermodynamic stability

We investigated the thermodynamics of hydrogen sorption in nanoconfined $LiBH_4$. The US National Institute of Standards[41] reports -190.8 kJ/mol and -90.46 kJ/mol as the standard heats of formation (Δ_fH^0) of $LiBH_4$ and LiH respectively. The entropy (S^0) values for $LiBH_4$, LiH, B and H_2 are 75.88, 20.03, 5.90 and 130.7 J/(mol K) respectively, resulting in enthalpy (Δ_rH^0) and entropy(Δ_rS^0) change of 66.6 kJ/(mol H_2) and 97.38 J/(K mol H_2) for reaction (3.1). This implies a decomposition temperature of 410 °C at 1 bar H_2. Mauron et al studied the stability of $LiBH_4$ by pressure-concentration-temperature (PCT) isotherm measurements and reported a dehydrogenation enthalpy and entropy values of 74 kJ/(mol H_2) and 115 J/(K mol H_2) respectively[26]. This results in an experimental hydrogen release temperature of approximately 370 °C at 1 bar H_2. We measured the hydrogen release from bulk $LiBH_4$ and $LiBH_4$/C nanocomposites (synthesized with purified carbon) in a magnetic suspension balance under a constant pressure of 1.05 bar H_2. Expectedly, no hydrogen release occurred from the bulk $LiBH_4$ upon heating to

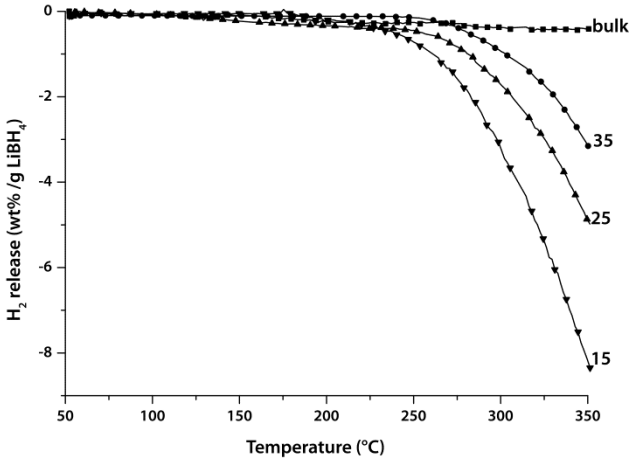

Figure 3.12: Hydrogen release from bulk and $LiBH_4$/PC nanocomposites (wt% $LiBH_4$ as indicated) measured in a suspension balance under 1.05 bar H_2

350 °C (figure 3.12). However in the nanocomposites, hydrogen release started around 255 °C which is more than 100 °C less than the thermodynamic decomposition temperature for bulk $LiBH_4$ at 1 bar H_2. Furthermore the onset of hydrogen release decreased slightly with decreasing $LiBH_4$ loading. The 15 wt% nanocomposites released 8 wt% H_2 while the 25 and 35 wt% samples released ~3 wt% and 5 wt% H_2 respectively, upon heating to 350 °C. This suggests that the decomposition pathway or stability of the nanoconfined $LiBH_4$ might be different than that of the bulk $LiBH_4$ as reported for $NaAlH_4$/C nanocomposites [42-44]. Furthermore $LiBH_4$ loading seems to also influence the thermodynamic hydrogen release temperatures of the nanoconfined $LiBH_4$.

3.10 General discussion

The results presented in the previous sections showed that melt infiltration was effective for the synthesis of $LiBH_4$/C nanocomposites using mesoporous turbostratic carbon material as template. The presence of impurities in carbon materials led to irreversible reactions which significantly influenced the hydrogen release and uptake capacities of $LiBH_4$ confined in nanoporous carbon. These side reaction(s) also influenced or complicated the kinetics and even the thermodynamics of the hydrogen sorption. This is most likely one of the reasons different hydrogen release/uptake temperatures and capacities have been observed

for $LiBH_4$ confined in carbon based nanoporous materials. Although the presence of impurities such as surface oxygen groups improves the wetting of carbon, purification of the carbon prior to use is necessary to minimize irreversible reactions and for accurate quantification of the hydrogen sorption performance of metal hydrides confined in nanoporous carbon materials.

Results from nitrogen physisorption and NMR measurements revealed that molten $LiBH_4$ readily wets the nanoporous carbon surface and preferentially fills the smallest pores and the larger ones are filled with increasing loading. Thus for a porous material with broad pore size distribution like our mesoporous carbon, varying the loading of $LiBH_4$ will lead to variation in the size features or nanostructure of $LiBH_4$ and its proximity to carbon since $LiBH_4$ was confined in carbon pores with different sizes. Therefore the observed depression (or absence) of the structural transition/melting temperatures of $LiBH_4$ and increase in its hydrogen sorption kinetics with decreasing loading can be explained by decrease in the average particle size of $LiBH_4$ and increase of its interface with carbon.

The structural transition and melting of $LiBH_4$ were not detected when less than half of the carbon pores were filled (< 15wt% $LiBH_4$). Similar observation have been reported for water confined in mesoporous silica (MCM-41) in which the melting/freezing process vanished once the pore diameter is 2.8 nm and below, and it was concluded that 2.8 nm is the lower limit for first-order melting/freezing of water in the pores[45]. For the $LiBH_4$ confined in nanoporous carbon materials, 10 nm is likely the lower limit for a first order structural phase transition and melting/solidification of $LiBH_4$ since the vast majority of the $LiBH_4$ is confined in carbon pores of diameter ≤ 10 nm at loadings < 15wt% $LiBH_4$. For loadings ≥ 15 wt% $LiBH_4$, structural transition and melting of $LiBH_4$ were detected since some of the $LiBH_4$ was confined in pores larger than 10 nm in diameter. The melting point depression ΔT_m of a material confined in a cylindrical shaped pore has been shown to increase with decreasing pore diameter d as described by the Gibbs–Thomson equation:

$$\Delta T_m(d) = T_m - T_m(d) = \frac{4T_m\gamma_{sl}}{d\Delta H_b\rho_s} \tag{3.5}$$

Where T_m and $T_m(d)$ are the melting temperatures of the material at the bulk state and when confined within a constant pore of diameter d. γ_{sl} represent the surface free energy (interfacial tension) of the solid/liquid interface, ΔH_b is the melting enthalpy in the bulk state and ρ_s is the molar density of the material in the bulk state.

From equation (4), broadening of the peaks due to phase transitions is expected due to confinement of $LiBH_4$ in pores of different sizes leading to variations in temperatures at which these phase transitions takes place. The ~10-50 °C decrease in melting point observed in the nanocomposites with ≥ 15 wt% $LiBH_4$ would corresponds to $LiBH_4$ confined in pores ~ 100 - 20 nm (using T_m = 548 K, ρ_s = 3.057×10^4 mol/m^3, ΔH_b = 7560 J/mol and assuming γ_{sl} = 0.12 J/m^2 for $LiBH_4$/C interface [46]). These values are supported by N_2 physisorption which indicated that ~ 3-10 % of the $LiBH_4$ in these nanocomposites are contained in pores with diameter > 10 nm.

The absence of, or decreased phase transition temperatures observed in nanoconfined $LiBH_4$ is interesting as this would mean that the high temperature (and hence more disordered) phase of $LiBH_4$ is stabilized at ambient conditions. The NMR results gave additional indication that the $LiBH_4$ is highly disordered when nanoconfined. It has been shown that the anisotropic displacement of the hydrogen atoms in the BH_4 units increased by almost 2 orders of magnitude in going from the low temperature to high temperature (hexagonal) phase[47-49] due to increased disorder in the high temperature phase[50-52]. The increase in disorder and/or rotation of the BH_4 units will lead to increase in the degrees of freedom or entropy of the nanoconfined $LiBH_4$ due to the increased vibration in the solid phase[53, 54] and thereby enhanced stability.

Although the rate limiting step(s) for dehydrogenation of $LiBH_4$ is not well known, two factors are most likely responsible for the increased kinetics with decreasing loading. Decreasing the particle sizes of metal hydrides to the nanoscales generally leads to increase in hydrogen release and uptake kinetics due to reduced mass transport distances (nanoscale) and an increase in nucleation site density. This is even more critical for rehydrogenation due to formation of segregated immobile solid phases after dehydrogenation. Since $LiBH_4$ is confined in smaller pores and

its average particle/ features sizes decreased with decreasing loading, it is expected that the hydrogen release and uptake rates will increase, as shown in this study. This is supported by results from carbon nanofibre supported-$NaAlH_4$ in which the hydrogen release kinetics increased with decreasing particle sizes of $NaAlH_4$[10]. Additionally, the increase in the interfacial area-volume of $LiBH_4$ in contact with the carbon (close contact) with decreasing loading might increase the average interaction between $LiBH_4$ and the carbon material(see below), and lower the activation barriers. The increase in the pre-exponential factor with decreasing loading suggest that more (nucleation) sites are available for de(re)hydrogenation reaction, perhaps due to the larger fraction of $LiBH_4$ that interacts directly with the surface of the carbon. The increase in average interaction between the $LiBH_4$ and carbon material with decreasing loadings is also most likely responsible for the full decomposition of the nanoconfined $LiBH_4$ into B and intercalated Li at relatively low temperatures.

It is interesting to speculate on the possible reasons for the significant decrease in the thermodynamic decomposition temperature of $LiBH_4$ when confined in the nanoporous carbon material. Firstly, for metal hydrides nanoparticles ($\leq$ 10 nm) or clusters such as MgH_2 it has been predicted that their standard enthalpy of formation could be significantly lower than that of the bulk due to the surface energy difference between the hydride and metal[55-57]. Although very little is known for complex hydrides, it is possible that such effects could also be important for nanoconfined $LiBH_4$. However, the high disorder or increased translational degrees of freedom in the nanoconfined $LiBH_4$ could possibly lead to a change in the dehydrogenation entropy and stabilize the hydride. A second reason could be the close contact and interaction between $LiBH_4$ and nanoporous carbon which could destabilize the $LiBH_4$ and/or change its decomposition pathway. It is generally believed that the presence of an element like carbon which is more electronegative than Li could weaken the ionic bond between the Li and BH_4 via electronic interactions. This will result in a lower dehydrogenation enthalpy, which implies a decrease in hydrogen release temperatures of nanoconfined $LiBH_4$[58-60]. This is supported by the fact that the nanoconfined $LiBH_4$ desorbs hydrogen in a single step as opposed to the multiple steps observed for the bulk. The observed decrease in the thermodynamic hydrogen release temperatures (at 1.05 bar H_2) suggests that

this electronic interaction increases with decreasing $LiBH_4$ loading. This is expected since a larger fraction of $LiBH_4$ is in close contact with the carbon surface. The formation of intercalated lithium and B (instead LiH and B) especially at low loadings is another proof that close contact and interaction with the carbon material could change decomposition pathway and equilibrium of nanoconfined $LiBH_4$. Finally anchoring of the $LiBH_4$ might change its stability due to possible restriction of volume changes which normally occur upon de(re)hydrogenation, and change in interface energy.

3.11 Conclusions

$LiBH_4$ was successfully melt infiltrated into nanoporous carbon material to form $LiBHR_4$/carbon nanocomposites. The melt infiltration process was studied in-situ using DSC and the effect of $LiBH_4$ loading on the structure and hydrogen sorption properties of nanoconfined $LiBH_4$ investigated. It was shown that purification of the nanoporous carbon material is necessary to avoid or to limit irreversible reactions during melt infiltration. The structural transition (~ 110 °C) and melting/solidification of $LiBH_4$ (~ 280 °C) where not detected when less than half of the carbon pores were filled with $LiBH_4$ (< 15 wt% $LiBH_4$) while nanocomposites with ≥ 15 wt% $LiBH_4$ showed ~ 10-50 °C shift to lower temperatures for these events. The nanoconfined $LiBH_4$ desorbed hydrogen at temperatures lower than that of the bulk by at least 100 °C. The dehydrogenation rates at 400 °C increased with decreasing loading, the apparent activation energy decreased from 169 ± 5 kJ/mol in the bulk to 110-140 kJ/mol, while the pre-exponential factor generally increased with decreasing loading. For loadings ≤ 15 wt%, $LiBH_4$ decomposes into B, intercalated Li and 18 wt% H_2 upon heating to 375 °C. Above this loading it decomposed into LiH/ intercalated Li, B, and ≤ 14 wt% H_2 at temperatures ≥ 400 °C. Partial reversibility of the dehydrogenated products was observed only in the nanocomposites at relatively mild conditions (325 °C, 50 bar H_2) and the reversible capacity increased with decreasing loading. At 1.05 bar H_2, the nanocomposites decomposed at temperatures ~100 °C lower than the thermodynamically expected decomposition temperature of $LiBH_4$ at 1 bar H_2, suggesting a possible destabilization of the $LiBH_4$ when confined in the nanoporous carbon material. Our investigation shows that the improved hydrogen

sorption of the $LiBH_4$/C nanocomposites with decreasing loading is due to the decrease in the average sizes of $LiBH_4$ and an increased interaction between $LiBH_4$ and the carbon surface.

Acknowledgements

The authors thank Dr. Margriet Verkuiljen of Radboud University, Nijmegen for her work and support regarding the NMR results. Charlotte Barre is acknowledged for her contributions to this work. We thank M.van Zwienen, A. van der Eerden and V. Koot for their technical support and Timcal Ltd. Switzerland for providing the high surface area graphite. This work was financially supported by NWO-Vidi Netherlands, Project Number 016.072.316. The Netherlands Organisation for Scientific Research (NWO) is acknowledged for its support of the solid-state NMR facility for advanced materials research at Radboud University Nijmegen.

References

1. A. F. Gross, J. J. Vajo, S. L. Van Atta and G. L. Olson, *J. Phys. Chem. C*, 2008, **112**, 5651-5657.
2. Z. Z. Fang, P. Wang, T. E. Rufford, X. D. Kang, G. Q. Lu and H. M. Cheng, *Acta Mater.*, 2008, **56**, 6257-6263.
3. S. Cahen, J. B. Eymery, R. Janot and J. M. Tarascon, *J. Power Sources*, 2009, **189**, 902-908.
4. N. Brun, R. Janot, C. Sanchez, H. Deleuze, C. Gervais, M. Morcrette and R. Backov, *Energy Environ. Sci*, 2010, **3**, 824-830.
5. Y. Zhang, W.-S. Zhang, A.-Q. Wang, S. Li-Xian, M.-Q. Fan, H.-L. Chu, J.-C. Sun and T. Zhang, *Int. J. Hydrogen Energy*, 2007, **32**, 3976-3980.
6. X. Liu, D. Peaslee, C. Z. Jost, T. F. Baumann and E. H. Majzoub, *Chem. Mater.*, 2011, **23**, 1331-1336.
7. X. F. Liu, D. Peaslee, C. Z. Jost and E. H. Majzoub, *J. Phys. Chem. C*, 2010, **114**, 14036-14041.
8. M. Christian and K. F. Aguey-Zinsou, *Nanoscale*, 2010, **2**, 2587-2590.
9. C. P. Baldé, B. P. C. Hereijgers, J. H. Bitter and K. P. de Jong, *Angew. Chem., Int. Ed.*, 2006, **45**, 3501-3503.

10. C. P. Baldé, B. P. C. Hereijgers, J. H. Bitter and K. P. De Jong, *J. Am. Chem. Soc.*, 2008, **130**, 6761-6765.
11. J. D. van Beek, *J. Magn. Reson.*, 2007, **187**, 19-26.
12. S. I. Orimo, Y. Nakamori, J. R. Eliseo, A. Züttel and C. M. Jensen, *Chem. Rev*, 2007, **107**, 4111-4132.
13. E.M. Fedneva, V. L. Alpatova and V. I. Mikheeva., *Russ. J. Inorg. Chem.*, 1964, **96**, 826-827.
14. A. Züttel, P. Wenger, S. Rentsch, P. Sudan, P. Mauron and C. Emmenegger, *J. Power Sources*, 2003, **118**, 1-7.
15. P. Adelhelm, J. B. Gao, M. H. W. Verkuijlen, C. Rongeat, M. Herrich, P. J. M. van Bentum, O. Gutfleisch, A. P. M. Kentgens, K. P. de Jong and P. E. de Jongh, *Chem. Mater.*, 2010, **22**, 2233-2238.
16. J. A. Menendez, J. Phillips, B. Xia and L. R. Radovic, *Langmuir*, 1996, **12**, 4404-4410.
17. L. Mosegaard, B. Moller, J. E. Jorgensen, Y. Filinchuk, Y. Cerenius, J. C. Hanson, E. Dimasi, F. Besenbacher and T. R. Jensen, *J. Phys. Chem. C*, 2008, **112**, 1299-1303.
18. M. Brun, A. Lallemand, J.-F. Quinson and C. Eyraud, *Thermochim. Acta*, 1977, **21**, 59-88.
19. A. Schreiber, I. Ketelsen and G. H. Findenegg, *Phys. Chem. Chem. Phys.*, 2001, **3**, 1185-1195.
20. T. M. Eggenhuisen, M. J. van Steenbergen, H. Talsma, P. E. de Jongh and K. P. de Jong, *The Journal of Physical Chemistry C*, 2009, **113**, 16785-16791.
21. T. M. Eggenhuisen, J. P. den Breejen, D. Verdoes, P. E. de Jongh and K. P. de Jong, *J. Am. Chem. Soc.*, 2010, **132**, 18318-18325.
22. P. Ngene, P. Adelhelm, A. M. Beale, K. P. de Jong and P. E. de Jongh, *J. Phys. Chem. C*, 2010, **114**, 6163-6168.
23. H. E. Kissinger, *Journal of Research of the National Bureau of Standards*, 1956, **57**, 217-221.
24. D. W. Henderson, *J. Non-Cryst. Solids*, 1979, **30**, 301-315.
25. J. Vázquez, P. L. López-Alemany, P. Villares and R. Jiménez-Garay, *J. Phys. Chem. Solids*, 2000, **61**, 493-500.
26. P. Mauron, F. Buchter, O. Friedrichs, A. Remhof, M. Bielmann, C. N. Zwicky and A. Zuttel, *J. Phys. Chem. B*, 2008, **112**, 906-910.

27. X. Y. Song, K. Kinoshita and T. D. Tran, *J. Electrochem. Soc.*, 1996, **143**, L120-L123.
28. G. Maurin, C. Bousquet, F. Henn, P. Bernier, R. Almairac and B. Simon, *Chem. Phys. Lett.*, 1999, **312**, 14-18.
29. D. Billaud, E. McRae and A. Hérold, *Materials Research Bulletin*, 1979, **14**, 857-864.
30. P. Adelhelm, K. P. de Jong and P. E. de Jongh, *Chem. Commun.*, 2009, 6261-6263.
31. N. A. Kaskhedikar and J. Maier, *Adv. Mater*, 2009, **21**, 2664-2680.
32. P. Ngene, M. H. W. Verkuijlen, Q. Zheng, J. Kragten, P. J. M. van Bentum, J. H. Bitter and P. E. de Jongh, *Faraday Discuss.*, 2011, **151**, 47-58.
33. M. H. W. Verkuijlen, J. B. Gao, P. Adelhelm, P. J. N. van Bentum, P. E. de Jongh and A. P. M. Kentgens, *J. Phys. Chem. C*, 2010, **114**, 4683-4692.
34. N. Imanishi, K. Kumai, H. Kokugan, Y. Takeda and O. Yamamoto, *Solid State Ionics*, 1998, **107**, 135-144.
35. O. Friedrichs, A. Remhof, S. J. Hwang and A. Züttel, *Chem. Mater.*, 2010, **22**, 3265-3268.
36. S. J. Hwang, R. C. Bowman, J. W. Reiter, J. Rijssenbeek, G. L. Soloveichik, J. C. Zhao, H. Kabbour and C. C. Ahn, *J. Phys. Chem. C*, 2008, **112**, 3164-3169.
37. K. J. D. Mackenzie and M. E. Smith, *Multinuclear Solid-State NMR of Inorganic Materials. Pergamon*, 2002.
38. A. D. Irwin, J. S. Holmgren and J. Jonas, *J. Non-Cryst. Solids*, 1988, **101**, 249-254.
39. G. D. Soraru, N. Dallabona, C. Gervais and F. Babonneau, *Chem. Mater.*, 1999, **11**, 910-919.
40. O. Friedrichs, A. Remhof, S. J. Hwang and A. Züttel, *Chem. Mater.*, **22**, 3265-3268.
41. *CRC Handbook of Chemistry and Physics, 2010-2011*, **91st Edition**.
42. J. Gao, P. Adelhelm, M. H. W. Verkuijlen, C. Rongeat, M. Herrich, P. J. M. Van Bentum, O. Gutfleisch, A. P. M. Kentgens, K. P. de Jong and P. E. de Jongh, *J. Phys. Chem. C*, 2010, **114**, 4675-4682.
43. W. Lohstroh, A. Roth, H. Hahn and M. Fichtner, *ChemPhysChem*, 2010, **11**, 789-792.

44. C. P. Baldé, O. Leynaud, P. Barnes, E. Peláez-Jiménez, K. P. De Jong and J. H. Bitter, *Chem. Commun.*, **47**, 2143-2145.
45. S. Jähnert, F. Vaca Chavez, G. E. Schaumann, A. Schreiber, M. Schonhoff and G. H. Findenegg, *Phys. Chem. Chem. Phys.*, 2008, **10**, 6039-6051.
46. Q. Ge, *The Journal of Physical Chemistry A*, 2004, **108**, 8682-8690.
47. F. Buchter, Z. Łodziana, P. Mauron, A. Remhof, O. Friedrichs, A. Borgschulte, A. Züttel, D. Sheptyakov, T. Strässle and A. J. Ramirez-Cuesta, *Physical Review B*, 2008, **78**, 094302.
48. M. R. Hartman, J. J. Rush, T. J. Udovic, R. C. Bowman Jr and S.-J. Hwang, *J. Solid State Chem.*, 2007, **180**, 1298-1305.
49. Y. Filinchuk, D. Chernyshov and R. Cerny, *J. Phys. Chem. C*, 2008, **112**, 10579-10584.
50. H. Hagemann, S. Gomes, G. Renaudin and K. Yvon, *J. Alloys Compd.*, 2004, **363**, 129-132.
51. I. Tamio, T. Eiji, I. Kazutaka, M. Motoaki, L. Hai-Wen, K. Yoshiyuki and O. Shin-ichi, *Diffuse and doubly split atom occupation in hexagonal LiBH4*, AIP, 2009.
52. A. Remhof, Z. Łodziana, P. Martelli, O. Friedrichs, A. Züttel, A. V. Skripov, J. P. Embs and T. Strässle, *Physical Review B - Condensed Matter and Materials Physics*, 2010, **81**.
53. D. J. Siegel, C. Wolverton and V. Ozolins, *Physical Review B*, 2007, **76**.
54. E. R. Andresen, R. Gremaud, A. Borgschulte, A. J. Ramirez-Cuesta, A. Züttel and P. Hamm, *The Journal of Physical Chemistry A*, 2009, **113**, 12838-12846.
55. V. Berube, G. Chen and M. S. Dresselhaus, *Int. J. Hydrogen Energy*, 2008, **33**, 4122-4131.
56. V. Bérubé, G. Radtke, M. Dresselhaus and G. Chen, *International Journal of Energy Research*, 2007, **31**, 637-663.
57. R. W. P. Wagemans, J. H. Van Lenthe, P. E. de Jongh, A. J. Van Dillen and K. P. de Jong, *J. Am. Chem. Soc.*, 2005, **127**, 16675-16680.
58. Y. Nakamori, H. W. Li, K. Kikuchi, M. Aoki, K. Miwa, S. Towata and S. Orimo, *J. Alloys Compd.*, 2007, **446**, 296-300.
59. Y. Nakamori, K. Miwa, A. Ninomiya, H. W. Li, N. Ohba, S. I. Towata, A. Zuttel and S. I. Orimo, *Physical Review B*, 2006, **74**.
60. M. S. Wellons, P. A. Berseth and R. Zidan, *Nanotechnology*, 2009, **20**.

Chapter 4

$LiBH_4$(Ni)/C Nanocomposites: Synergetic effects of nanoconfinement and Ni addition

Abstract

Nanoconfinement and the use of catalysts are promising strategies to enhance the reversibility of hydrogen storage in light metal hydrides. We combined nanoconfinement of $LiBH_4$ in nanoporous carbon material with the addition of Ni. Samples were prepared by deposition of 5-6 nm Ni nanoparticles inside the nanoporous carbon material, followed by melt infiltration with $LiBH_4$. The Ni addition has only a slight influence on the $LiBH_4$ hydrogen desorption, but significantly enhances the subsequent uptake of hydrogen under mild conditions. Reversible, but limited, intercalation of Li is observed during hydrogen cycling. X-ray diffraction shows that the initial crystalline 5-6 nm Ni nanoparticles are not present anymore after melt infiltration with $LiBH_4$. However, transmission electron microscopy showed Ni-containing nanoparticles in the samples. Extended X-ray absorption fine structure spectroscopy proved the presence of Ni_xB phases with the Ni-B coordination numbers changing reversibly with dehydrogenation and rehydrogenation of the sample. Ni_xB can act as a hydrogenation catalyst, but solid state ^{11}B NMR proved that the addition of Ni also enhanced the reversibility of the system by influencing the microstructure of the nanoconfined $LiBH_4$ upon cycling.

This chapter is based on the following manuscripts: P. Ngene, M. Rien van Zwienen and P. E. de Jongh. *Reversibility of the hydrogen desorption from LiBH4: a synergetic effect of nanoconfinement and Ni addition. Chem. Commun.,* 2010, **46**, 8201

P. Ngene, M. H. W. Verkuijlen, Q. Zheng, J. Kragten, P. Jan M. van Bentum, J. H. Bitter and Petra E. de Jongh. *The role of Ni in increasing the reversibility of the hydrogen release from nanoconfined $LiBH_4$.* Faraday Discussions, 2011, **151**, 47-58

4.1 Introduction

Nanoconfinement of $LiBH_4$ in nanoporous carbon materials is an effective strategy to lower its hydrogen release temperatures and enable partial reversibility under relatively mild conditions as described in chapter 3. However despite the decrease in hydrogen release temperatures and improved reversibility, hydrogen release from nanoconfined $LiBH_4$ still occur at temperatures higher than is required for fuel cell applications. Furthermore, the dehydrogenated $LiBH_4$/nanoporous carbon nanocomposites absorbed less than 50 % of its original hydrogen capacity during rehydrogenation. This shows that the hydrogen release from the nanoconfined $LiBH_4$ is only partially reversible at the rehydrogenation conditions most likely due to slow hydrogen uptake kinetics. Therefore further improvements in the hydrogen release kinetics and especially reversible capacity in nanoconfined $LiBH_4$ is desirable.

Use of catalysts or additives is another strategy to improve the hydrogen release and uptake kinetics in metal hydrides[1-7]. Bogdanovič et al first showed that Ti-based compounds such as $TiCl_3$ are effective catalysts for the dehydrogenation and rehydrogenation reactions of $NaAlH_4$[8]. Although the exact role of Ti is still not well understood, the discovery led to a new interest in finding catalysts that could also be effective for other complex hydrides such as $LiBH_4$. Züttel *et al*. first reported that SiO_2 acted as a catalyst for the dehydrogenation of $LiBH_4$[1]. However as discussed in chapter 2, SiO_2 does not catalyze the decomposition of $LiBH_4$. It reacts with the decomposition product(s) of $LiBH_4$ to form stable silicates[9, 10, 11] while irreversibly releasing hydrogen, as is the case with most metal oxide additives[12, 13]. A large range of materials, including metal halides [2, 4, 14], Al, Pt, carbon nanotubes, fullerene and Ni[3, 5-7, 15], has been investigated in an effort to identify an effective catalyst for $LiBH_4$ de/rehydrogenation. Addition of these materials generally led to a decrease in the dehydrogenation temperatures but most of the systems still required temperatures above 400 °C and hydrogen pressures above 40 bar for only achieving partial rehydrogenation of the desorbed material. For example 600 °C, 100 bar H_2 and 30 h were required for partial (12 wt% H_2) reversibility in $LiBH_4$ ball milled with Ni[6] (600 °C and 350 bar hydrogen for bulk $LiBH_4$), while $LiBH_4$ catalyzed by carbon- supported Pt nanoparticles absorbed only 6 wt% H_2 upon rehydrogenation for 24 h at 600 °C and 30 bar H_2.

Failure of classical hydrogenation catalysts like Pt and Pd to have significant impact on the hydrogen uptake kinetics indicates that hydrogen dissociation is not the rate limiting step for the rehydrogenation reaction of desorbed $LiBH_4$. Rather solid state diffusion, microstructure, and nucleation of phase transformations seem to play a role as discussed in chapter 3. It is possible that these catalysts could be effective during hydrogen uptake if phase segregation of the dehydrogenation products is restricted. Hence in the present study we investigate how nanoconfinement in nanoporous carbon materials can be combined with additives to improve especially the reversibility of the hydrogen release from $LiBH_4$. We show that the addition of Ni nanoparticles increases the reversibility of the hydrogen release from nanoconfined $LiBH_4$. We discuss the structural changes and phase evolution of the nanoconfined $LiBHR_4$ during cycling in the presence and absence of Ni.

4.2 Experimental Details

Carbon-supported Ni nanoparticles were prepared by incipient wetness impregnation [16]. Nickel nitrate (99%, Acros) and citric acid (99.5%, Acros) were mixed in a 3:2 molar ratio in demineralized water resulting in a bright green nickel citrate solution. Typically, 0.66 ml of the solution was added to 1 g high surface area graphite (HSAG 500) under static vacuum. HSAG 500 is high purity (99.9%) graphitic carbon from Timcal Switzerland. It contains mesopores (mostly 2-3 nm) up to 20 nm in diameter, has 500 $m^2 g^{-1}$ BET surface area and a total pore volume of 0.66 $cm^3 g^{-1}$. The impregnated sample was dried in air overnight at 120 °C, calcined by heating to 450 °C under N_2 flow and reduced in a flow of a gas mixture of 5% H_2 in N_2 with 1 h dwell at 400 °C.

25 wt% $LiBH_4$ (Acros-organics 95% pure) was incorporated into the Ni–impregnated carbon by melt infiltration. The required amounts of Ni/C nanocomposites and $LiBH_4$ were placed in a graphite sample holder and inserted into a stainless steel autoclave. An initial pressure of 50 bar H_2 was applied and the sample was heated at 3 °C min^{-1} to 295 °C and allowed to stay for 30 min at 295 °C at a final pressure of ≈ 100 bar H_2. The sample was then allowed to cool down to room temperature, the pressure was released and the samples were stored in a glove box. Apart from Ni impregnation, all other sample handling was under Ar

atmosphere in a glove-box (contamination typically less than 1 ppm of O_2 and H_2O) to avoid exposure and contamination. Nanocomposites containing 25wt% $LiBH_4$ and different Ni loadings on carbon (0, 5 and 10 wt %) were synthesized and labelled according to the weight percentage of these materials in the composites. For example the sample $25LiBH_4/3.75Ni/C$ contains 25 wt% $LiBH_4$, 3.75 wt% Ni and 71.25 wt% C.

Sample characterization was performed using X-Ray Diffraction (XRD), N_2-physisorption, Transmission Electron Microscopy (TEM), Extended X-ray Absorption Fine Structure spectroscopy (EXAFS) and solid state Nuclear Magnetic Resonance (NMR) measurements. All measurements (except TEM) were done in air tight sample holders. XRD patterns were obtained at room temperature from 18 to 80° 2θ with a Bruker-AXS D-8 Advance X-ray diffractometer setup using $CoK\alpha_{1,2}$ radiation with λ= 1.790 Å. The Ni crystallite sizes were derived from analysis of the width of the 52.2° 2θ diffraction peak using the Debye-Scherrer method and assuming a Scherrer constant of 0.94 and corrected for experimental line broadening. N_2-physisorption measurements were performed at -196 °C, using a Micromeritics Tristar 3000 apparatus. The pore size distributions of the samples were calculated from the desorption branch using BJH theory with the Harkins and Jura thickness equation. Transmission Electron Micrographs (TEM) were obtained using a Tecnai 20F microscope operating at 200 kV acceleration voltage, equipped with a LaB_6 electron source and a TWIN objective lens. Particle size histograms were determined from dark-field images analyzing 100-200 crystallites. The electron diffraction pattern was determined using a camera constant of 720

Nickel K-edge (8333 eV) EXAFS spectra of the as-prepared, dehydrogenated and rehydrogenated Ni- containing nanocomposites($25LiBH_4/3.75Ni/C$) were recorded at beamline C of the DORIS III storage ring at the Deutsches Elektronen-Synchrotron (DESY), Hamburg. The beamline is equipped with a Si (111) double-crystal monochromator, which is detuned to 60 % of the Bragg peak intensity to suppress higher harmonics. About 50 mg sample was pressed into a pellet, mounted to the cell, and transferred to the beamline without air exposure. The samples were measured in transmission mode at room temperature in Ar flow. A 7 μm thick Ni foil (99.99%) and Ni_2B power (99.5%, Acros) were measured at liquid nitrogen temperature as reference materials. Data reduction was performed with

XDAP[17] in order to obtain the Fourier transformed (FT) EXAFS, phase-uncorrected Fourier transformed $\chi(k)$ EXAFS and the FEFF fits from the measured spectra. At least three scans from a sample were averaged. The edge-energy was determined from the maximum of the first derivative of the spectrum using the Ni foil as a standard reference. The background signal before the edge jump was fitted with a smooth spline, and substracted[18]. The obtained data were normalized by setting the signal height (50 eV) after the edge to 1. Experimental data are fitted in R-space with k^2 weighting using the difference file techniques in real space[19] and the quality of the fit checked by applying k^1 and k^3 weightings

Solid-state NMR experiments were performed on a 600 MHz Varian spectrometer using a 2.5 mm HX MAS probe. ^{11}B single pulse excitation spectra were obtained using a short hard pulse of 0.20 μs at effective rf-field strength of 140 kHz after taking pulse rise and decay times into account. A sample spinning speed of 15 kHz was applied. The ^{11}B spectra were referenced with respect to an aqueous solution of H_3BO_3 (δ = 19.6 ppm) and shifts are given relative to $BF_3 \cdot OEt_2$ (δ = 0 ppm).

Hydrogen release properties of the nanocomposites was measured by temperature programmed desorption (TPD) using a Micromeritics AutoChem II 2920 apparatus. 100 to 150 mg of sample was heated at 5 °C/min from room temperature to 400 or 450 °C in 25 ml min^{-1} Ar flow with a dwell time of 25 min at the maximum temperature. The composition of the desorbed gas was analyzed using a quadrupole mass spectrometer (MS) with purified Ar as carrier gas. Rehydrogenation of the desorbed samples was performed in an autoclave by heating at 2 °C min^{-1} with initial pressure of 20 bar H_2 to 320 °C and dwelling at 320 °C for 120 min at a final pressure of 40 bar. Isothermal manometric hydrogen uptake measurement was done using a Sievert type apparatus (PCTPro-2000, Hy-Energy & Setaram, pressure measurement accuracy: 1% of reading). About 150 mg sample which had been dehydrogenated in a stainless steel sample holder (~ 5 ml) at 400 °C, is evacuated for 1 h and subsequently rehydrogenated by charging the sample with an initial pressure of approximately 28 bar H_2 at 330 °C (reservoir volume of 4.6 ml). The hydrogen uptake by the nanocomposite was evaluated from the pressure drop (final pressure typically > 15 bar). Prior to hydrogen uptake measurement, the volume of the sample holder at 330 °C was determined by volume calibration using Ar.

Results and Discussion

4.3 Hydrogen Sorption

Figure 4.1 show the hydrogen release from samples heated to 400 °C and dwelled at this temperature for 25 min. As a reference the desorption pattern from 25 wt% $LiBH_4$ melted with non porous graphite (BET surface area 7 m^2/g) is included. Hydrogen release started in the $LiBH_4$/graphite sample around 280 °C with two minor hydrogen release peaks around 280 °C and 350 °C. The majority of the hydrogen is desorbed only at higher temperatures as reported in literature[9, 20]. For the $LiBH_4$/C nanocomposite, hydrogen desorption started around 200 °C, with a maximum release rate at 350 °C. The onset temperature of hydrogen release is slightly lower (below 200 °C) in the Ni containing nanocomposites. Increasing the Ni concentration from 3.75 to 7.5 wt% did not have a significant effect on the hydrogen release. Quantitative analysis of the hydrogen desorption shows that all the nanocomposites had released about 14 wt% H_2 per g $LiBH_4$ (3.5 wt% H_2/g sample) after dwelling for 25 min at 400 °C. Ni is a typical catalyst for hydrogen dissociation and recombination. However its addition did not have a significant effect on the hydrogen desorption, suggesting that either the recombination of

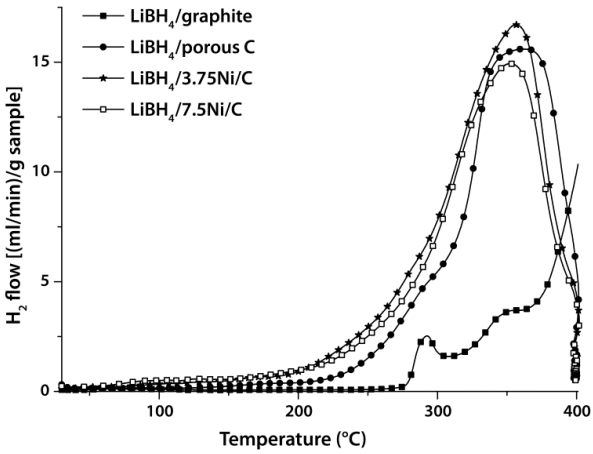

Figure 4.1: Hydrogen release from 25 wt% $LiBH_4$ melted with: non porous graphite, nanoporous carbon material, and nanoporous carbon material doped with different concentration (wt %) of Ni as indicated.

atomic hydrogen to molecular hydrogen is not the rate limiting step in the dehydrogenation of $LiBH_4$ or that the Ni has reacted during synthesis

To evaluate the reversible hydrogen uptake behaviour of the nanocomposites at mild conditions, the dehydrogenated samples were rehydrogenated in an autoclave at 320 °C, 40 bar H_2 for 120 min. Figure 4.2 shows the hydrogen release from the rehydrogenated samples upon heating to 400 °C and dwelling at this temperature for 25 min. Only a negligible amount of hydrogen was released from the rehydrogenated $LiBH_4$/graphite sample. This suggests rehydrogenation was not successful which is in line with the fact that bulk $LiBH_4$ requires about 600 °C and 350 bar H_2 for rehydrogenation [21, 22]. In contrast, the rehydrogenated $LiBH_4$/porous carbon nanocomposites released about 6 wt% H_2/g $LiBH_4$ (1.5 wt% H_2/g sample) indicating that hydrogen was absorbed during rehydrogenation. Surprisingly, the two Ni containing samples released about 9.2 wt% H_2 (2.3 wt% H_2/g sample). Similar to the first hydrogen release cycle, increasing the concentration of Ni did not lead to an increase in the hydrogen desorption rate nor in the amount of hydrogen released in the second cycle. However, in contrast to the first hydrogen desorption cycle, in the second cycle there is a clear difference in the hydrogen desorption pattern of the nanocomposites with and without Ni. With Ni the onset temperature of the hydrogen release was significantly lower, and more hydrogen

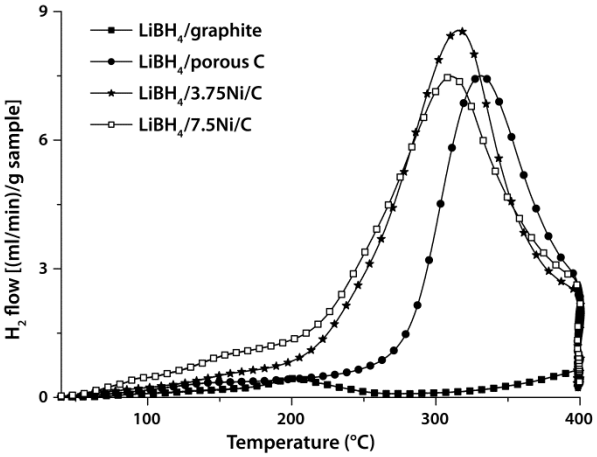

Figure 4.2: Hydrogen release from the samples after rehydrogenation for 120 min at 320 °C and 40 bar H_2

was released between 250 and 300 °C. These differences in the hydrogen release profiles for the rehydrogenated nanocomposites suggest that the nanostructure of the $LiBH_4$ formed after rehydrogenation might be influence by the presence of Ni,

or that a Ni-containing catalytic active component was only formed after the first dehydrogenation.

To further investigate the influence of the Ni during rehydrogenation, we gravimetrically followed the H_2 uptake of the nanocomposites after the first desorption, rehydrogenating at 320 °C under 40 bar H_2 pressure. Figure 4.3 shows that negligible amount of H_2 was absorbed in the sample containing $LiBH_4$ and graphite. The confined $LiBH_4$ without Ni absorbed about 6 wt% H_2/(g $LiBH_4$) while the Ni containing sample absorbed about 10 wt% H_2/(g $LiBH_4$), in fair agreement with the amount of H_2 released in the second desorption run. It is clear that the uptake of H_2 rather than the release is the critical step limiting the reversibility. Especially for the sample without Ni, it seems that the uptake levels off after about 1 h of absorption.

Although the gravimetric hydrogen uptake measurements is very accurate in measuring the amount of H_2 absorbed, it does not accurately reflect the initial uptake kinetics (as ~ 40 min are needed to reach the designated pressure of 40 bar). Additional manometric (volumetric) uptake measurements at initial pressure of ~ 28 bar show a very fast initial hydrogen uptake (figure 4.4). Hence it seems that a

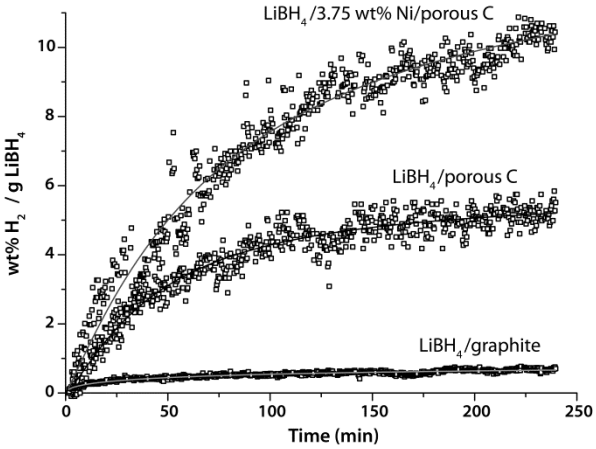

Figure 4.3: Hydrogen uptake of $LiBH_4$(Ni)/C nanocomposites measured gravimetrically at 320 °C under 40 bar H_2.

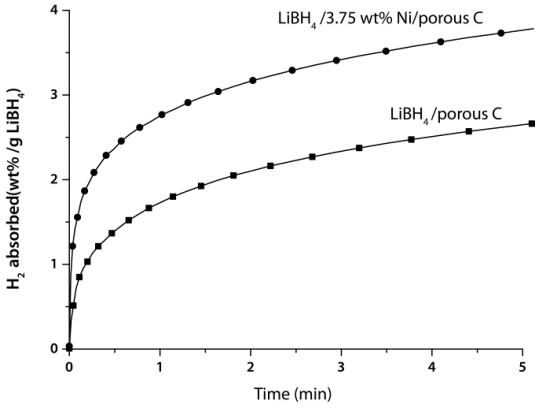

Figure 4.4 Manometric H_2 uptake measurements for the 25 wt% $LiBH_4$/C nanocomposites with and without Ni.

fraction of the material can be hydrogenated very rapidly under mild conditions, while for another part of the sample the H_2 uptake is much more sluggish.
Xia et al recently showed that $LiBH_4$ ball milled with Ni can reversibly absorb about 12 wt % H_2 only when rehydrogenated for 30 h at 600 °C and 100 bar H_2 [6]. Hence, the results presented above clearly show the effectiveness of combining nanoconfinement and Ni addition in enhancing reversibility of the hydrogen release from $LiBH_4$ under mild conditions. Remarkable is the fact that the samples can be partially rehydrogenated at pressures as low as 28 bar H_2.

4.4 Bulk Characterization

It is interesting to investigate the role of Ni in more detail. To this end, possible structural changes occurring in the nanocomposites during the different stages were analyzed using XRD and TEM. Figure 4.5 shows the XRD patterns of the porous carbon, 5wt% Ni/C nanocomposites, and the $LiBH_4$/Ni/C nanocomposites after synthesis, dehydrogenation and rehydrogenation. The XRD pattern of the carbon shows three diffraction lines at 31° 52° and 64° 2θ that are typical for turbostratic carbon materials. In addition to these diffraction lines, the Ni impregnated carbon shows two broad diffraction peaks around 53° and 60° 2θ that are due to crystalline Ni with an average crystallite size of 6 nm. After melt infiltration with $LiBH_4$, the Ni diffraction lines have disappeared. Upon dehydrogenation, no diffraction line

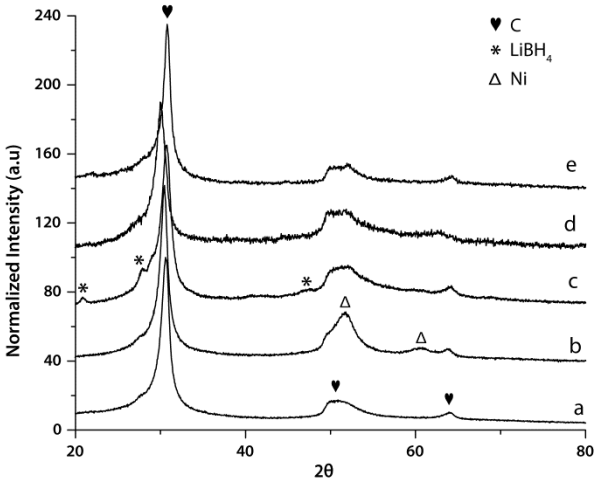

Figure 4.5: XRD patterns of pure porous carbon (a) pure porous carbon, 5wt%Ni/C (b); and 25$LiBH_4$/3.75Ni/C nanocomposites after synthesis(c), dehydrogenation (d) and rehydrogenation (e)

other than that of the carbon material was seen and this is same for the rehydrogenated samples. This shows that the crystalline Ni nanoparticles are no longer present after melt infiltration, probably due to reaction with $LiBH_4$ during melt. For the $LiBH_4$, only very weak diffraction lines were seen after melt infiltration (figure 4.5, spectra c) indicating that the material is not crystalline and most likely confined in the nanopores[9, 23]. A comparison of pattern (d) and (e) shows a reversible shift in the C(002) diffraction line from 31° to 29.9 2θ and back upon dehydrogenation and rehydrogenation. This is ascribed to reversible intercalation of Li into the graphitic nanoporous carbon material to form $Li_{0.23}C_6$ as discussed in Chapter 3. Similar behaviour is observed for the samples with and without Ni indicating that presence of Ni does not influence lithium intercalation into the carbon.

To investigate whether the Ni nanoparticles had withstood melt infiltration with $LiBH_4$, we further investigated the microstructure of the nanocomposites by acquiring TEM micrographs of the samples at different stages of treatment. A representative TEM micrograph of the 5 wt% Ni/C nanocomposites (figure 4.6A) shows well dispersed and homogenously distributed Ni nanoparticles with a number-averaged particle size of 5-6 nm which is in good agreement with the volume-averaged crystallite size of 6 nm obtained from XRD pattern using

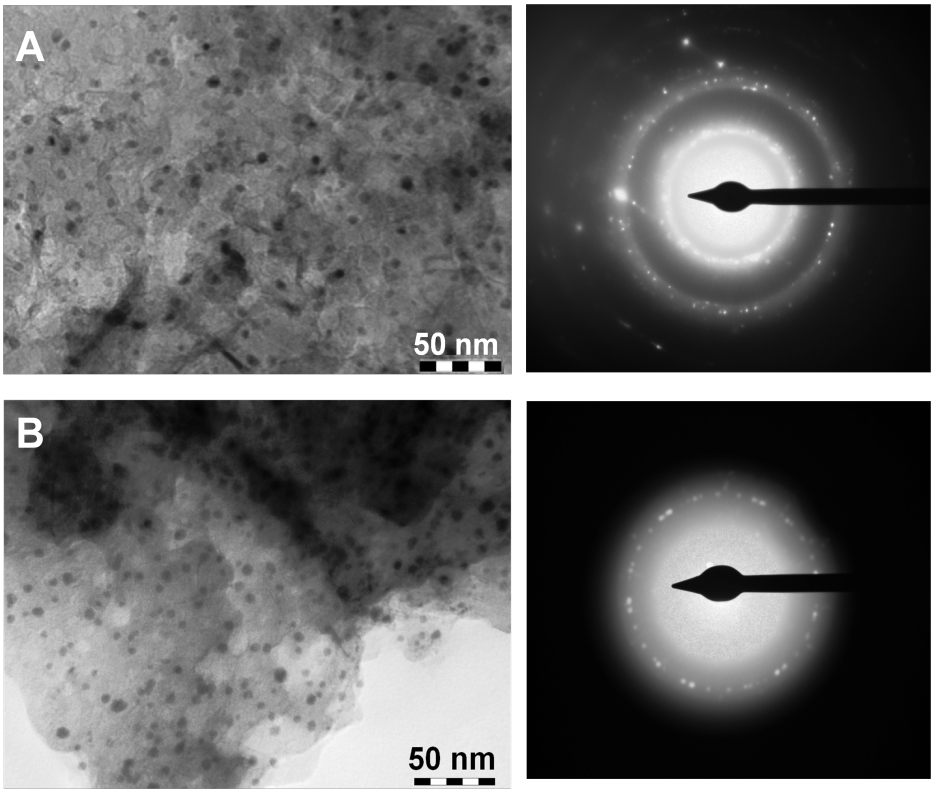

Figure 4.6 TEM images and electron diffraction of (A) 5%wt% Ni/C; (B) 5 wt% Ni/C after melt infiltrating with 25 wt% $LiBH_4$ ($25LiBH_4/3.75Ni/C$)

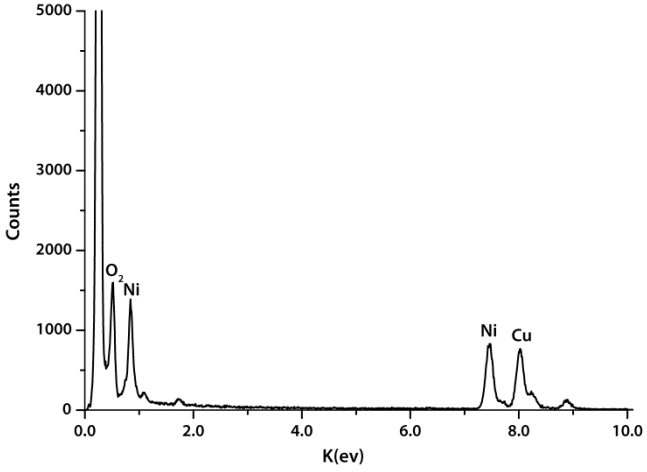

Figure 4.7: EDX signal from $LiBH_4$/Ni/C nanocomposite after synthesis (of figure 4.6B)

Scherrer formula. Analysis of the electron diffraction pattern (data not shown) shows that the signal is due to diffraction from the graphitic carbon (d-values of 1.68 and 1.54 Å) and Ni (2.03 and 1.25 Å). Figure 4.6b shows that after melt infiltrating the Ni/C nanocomposites with 25 wt% $LiBH_4$ (to $LiBH_4$/Ni/C nanocomposites), nanoparticles with average size of 7 nm were still present but the electron diffraction detects only graphitic carbon (d values of 1.67 and 1.54 Å) as a crystalline phase, showing that these nanoparticles are amorphous. Energy-dispersive X-ray (EDX) measurement on the same sample reveals that the nanoparticles contain Ni (figure 4.7). $LiBH_4$ cannot be reliably imaged with TEM due to weak scattering of electrons by the light elements Li and B. The electron micrographs of the dehydrogenated and rehydrogenated samples (data not shown here) looked similar to that of the melt infiltrated sample, with amorphous Ni-containing nanoparticles. Apparently the Ni has reacted during melt infiltration with the $LiBH_4$, forming amorphous or non crystalline nanoparticles that are rich in Ni, and roughly maintain their morphology upon cycling.

Carbon has a low surface energy, and Ni has been used as an effective wetting agent for melt infiltration of carbon with Mg[24, 25]. Hence we investigated the influence of Ni on the wetting of the nanoporous carbon material by $LiBH_4$. However as shown in figure 4.8, the wetting of carbon with molten $LiBH_4$ does not

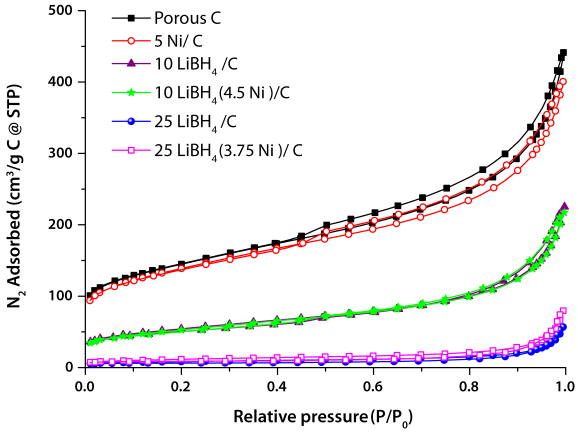

Figure 4.8 N_2-physisorption measurements for nanoporous carbon, 5 wt% Ni/nanoporous carbon nanocomposites and $LiBH_4$ (Ni)/carbon nanocomposites with different wt% loadings of $LiBH_4$ and Ni as indicated. Addition of Ni did not have any significant impact on the pore volume lost by the carbon.

seem critical, and no significant difference is seen in the pore volume filled with and without Ni, even when the $LiBH_4$ loading was varied.

4.5 Characterization of the Ni chemical environment

As these particles are non-crystalline, Extended X-ray Absorption Fine Structure (EXAFS) at the Ni K-edge was used to characterize the local environment of Ni. Figure 4.9 shows the phase-uncorrected Fourier transform (FT) of the EXAFS spectra of the 5 wt% Ni/C, and the $LiBH_4$/Ni/C nanocomposites after synthesis,

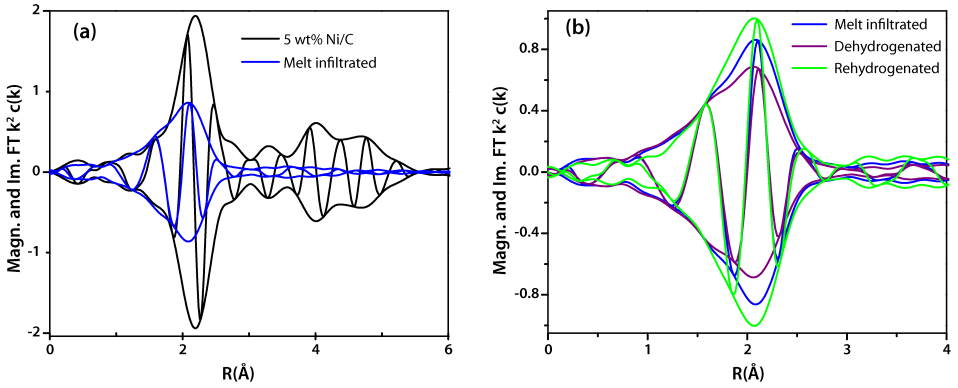

Figure 4.9: Magnitude and Imaginary part of the phase-uncorrected Fourier transformed (FT) $k^2\chi$ (k) for (a) 5 wt % Ni/C and the $25LiBH_4/3.75Ni/C$ nanocomposite after melt infiltration, (b) melt infiltrated, dehydrogenated and rehydrogenated states of the $25LiBH_4/3.75Ni/C$ nanocomposites.

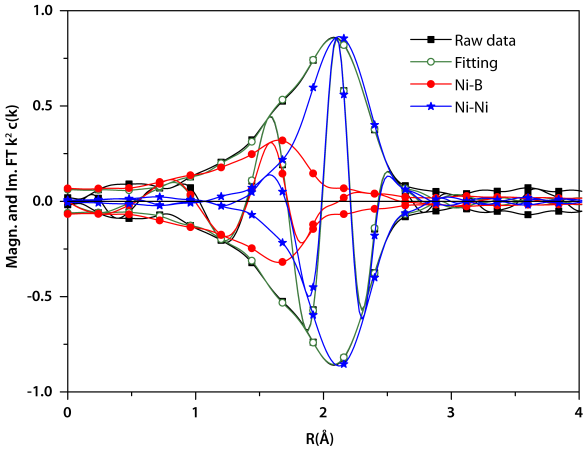

Figure 4.10: Magnitude and Imaginary part of the phase-uncorrected Fourier transformed χ(k) for the as-synthesized $LiBH_4$/Ni/C nanocomposites. The fit is optimized with Δk=3-13 $Å^{-1}$ and ΔR=1.2-3.0 with the k-weighting parameter of 2. The individual contributions of Ni-B and Ni-Ni are also included.

dehydrogenation and rehydrogenation. For 5 wt% Ni/C a main peak is visible around 2.2 Å which is representative for Ni-Ni scattering in metallic Ni (figure 4.9 (a)). The signals at larger distances are representative for Ni present in higher coordination shells as expected for crystalline metallic Ni. The main peak at 2.2 Å shifted to 2.1 Å and decreased in intensity after melt infiltration of $LiBH_4$. This indicates a significant change of the coordination around Ni after melt infiltration. In addition, after melt infiltration, no higher shells were observed which suggests that the sample lacked long range order, or consisted of nanosized clusters, in line with XRD and TEM results.

The fitting results and theoretical crystal structure of Ni-B compounds are listed in table 4.1. The quality of the fit can be appreciated from figure 4.10. For the Ni/C, Ni was surrounded by 8 Ni-neighbors at 2.47 Å indicative of Ni particles of a few nanometers. After melt infiltration with $LiBH_4$, Ni was surrounded by 4.6 B neighbors at 2.07 Å and 4.2 Ni neighbors at 2.47 Å. By comparing these values to those of the reference compounds (Ni, NiB, Ni_2B and Ni_3B), it can be concluded that the structure of the sample is most similar to that of Ni_2B. A smaller amount of other phases must be present as well, although the data do not allow a more detailed analysis of the composition. The Ni-Ni distances in Ni_2B and Ni_3B are close to that in metallic Ni, making it difficult to discuss the exact nature of the Ni-Ni scattering. Large E_0 shifts were observed for Ni-Ni and Ni-B scattering in the samples indicating that coordination and/or nature of the scattering in the references used to fit the data was different from that in the samples. For Ni-Ni this is logical as a Ni-foil was used to extract the reference data while Ni-Ni in Ni-B compounds is different in nature. For Ni-B this is more difficult to explain since Ni_2B was used as reference. However the fitting of the data does not show a perfect fit with Ni_2B as discussed above which might indicate the sample consist of a number of phases which makes the choice of a proper reference challenging.

A comparison of the FT EXAFS data after melt infiltration, dehydrogenation and rehydrogenation is shown in Figure 4.9 (b). After dehydrogenation the signal at 2.1 Å decreased in intensity and increased again after rehydrogenation. The fitting results of these samples are shown in Table 4.1. After dehydrogenation the Ni-B coordination number increased, from 4.6 to 5.3, while the Ni-Ni coordination

Table 4.1: Local structure parameters including neighbour type, inter atomic distance (R) and Debye-Waller factor (σ^2) for Ni in the 5 wt % Ni/C and $LiBH_4$/Ni/C nanocomposites afer melt infiltration(melt), dehydrogenation (Deh.) and rehydrogenation (Reh.). The fit is optimized with Δk=3-13 $Å^{-1}$ and ΔR=1.2-3.0 with the k-weighting parameter of 2. The parameters of NiB, Ni_2B, Ni_3B and Ni references are included for comparison.

Sample	Shell	N	$\Delta\sigma^2$ (10^{-3} $Å^2$)	R (Å)	ΔE_0 (ev)	k^2-variance Abs.	Img.
5% Ni/C	Ni-Ni	8.1	1.46	2.474	0.03	0.09	0.11
Melt	Ni-B	4.6	1.62	2.07	10.7	0.06	0.28
	Ni-Ni	4.2	5.83	2.47	7.9		
Deh.	Ni-B	5.3	2.56	2.07	11.4	0.03	0.25
	Ni-Ni	3.4	6.03	2.48	8.4		
Reh.	Ni-B	3.8	2.19	2.07	11.9	0.08	0.28
	Ni-Ni	6.9	9.08	2.46	9.4		
NiB [36]	Ni-B	7	---	2.16	---	---	---
	Ni-Ni	6	---	2.60	---	---	---
	Ni-Ni	4	---	2.95	---	---	---
Ni_2B [35]	Ni-B	4	---	2.14	---	---	---
	Ni-Ni	3	---	2.40	---	---	---
	Ni-Ni	8	---	2.67	---	---	---
Ni_3B [34]	Ni-B	3	---	2.13	---	---	---
	Ni-Ni	8	---	2.50	---	---	---
	Ni-Ni	3	---	2.74	---	---	---
Ni	Ni-Ni	12	---	2.49	---	---	---

decreased from 4.2 to 3.4. This indicates that more B reacted with Ni during dehydrogenation which can be expected since dehydrogenation resulted in the formation of significant amounts of B. After rehydrogenation the Ni-B coordination decreased again from 5.3 to 3.8 while the Ni-Ni coordination increased again from 3.4 to 6.9. This shows the reversible behavior of the sample. Since the Ni-Ni coordination is higher than in the melt infiltrated sample and the Ni-B is lower, it is tempting to speculate that more Ni_3B is formed after

rehydrogenation. This is in line with the stability of different Ni-B compounds at room temperature: $Ni_3B > NiB > Ni_2B$[26].

The EXAFS results show that nickel borides (Ni_xB) are formed after synthesis, dehydrogenation and rehydrogenation of the $LiBH_4$/Ni/C, with the value of x depending on the state. Therefore the improved reversibility in this system is related to the formation of the nickel boride nanoparticles. Although nickel boride has been used as a catalyst in hydrogenation processes [27-32], an interesting question is how does Ni_xB improve the reversible hydrogen uptake in the $LiBH_4$/Ni/C nanocomposites. A possible explanation is that the nickel boride acts as hydrogenation catalyst, lowering the barrier for the formation of borohydride anions (BH_4^-) as recently reported in literature[33]. In this case it is expected that the rate at which hydrogen is absorbed in the Ni containing nanocomposites will be higher, reaching the maximum capacity faster than the sample without Ni. However an investigation of the hydrogen uptake behavior (figure 4. 3 and 4.4) in the nanocomposites shows that the nickel boride does not only enhance the overall uptake rates but its presence also seems to enlarge the fraction of the material that can be rehydrogenated under mild conditions. Other possible roles of nickel boride in the nanocomposite could be to act as a nucleation site for the reversible formation of $LiBH_4$ from the dehydrogenated products, and/or that its presence influences the microstructure of the nanocomposites during desorption and rehydrogenation.

4.6 NMR investigation of the nanostructure

EXAFS is not suitable to investigate the lighter elements such as Li and B. Therefore, we further investigated the B-containing compounds present in the nanocomposites at different stages using solid-state ^{11}B NMR. Note that the Ni-containing species will not be evident from the NMR due to a paramagnetic effect of the Ni. This effect results in a very fast relaxation of the ^{11}B magnetization and/or a distortion of the local magnetic field homogeneity and the intensity will be smeared out in the baseline. Therefore an accurate quantification of the phases is not possible at present due to unknown effects of the carbon susceptibility on the local RF field strength and penetration depths and possible paramagnetic effects of

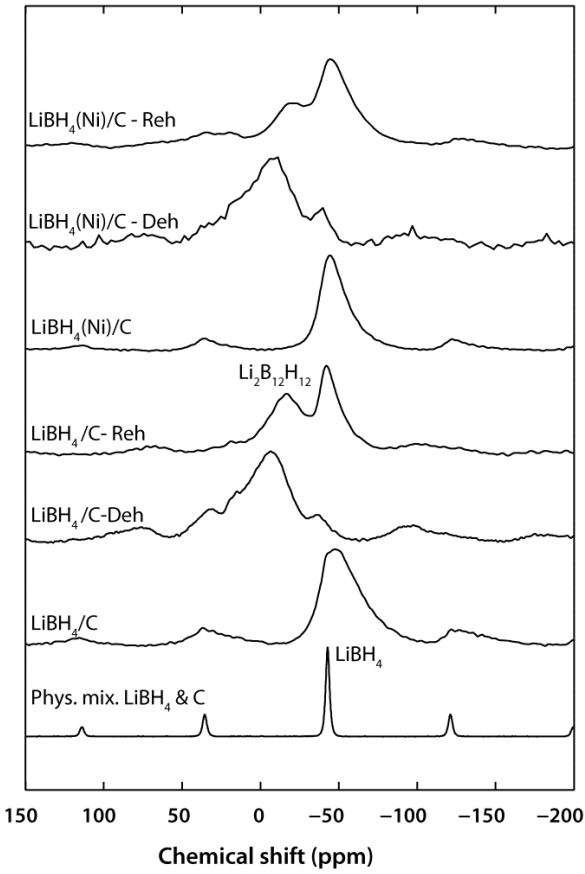

Figure 4.11 Solid-state ^{11}B NMR spectra of a physical mixture of 25 wt% $LiBH_4$ and porous carbon, and the melt infiltrated nanocomposites with and without Ni after synthesis, dehydrogenation(deh) and rehydrogenation (reh) at 320 °C, 40 bar H_2

the Ni. Figure 4.11 shows ^{11}B NMR spectra of the nanocomposites after synthesis, dehydrogenation and rehydrogenation, including the spectra for $LiBH_4$ physically mixed with porous carbon. The ^{11}B spectrum of a physical mixture of $LiBH_4$ and porous carbon shows a well defined sharp peak at - 42 ppm. The $LiBH_4$ lineshape is clearly broadened in both nanocomposites after synthesis due to close contact of the $LiBH_4$ with the carbon. The broadening can be explained by a variation in local magnetic field due to the anisotropic susceptibility of the carbon. In addition, we expect a broadening due to the higher disorder, which results in a distribution in chemical shift and quadrupolar interaction parameters, as reported for $NaAlH_4$ confined in nanoporous carbon[34, 35]. After dehydrogenation, a broad (50 to -25 ppm) peak is seen in both sample which is most likely due to elemental B[36] and/or $Li_2B_{12}H_{12}$. For the rehydrogenated samples in addition to the peak due to $LiBH_4$,

both samples show the presence of another peak around -15 ppm chemical shift and is assigned to the intermediate compound $Li_2B_{12}H_{12}$[37, 38]. However two major differences exist between the rehydrogenated samples. Firstly, the intensity of $Li_2B_{12}H_{12}$ is smaller in the sample with Ni, which is in line with the fact that more of the desorbed components are rehydrogenated back to $LiBH_4$ in this sample. Secondly, the rehydrogenated Ni containing samples have a $LiBH_4$ peak which is very similar to that in the as-synthesized samples both in the intensity and line width, while the sample without Ni shows a narrower $LiBH_4$ peak with lower intensity compared to both the as-synthesized sample and the rehydrogenated Ni containing nanocomposites. These results suggest a change in the nanostructure or distribution of $LiBH_4$ in the carbon material for the sample without Ni upon cycling, with a tendency toward phase separation and increased cluster size. Since the broadening of the linewidth is related to the contact between the $LiBH_4$ and porous C, [34, 35] the $LiBH_4$ in the as synthesized sample possibly has a closer contact with the carbon than in the rehydrogenated sample. For the Ni containing sample the NMR data suggest that the $LiBH_4$ distribution is retained upon cycling as similar lineshapes are observed before and after rehydrogenation. This could also explain the observed lower desorption temperatures in the rehydrogenated nanocomposites with Ni compared to the sample without Ni (figure 4.2). Therefore the observed differences in the ^{11}B NMR of the rehydrogenated nanocomposites shows that the presence of the nickel boride nanoparticles influenced the structural evolution of the boron phases in the compound upon dehydrogenation and rehydrogenation thereby limiting the redistribution of the active phases during hydrogen release and uptake.

4.7 Conclusion

We have shown that the hydrogen sorption properties of $LiBH_4$ were markedly increased by the synergetic effects of nanoconfinement and Ni addition. Confining $LiBH_4$ in nanoporous carbon resulted in a 100-150 °C decrease in the dehydrogenation temperature compared to bulk $LiBH_4$. The amount of material that could be rehydrogenated rapidly and under mild conditions was further enhanced significantly upon the addition of Ni to the system. We studied the

structure and phase evolution in the $LiBH_4$/Ni/C nanocomposites, and the role of Ni, during hydrogen cycling. XRD and TEM measurements show that after sample preparation Ni-containing nanoparticles are present. However, they are neither metallic Ni nor crystalline. EXAFS revealed that the local structure of this nickel boride phase is most similar to that of Ni_2B, although a smaller amount of other phases was present as well. Interestingly, upon hydrogen cycling, the chemical environment in this nanophase changes reversibly, with a higher Ni-B coordination in the dehydrogenated state. Ni_xB is known to be able to act as a hydrogenation catalyst. However, ^{11}B NMR results showed that the presence of Ni also influenced the microstructural evolution of the $LiBH_4$. In the absence of Ni a change in the nanoconfined $LiBH_4$ microstructure upon cycling was observed, while this was not the case in the presence of Ni. From these structural studies it has become clear that Ni does not simply act as a (de)hydrogenation catalyst in these systems. It reacts to form Ni_xB nanoparticles which reversibly interact with the boron being formed upon dehydrogenation of the $LiBH_4$. The presence of these particles enhances the stability of the structure of the nanoconfined $LiBH_4$ upon cycling.

Acknowledgements

We acknowledge M. (Rien) van Zwienen, A. van der Eerden, A. Mens, and V. Koot, for their technical support, and NWO-Vidi 016.072.316 for financial support. The Nederlandse Organisatie voor Wetenschappelijk Onderzoek (NWO) is acknowledged for support of the "Solid-state NMR facility for advanced materials science". Support of HASYLAB and HASYLAB staff, Project Number II-20090124 EC, is gratefully acknowledged for the EXAFS, Johannes H. Meeldijk for TEM measurements and Timcal Switzerland for providing the carbon.

References

1. A. Züttel, S. Rentsch, P. Fischer, P. Wenger, P. Sudan, P. Mauron and C. Emmenegger, *J. Alloys Compd.*, 2003, **356-357**, 515-520.
2. M. Au, A. R. Jurgensen, W. A. Spencer, D. L. Anton, F. E. Pinkerton, S. J. Hwang, C. Kim and R. C. Bowman, *J. Phys. Chem. C*, 2008, **112**, 18661-18671.

3. Z. Z. Fang, X. D. Kang, P. Wang and H. M. Cheng, *J. Phys. Chem. C*, 2008, **112**, 17023-17029.
4. J. J. Vajo, S. L. Skeith and F. Mertens, *J. Phys. Chem. B*, 2005, **109**, 3719-3722.
5. M. S. Wellons, P. A. Berseth and R. Zidan, *Nanotechnology*, 2009, **20**.
6. G. L. Xia, Y. H. Guo, Z. Wu and X. B. Yu, *J. Alloys Compd.*, 2009, **479**, 545-548.
7. J. Xu, X. B. Yu, Z. Q. Zou, Z. L. Li, Z. Wu, D. L. Akins and H. Yang, *Chem. Commun.*, 2008, 5740-5742.
8. B. Bogdanovic and M. Schwickardi, *J. Alloys Compd.*, 1997, **253**, 1-9.
9. P. Ngene, P. Adelhelm, A. M. Beale, K. P. de Jong and P. E. de Jongh, *J. Phys. Chem. C*, 2010, **114**, 6163-6168.
10. Y. Zhang, W.-S. Zhang, M.-Q. Fan, S.-S. Liu, H.-L. Chu, Y.-H. Zhang, X.-Y. Gao and L.-X. Sun, *J. Phys. Chem. C*, 2008, **112**, 4005-4010.
11. L. Mosegaard, B. Moller, J. E. Jorgensen, Y. Filinchuk, Y. Cerenius, J. C. Hanson, E. Dimasi, F. Besenbacher and T. R. Jensen, *J. Phys. Chem. C*, 2008, **112**, 1299-1303.
12. X. B. Yu, D. A. Grant and G. S. Walker, *J. Phys. Chem. C*, 2008, **112**, 11059-11062.
13. S. M. Opalka, X. Tang, B. L. Laube and T. H. Vanderspurt, *Nanotechnology*, 2009, **20**.
14. M. An and A. Jurgensen, *J. Phys. Chem. B*, 2006, **110**, 7062-7067.
15. X. D. Kang, P. Wang, L. P. Ma and H. M. Cheng, *Applied Physics A*, 2007, **89**, 963-966.
16. R. Bogerd, P. Adelhelm, J. H. Meeldijk, K. P. de Jong and P. E. de Jongh, *Nanotechnology*, 2009, **20**, 204019.
17. M. Vaarkamp, J. C. Linders and D. C. Koningsberger, *Physica B*, 1995, **208-209**, 159-160.
18. J. W. Cook Jr and D. E. Sayers, *J. Appl. Phys.*, 1981, **52**, 5024-5031.
19. D. C. Koningsberger, B. L. Mojet, G. E. Van Dorssen and D. E. Ramaker, *Top. Catal.*, 2000, **10**, 143-155.
20. A. F. Gross, J. J. Vajo, S. L. Van Atta and G. L. Olson, *J. Phys. Chem. C*, 2008, **112**, 5651-5657.

21. P. Mauron, F. Buchter, O. Friedrichs, A. Remhof, M. Bielmann, C. N. Zwicky and A. Zuttel, *J. Phys. Chem. B*, 2008, **112**, 906-910.
22. S. Orimo, Y. Nakamori, G. Kitahara, K. Miwa, N. Ohba, S. Towata and A. Züttel, *J. Alloys Compd.*, 2005, **404**, 427-430.
23. Z. Z. Fang, P. Wang, T. E. Rufford, X. D. Kang, G. Q. Lu and H. M. Cheng, *Acta Mater.*, 2008, **56**, 6257-6263.
24. A. F. Gross, C. C. Ahn, S. L. Van Atta, P. Liu and J. J. Vajo, *Nanotechnology*, 2009, **20**.
25. R. Bogerd, P. Adelhelm, J. H. Meeldijk, K. P. De Jong and P. E. De Jongh, *Nanotechnology*, 2009, **20**.
26. O. Teppo and P. Taskinen, *Mater. Sci. Technol.*, 1993, **9**, 205-212.
27. H. C. Brown and C. A. Brown, *J. Am. Chem. Soc.*, 1963, **85**, 1005-1006.
28. R. Paul, P. Buisson and N. Joseph, *Ind. Eng. Chem. Res.*, 1952, **44**, 1006-1010.
29. C. M. Kaufman and B. Sen, *Dalton Trans.*, 1985, 307-313.
30. C. A. Brown and V. K. Ahuja, *J. Org. Chem.*, 1973, **38**, 2226-2230.
31. J. C. Walter, A. Zurawski, D. Montgomery, M. Thornburg and S. Revankar, *J. Power Sources*, 2008, **179**, 335-339.
32. D. Hua, Y. Hanxi, A. Xinping and C. Chuansin, *Int. J. Hydrogen Energy*, 2003, **28**, 1095-1100.
33. J. Graetz, S. Chaudhuri, T. T. Salguero, J. J. Vajo, M. S. Meyer and F. E. Pinkerton, *Nanotechnology*, 2009, **20**.
34. P. Adelhelm, J. B. Gao, M. H. W. Verkuijlen, C. Rongeat, M. Herrich, P. J. M. van Bentum, O. Gutfleisch, A. P. M. Kentgens, K. P. de Jong and P. E. de Jongh, *Chem. Mater.*, 2010, **22**, 2233-2238.
35. M. H. W. Verkuijlen, J. B. Gao, P. Adelhelm, P. J. N. van Bentum, P. E. de Jongh and A. P. M. Kentgens, *J. Phys. Chem. C*, 2010, **114**, 4683-4692.
36. N. Brun, R. Janot, C. Sanchez, H. Deleuze, C. Gervais, M. Morcrette and R. Backov, *Energy Environ. Sci*, 2010, **3**, 824-830.
37. O. Friedrichs, A. Remhof, S. J. Hwang and A. Züttel, *Chem. Mater.*, 2010, **22**, 3265-3268.
38. S. J. Hwang, R. C. Bowman, J. W. Reiter, J. Rijssenbeek, G. L. Soloveichik, J. C. Zhao, H. Kabbour and C. C. Ahn, *J. Phys. Chem. C*, 2008,**112**,3164-3169.

Chapter 5

$NaBH_4$ in Nanoporous Carbon materials

Abstract

$NaBH_4$ is an interesting hydrogen storage material for mobile applications due to its high hydrogen content of 10.8 wt%. However, its practical use is hampered by the high temperatures (above 500 °C) required to release the hydrogen and by the non reversibility of the hydrogen sorption. In this study, we show that upon heating to 600 °C, bulk $NaBH_4$ decomposed into Na and $Na_2B_{12}H_{12}$, releasing the expected 8.1 wt% of hydrogen. Nanosizing and confinement of $NaBH_4$ in porous carbon resulted in much faster hydrogen desorption kinetics. The onset of hydrogen release was reduced from 470 °C for the bulk to below 250 °C for the nanocomposites. Furthermore, the dehydrogenated nanocomposites were partially rehydrogenated to form $NaBH_4$, with the absorption of about 43% of the initial hydrogen capacity at relatively mild conditions (60 bar H_2 and 325 °C). Reversibility in this system was limited due to partial loss of Na during dehydrogenation. The dehydrogenated boron compounds were almost fully rehydrogenated to $NaBH_4$ (98 %) when extra Na was added to the nanocomposites. To the best of our knowledge, this is the first time that reversibility for $NaBH_4$ has been demonstrated.

This chapter is based on the following manuscripts: P. Ngene, P. Ngene, R. van den Berg, M. H. W. Verkuijlen, Krijn P. de Jong and Petra E. de Jongh. *Reversibility of the Hydrogen Desorption from $NaBH_4$ by Confinement in Nanoporous Carbon. Energy Environ. Sci., 2011, 4, 4108–4115*

5.1 Introduction

$NaBH_4$ has been known since 1940's, and widely used as a reducing agent in organic chemistry, especially in the reduction of functional groups like aldehydes and ketones into alcohols[1] and more recently in metal colloid synthesis. Apart from its use as reducing agent, it can also be used as a solid state hydrogen storage material. $NaBH_4$ is relatively stable in air, and has gravimetric and volumetric hydrogen contents of 10.8 wt% and 115 kg of H_2 m^{-3} respectively, fulfilling the capacity requirements for onboard hydrogen storage as set by the US department of energy (DOE). Since its discovery, extensive studies have been undertaken on the use of $NaBH_4$ as a hydrogen storage material. Most of these studies focussed on hydrogen release via catalyzed hydrolysis of $NaBH_4$[1, 2]. However, DOE recently recommended a no-go for $NaBH_4$ hydrolysis as a hydrogen source for vehicular applications due to the formation of stable $NaBO_2$ that can not be recycled efficiently[3].

An alternative method to release the hydrogen from $NaBH_4$ is by thermal decomposition into H_2, B and Na (or NaH)[4-7]. However, like most alkali borohydrides, $NaBH_4$ is thermodynamically very stable (standard enthalpy of formation $\Delta_f H^0 = -188.6$ kJ per mol $NaBH_4$ and entropy of formation $S^0 = 101.3$ JK^{-1} per mol $NaBH_4$)[8] and releases hydrogen only when heated to temperatures exceeding 500 °C[5, 6, 9, 10] which is too high for practical applications in hydrogen fuel cell cars. Furthermore, reversibility of the hydrogen desorption which is a very important criterium for a hydrogen storage material, has never been reported for $NaBH_4$ as far as we are aware.

For $LiBH_4$, a compound similar to $NaBH_4$, the thermal hydrogen sorption properties have been widely investigated and the kinetics of its hydrogen release and uptake improved using techniques such as destabilization, addition of catalysts and nanosizing/ nanoconfinement [11-23] as also shown in previous chapters. However only few reports in literature exists on the thermal hydrogen sorption properties of $NaBH_4$ and they mainly focused on mixtures of $NaBH_4$ and other hydrides, especially MgH_2[9, 24-28]. Martelli et al[5] recently studied the stability and decomposition of $NaBH_4$ and reported that the compound decomposes in one step (unlike other complex metal hydrides such

as $NaAlH_4$ and $LiBH_4$) to Na and an unidentified boron rich phase. However no further report was made on the identification of the composition of the boron rich phases and no reversibility of the hydrogen desorption from the bulk $NaBH_4$ was reported. The reversibility of the hydrogen desorption from metal hydrides can be improved by nanostructuring and/or nanoconfinement in porous material[15, 29-35]. However in the case of $NaBH_4$, it has been shown that mechanical milling which is commonly employed to produce nanosized metal hydrides[36] is not effective in nanostructuring the compound due to its high structural stability even under heavy deformation conditions imposed by milling[37]. Ampoumogli et al[38] recently synthesized $NaBH_4$/carbon nanocomposites via impregnation of nanoporous carbon with $NaBH_4$ dissolved in liquid ammonia and showed that the nanocomposites releases hydrogen at lower temperatures than bulk $NaBH_4$. However, the hydrogen release was associated with ammonia and no reversibility was observed in this nanocomposite.

In this work, we study the thermal hydrogen release from $NaBH_4$ and investigate how confinement of $NaBH_4$ in nanoporous carbon material using different preparation routes affects the hydrogen sorption properties. Our study reveals that $NaBH_4$ decomposes into metallic Na, $Na_2B_{12}H_{12}$ and H_2 rather than into Na or NaH, B and H_2 as postulated earlier[6, 39]. In addition, we show that confining $NaBH_4$ in nanoporous carbon resulted in a significant increase in the dehydrogenation kinetics and remarkably enabled the rehydrogenation of the decomposition products to $NaBH_4$ at relatively mild conditions.

5.2 Experimental

$NaBH_4$/C nanocomposites were prepared using pore volume impregnation with an aqueous $NaBH_4$ solution (denoted SI) or melt infiltration (MI). For pore volume impregnation, 1.1g $NaBH_4$ (98+% pure, Acros Organics) was dissolved in 2 ml water of pH 13, which was prepared by adding 0.3 g NaOH(Merk 99%) to 10 ml demineralized water. 1g of high surface area carbon (HSAG-500, Timcal Ltd., pore volume 0.66 $cm^3\ g^{-1}$, BET surface area 500 $m^2\ g^{-1}$, broad pore size distribution dominated by 2-3 nm pores) that had been previously dried overnight under vacuum at 200 °C was impregnated with 0.66 ml of the

$NaBH_4$ solution. The water in the impregnated sample was removed by drying overnight at 165 °C under vacuum (~ 9 mbar). The impregnation and drying were done using a Schlenk technique while $NaBH_4$ handling and storage was conducted under Ar atmosphere in a glovebox (< 0.1 ppm of O_2 and H_2O). For melt infiltration, the required amounts of carbon (which had been dried at 500 °C under Ar) and $NaBH_4$ were mixed in a graphite sample holder and placed in stainless steel autoclave. The mixture was heated under hydrogen atmosphere at 5 °C/min to 520 °C (melting point of $NaBH_4$ ~ 500 °C) and dwelled at 520 °C for 25 min at approximately 5 bar H_2. Nanocomposites containing various compositions of $NaBH_4$ and C were synthesized and labeled according to the weight percentage of $NaBH_4$ in the composite. As a reference, physically mixed samples of $NaBH_4$ and C or graphite (BET surface area 7 $m^2\ g^{-1}$) were prepared by mixing the required amounts in a mortar using a pestle.

Structural characterization was performed using X-ray diffraction (XRD), N_2-physisorption and both ^{11}B and ^{23}Na solid-state Nuclear Magnetic Resonance (NMR) spectroscopy. All measurements were done in air tight sample holders. XRD patterns were obtained at room temperature from 18 to 80° 2θ with a Bruker-AXS D-8 Advance X-ray diffractometer setup using $CoK\alpha_{1,2}$ radiation with λ= 1.79026 Å. N_2-physisorption measurements were performed at -196 °C, using a Micromeritics Tristar 3000 apparatus. The pore size distributions of the samples were calculated from the desorption branch using BJH theory with the Harkins and Jura thickness equation. Solid-state NMR experiments were performed on a 600 MHz Varian spectrometer using a 2.5 mm HX MAS probe. ^{11}B and ^{23}Na single pulse excitation spectra were obtained using a short hard pulse of 0.20 μs at an effective rf-field strength of 140 kHz after taking pulse rise and decay times into account. Spectra were acquired without proton decoupling. A sample spinning speed of 15 kHz was applied. The ^{11}B spectra were referenced using an aqueous solution of H_3BO_3 as secondary reference with a chemical shift of δ = 19.6 ppm relative to $BF_3{\cdot}OEt_2$ (δ = 0 ppm). The ^{23}Na spectra were referenced with respect to an aqueous solution of NaCl (δ = 0 ppm).

Hydrogen release from the samples was measured by temperature programmed desorption (TPD) using a Micromeritics AutoChem II 2920 apparatus. 100 to

150 mg of sample was heated at 5 °C/min from room temperature to 450-600 °C in 25 ml/min Ar (99.99 % purity) flow with a dwell time of 25 min at the maximum temperature. The composition of the desorbed gas was analyzed using a quadrupole mass spectrometer (Pfeifer) attached to the TPD gas outlet. Rehydrogenation of desorbed samples was performed in an autoclave at 60 bar H_2 and 325 °C for 5 h after which the amount of H_2 absorbed by the sample was determined by a second TPD run. Cycling of the sample under Ar was performed in a magnetic suspension balance from Rubotherm. About 100 mg of the sample was loaded in a graphitic cup and inserted into a stainless steel sample holder. The sample was heated at 5 °C/min to 400 °C in 25 ml/min Ar flow. Rehydrogenation of the desorbed sample was performed at 325 °C by increasing the H_2 pressure from zero to 60 bar in 60 min and remaining at this pressure and temperature for 5 h. Hydrogen uptake and release were determined from the weight changes after having corrected for buoyancy effects.

5.3 Structure of the $NaBH_4$/C nanocomposites

The X-ray diffraction (XRD) patterns of a physical mixture of 25 wt% $NaBH_4$ and nanoporous carbon (PM), and 25 wt% $NaBH_4$/C nanocomposites prepared through solution impregnation (SI) and melt infiltration (MI) are shown in figure 5.1. The XRD pattern of the carbon shows two diffraction lines at 31° (002) and around 52° (10) 2θ that are typical for turbostratic graphitic materials. After synthesis, all diffraction lines can be ascribed to either carbon or $NaBH_4$. A comparison of the diffraction patterns of the physical mixture and the nanocomposites show a clear broadening and a huge reduction in the intensity of $NaBH_4$ diffraction lines in the nanocomposites. A decrease in the amount of $NaBH_4$ in the nanocomposites to 20 and 15 wt% led to nanocomposites with no detectable diffraction from the $NaBH_4$ (data not shown). Similar observations were reported for $LiBH_4$ confined in porous carbon and silica, and were attributed to a decrease in the long-range order of the compound due to nanozing and confinement in the porous hosts[21, 22]. Hence, we conclude that the $NaBH_4$ is confined in the porous carbon.

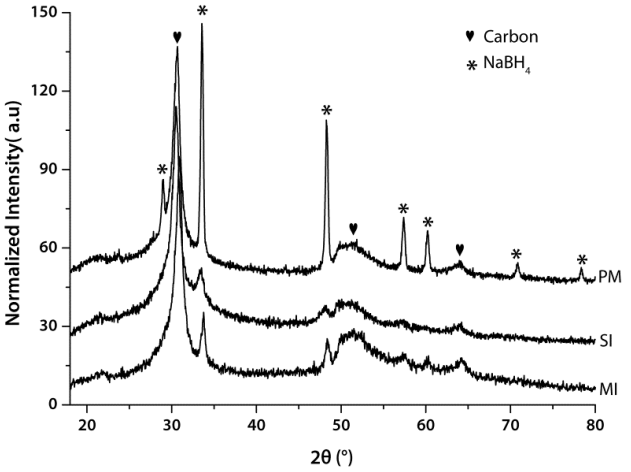

Figure 5.1: XRD Pattern of a physical mixture of 25wt% $NaBH_4$ and carbon (PM), and 25 wt% $NaBH_4$/C nanocomposites synthesized via melt infiltration (MI), solution impregnation (SI)

Further evidence for the incorporation of the $NaBH_4$ into the pores of the carbon is from nitrogen physisorption measurements (figure 5.2) which show that the total pore volume of the carbon decreased from 0.64 cm^3/g carbon in the physically mixed sample to 0.31 and 0.24 cm^3/g carbon in the solution impregnated and melt infiltrated nanocomposites respectively. This decrease in

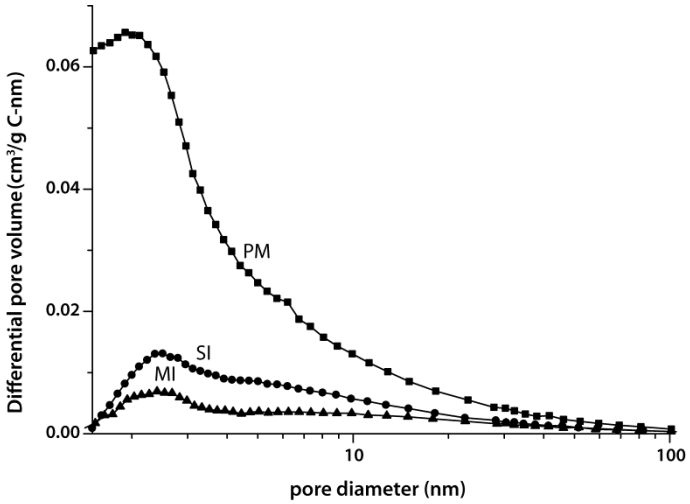

Figure 5.2 Differential pore volume versus pore diameter for a physical mixture of $NaBH_4$ and carbon (PM), solution impregnated (SI) and melt infiltrated (MI) $NaBH_4$/C nanocomposites, showing loss of carbon porosity upon $NaBH_4$ incorporation

pore volume (0.33 cm^3/g C in SI and 0.40 cm^3/g C in the MI) is close to the volume of $NaBH_4$ (0.31cm^3) added in the mixture, in agreement with the fact that the $NaBH_4$ is in the pores of the carbon. The slight difference is most likely due to minor pore blocking and some pore loss (≈ 0.05 cm^3/g) during heat treatment.

5.4 Hydrogen release

Figure 5.3 shows the hydrogen release from bulk $NaBH_4$, a physical mixture of 25wt% $NaBH_4$ and porous carbon (PM), and the MI and SI 25wt% $NaBH_4$/C nanocomposites. Hydrogen release started in the bulk $NaBH_4$ around 470 °C with two major peaks at 515 °C and 560 °C, in line with literature[6]. The onset of hydrogen release is significantly lower (about 320 °C) for the PM sample than for the bulk $NaBH_4$. However, hydrogen release also occurs slightly above 500 °C which is the melting point of $NaBH_4$. For the MI nanocomposite, hydrogen release started at much lower temperatures (below 300 °C) and the majority of the hydrogen was released around 450 °C. Remarkably, for the impregnated sample hydrogen release started below 250 °C, about 220 °C lower in temperature than bulk $NaBH_4$ and with a maximum release rate at 350 °C

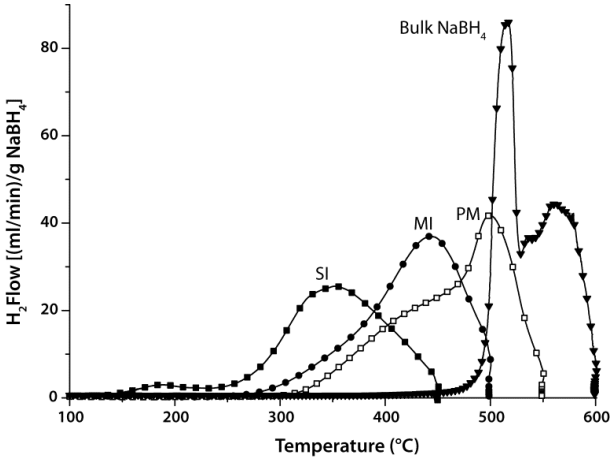

Figure 5.3 Temperature programmed desorption- TPD (while heating with 5 ^oC/min in Ar flow) showing hydrogen release from bulk $NaBH_4$, physical mixture of 25 wt % $NaBH_4$ and porous carbon (PM), Solution impregnated (SI) and melt infiltrated (MI) 25 wt% $NaBH_4$/C nanocomposites.

which is in agreement with previous report for $NaBH_4$/C nanocomposites synthesized via impregnation of $NaBH_4$/liquid ammonia solution[38]. These observations clearly demonstrate that nanoconfinement in porous carbon enhances the dehydrogenation of $NaBH_4$ significantly. The difference in the hydrogen release temperatures of the MI and SI samples suggests the presence of different $NaBH_4$ feature sizes in the two samples which might be due to differences in the interaction of carbon with molten $NaBH_4$ and aqueous $NaBH_4$ solution. Lowering the loading of $NaBH_4$ in the MI nanocomposites led to hydrogen release at lower temperatures, similar to those for the SI sample. Qualitative analysis of the desorbed gas using mass spectrometry (not shown) proved that hydrogen was released in all cases and if other gases were released, the amount was below the detection limit.

The SI nanocomposite released approximately 6.7 wt% H_2 (normalized to the $NaBH_4$ content) after heating to 450 °C and dwelling for 25 min, the MI nanocomposites released 7.9 wt% H_2/g $NaBH_4$ (≈ 2.1wt% H_2/ g sample) with same dwell time at 500 °C, while 8.1 wt% H_2 was released in the physically mixed sample and the bulk $NaBH_4$ after heating to 600 °C and dwelling for 25 min. The minor difference in hydrogen release for the nanocomposites and the physical mixtures is most likely due to partial decomposition or oxidation of the sample during synthesis and handling. Decomposition of $NaBH_4$ into NaH and B would release 8.1 wt% H_2 while 10.8 wt% H_2 would be expected for decomposition into elemental Na and B.

5.5 Reversibility

Reversibility of the hydrogen sorption in the composites was evaluated by rehydrogenating the dehydrogenated samples in an autoclave at 325 °C and 60 bar H_2 for 5 h. The hydrogen release from the rehydrogenated samples is shown in figure 5.4. About 0.9 wt% hydrogen was released from the rehydrogenated bulk $NaBH_4$ indicating minor hydrogen uptake during rehydrogenation. Remarkably, the nanocomposites and the physically mixed $NaBH_4$/nanoporous carbon released about 3.4 wt% H_2/g $NaBH_4$, indicating about 43% reversibility under these mild conditions. As far as we are aware, this is the first report of a

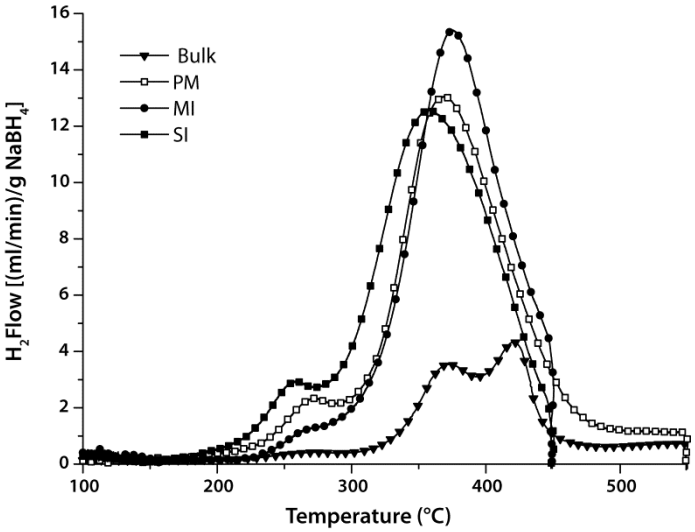

Figure 5.4 Hydrogen release from the rehydrogenated bulk $NaBH_4$, physically mixed (PM), melt-infiltrated (MI) and solution impregnated (SI) nanocomposites. Rehydrogenation was done under 60 bar H_2 and 325 °C for 5 h

successful rehydrogenation of $NaBH_4$ decomposition products. Furthermore, the nanocomposites can be cycled repeatedly as shown in Figure 5.5, although the capacity decreases steadily as in the case of nanoconfined $LiBH_4$[15]. These results show that nanoconfinement in the pores of the carbon material plays an important role in determining reversibility. The reversibility seen in the physically mixed sample (PM) results from the fact that $NaBH_4$ melts (500 °C) during the first cycle desorption and infiltrates the pores of the nanoporous carbon material thereby forming nanoconfined products after decomposition that can be rehydrogenated. This was confirmed from nitrogen physisorption measurements which showed that the total pore volume of carbon decreased by 0.26 cm^3/g after dehydrogenation (Figure 5.6). Such reversibility was not observed for a similar experiment with non porous carbon or graphite (data not shown).

Notably, all the rehydrogenated nanocomposites released hydrogen in the same temperature range, which means that the desorption temperatures especially for the MI nanocomposites had shifted to lower values. This suggests a possible structural change and/or redistribution of the $NaBH_4$ in the carbon after

rehydrogenation. The bulk $NaBH_4$ showed some reversibility (~0.9 wt% H_2 released) but only if the first desorption cycle is done in a closed system.

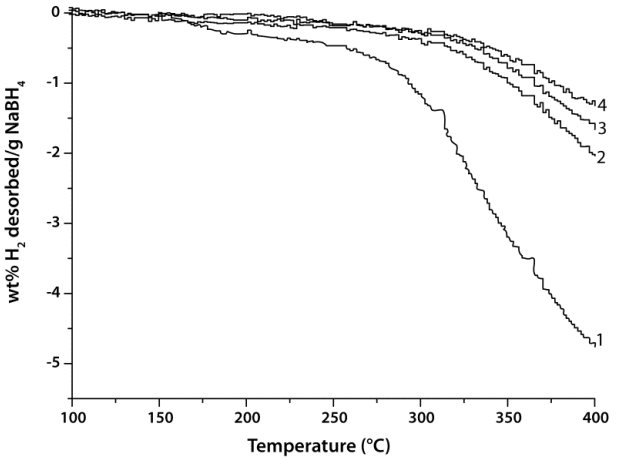

Figure 5.5 Cycling of the nanocomposites in Rubotherm suspension balance. After desorption cycle, the dehydrogenated nanocomposites are rehydrogenated under 60 bar H_2, 325 °C for 5h.

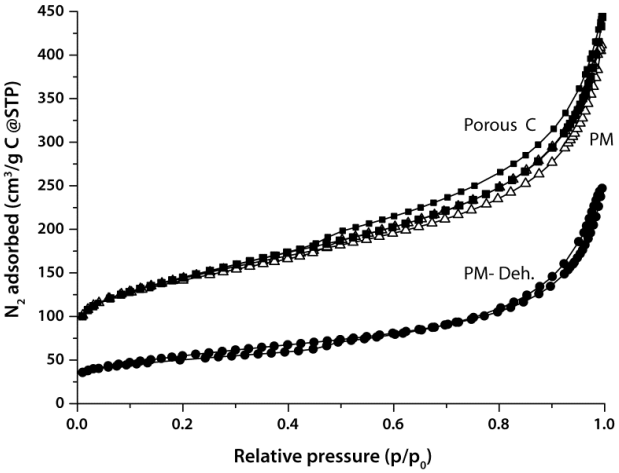

Figure 5.6: N_2 physisorption showing a decrease in the volume of nitrogen adsorbed: The total pore volume of the carbon decreased from 0.64 cm^3/g C for a physical mixture of 25 wt% $NaBH_4$ and porous carbon (PM) to 0.38 cm^3/g C after dehydrogenation (PM- Deh.). The volume of $NaBH_4$ added in the mixture before desorption is 0.31 cm^3.

To investigate structural changes occurring in the samples during hydrogen release and uptake, XRD patterns of the desorbed and rehydrogenated samples were acquired and compared to the pure $NaBH_4$. For bulk $NaBH_4$, we physically observed two distinct solid phases after dehydrogenation as recently reported for dehydrogenated bulk $NaBH_4$[5]. However XRD (figure 5.7a) shows diffractions mainly from Na and unidenfied phase with peak at 45° (2θ). After rehydrogenation, two distinct phases were still physically observed but only NaH was detected from the XRD, showing that for the bulk $NaBH_4$, part of the de- and re-hydrogenated material is amorphous. For both nanocomposites (MI and SI), only C diffraction peaks were observed after hydrogen desorption indicating that the desorption products are amorphous (figure 5.7b). After rehydrogenation, in addition to the C, diffraction peaks due to $NaBO_2$ were observed in the impregnated nanocomposites. The $NaBO_2$ is probably due to reaction between NaOH (used to stabilize the $NaBH_4/H_2O$ solution) and $NaBH_4$ or its decomposition products at high temperatures. In contrast, no diffraction peak other than that from the nanoporous carbon material was observed for the melt infiltrated samples. This shows that for both samples, the hydrogenated phases are amorphous as also reported in literature for $LiBH_4$ and $NaAlH_4$ confined in nanoporous carbon materials[15, 21, 29, 40].

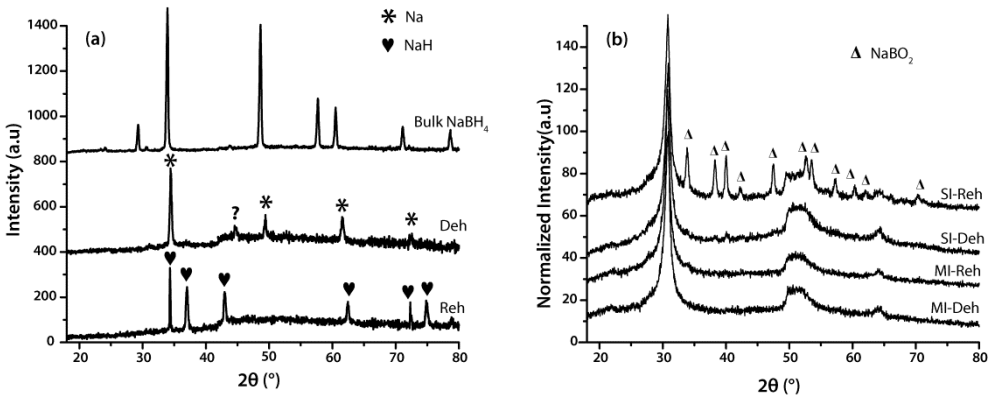

Figure 5.7: XRD pattern of (a): Bulk $NaBH_4$ at room temperature and after dehydrogenation (Deh) and rehydrogenation (Reh). (b): the melt infiltrated (MI) and solution impregnated (SI) 25wt% $NaBH_4$/C nanocomposites after dehydrogenation and rehydrogenation.

5.6 Characterization of the non crystalline phases

A convenient technique to investigate the local structure of non-crystalline solids is solid-state magic angle spinning (MAS) NMR. Figure 5.8 shows the ^{11}B NMR spectra of a physical mixture of $NaBH_4$ and porous carbon, and the nanocomposites after synthesis, dehydrogenation and rehydrogenation. The ^{11}B

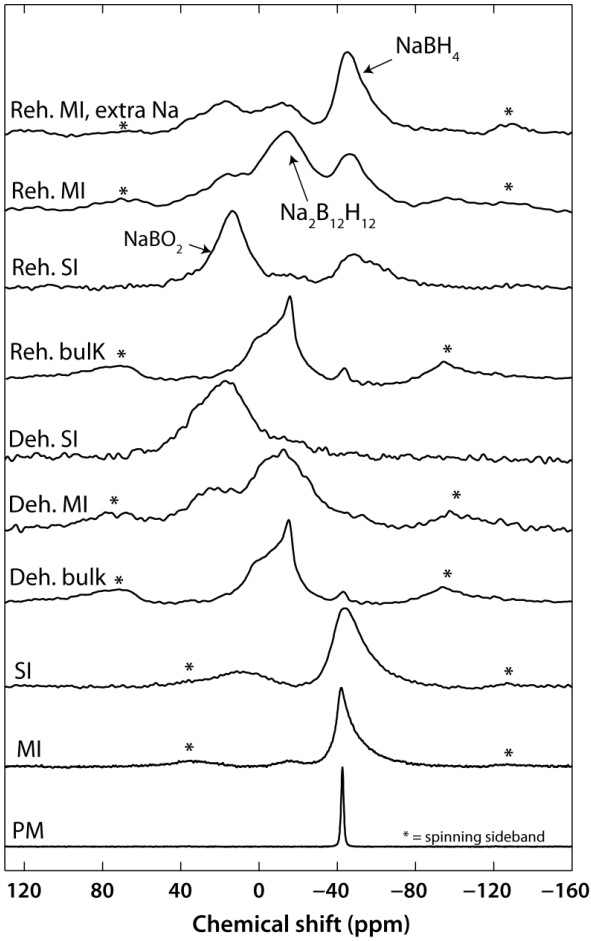

Figure 5.8: Solid-state ^{11}B MAS-NMR spectra of bulk $NaBH_4$ and 25 wt% $NaBH_4$/porous carbon nanocomposites: (PM) Physical mixture; (SI) and MI are nanocomposites prepared by solution impregnation; melt infiltration respectively; (Deh bulk), (Deh. SI) and (Deh.MI) are bulk $NaBH_4$, Sample SI and Sample respectively after dehydrogenation; (Reh. bulk), (Reh. SI), and (Reh. MI) are the rehydrogenated sample of bulk $NaBH_4$, SI and MI nanocomposites respectively. (Reh. MI, extra Na) MI sample containing extra Na. Asterisks indicate spinning sidebands.

spectrum of a physical mixture of $NaBH_4$ and porous carbon shows a well defined sharp peak at -42.6 ppm. For the nanocomposites (both melt infiltrated and volume impregnated), the lineshape of $NaBH_4$ is broadened. As reported previously for $NaAlH_4$/C nanocomposites[40, 41], this line broadening is explained by distortions of the local field homogeneity because of the magnetic susceptibility of the carbon and/or a higher disorder in the material, which results in a distribution in chemical shift and quadrupolar interaction parameters. The impregnated nanocomposite exhibits a significantly larger linewidth with a full width at half maximum (FWHM) of 17.1 ppm compared to the melt infiltrated sample with a FWHM of 9.4 ppm. This means that the microstructure and/or distribution over the carbon depends on the preparation method as was also clear from the physisorption and hydrogen release measurements.

After dehydrogenation, all $NaBH_4$ disappeared in both MI and SI samples, but minor traces of unreacted $NaBH_4$ are present in the dehydrogenated bulk sample. The dehydrogenated bulk $NaBH_4$ and MI sample shows mainly a broad resonance with a maximum at -13 ppm which is assigned to $Na_2B_{12}H_{12}$[45-47]. A small amount of $Na_2B_{12}H_{12}$ is also observed in the sample after melt infiltration which is most likely due to partial desorption, or reaction between $NaBH_4$ and minor impurities in the carbon during melt infiltration. For the dehydrogenated SI sample, a large resonance peak with a maximum at 16 ppm is present. ^{11}B has typical isotropic chemical shifts between 12 and 19 ppm in materials with trigonal B-O coordination[42-44]. Hence this peak can be assigned to $NaBO_2$ in agreement with the XRD results. Most likely, the smaller contribution at 18 ppm in the dehydrogenated MI sample also corresponds to $NaBO_2$. No clear evidence of the formation of elemental boron after desorption was observed. Boron gives a broad line around 5 ppm[48] and therefore, its resonance might overlap with the resonances of $Na_2B_{12}H_{12}$ and/or $NaBO_2$.

No significant change was observed after rehydrogenation of the desorbed bulk $NaBH_4$. In contrast, nanoconfined $NaBH_4$ was reformed in both the MI and SI samples. This clearly proves the partial reversibility for these nanocomposites. Clear differences exist between the MI and SI samples. Besides nanoconfined $NaBH_4$, the MI samples show mainly $Na_2B_{12}H_{12}$ and little $NaBO_2$, while the SI

samples show mainly $NaBO_2$ and only a minor amount of $Na_2B_{12}H_{12}$. The linewith of the $NaBH_4$ resonance increased slightly after rehydrogenation especially for the MI sample. This suggests a possible change in the microstructure and/or distribution of $NaBH_4$ in the carbon after rehydrogenation and is most likely responsible for the lower hydrogen release temperatures in rehydrogenated MI sample (Reh. MI) when compared to the as synthesized sample (MI).

^{23}Na NMR of the samples was also measured in order to investigate the evolution of the Na phase(s). Unfortunately, for the nanocomposites, ^{23}Na NMR gave very broad spectra from which no useful information about the Na phases could be extracted. In general, the chemical shift range for ^{23}Na is relatively small (~30 ppm) compare to ^{11}B, which results in an overlap of the resonances of different compounds especially when the peaks are broad. This broadening is most likely caused by the high dispersion of Na when confined and in close contact with the carbon. Meanwhile ^{23}Na NMR for the bulk $NaBH_4$ (Figure 5.9) shows resonances due to elemental Na and $Na_2B_{12}H_{12}$ after dehydrogenation. After rehydrogenation, the Na resonance disappeared while $Na_2B_{12}H_{12}$ and a peak at a chemical shift due to NaH are seen, in agreement with the XRD results. The formation of NaH (instead of $NaBH_4$) after the rehydrogenation of the bulk $NaBH_4$ explains the differences in the hydrogen release profile of the rehydrogenated nanocomposites and the rehydrogenated bulk $NaBH_4$.

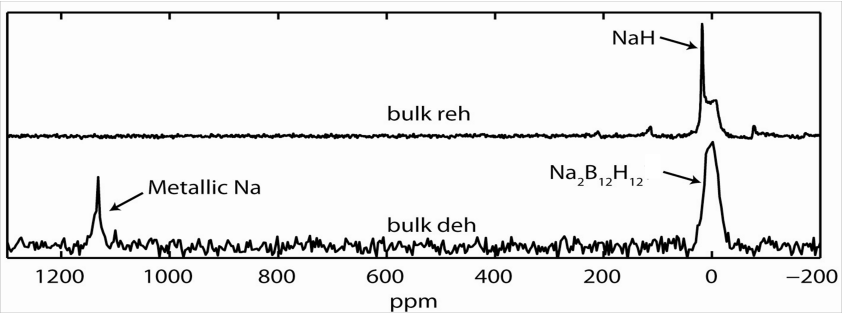

Figure 5.9: Solid-state ^{23}Na NMR spectra of $NaBH_4$ after dehydrogenated (bulk deh) and rehydrogenated (bulk reh) $NaBH_4$. The assignment of $Na_2B_{12}H_{12}$ in the ^{23}Na spectra is done based on the fact that large amount of $Na_2B_{12}H_{12}$ was also observed in the ^{11}B spectra (and not by a comparison with a ^{23}Na reference spectrum of $Na_2B_{12}H_{12}$). The resonance has a maximum at 3 ppm, and it is clearly not NaH which is at 18.3 ppm.

5.7 Addition of extra sodium

The reversibility achieved in the nanoconfined $NaBH_4$ is relatively low when compared to that of other complex hydrides such as $NaAlH_4$ and $LiBH_4$ confined in similar carbon[15, 30, 49]. Apart from partial oxidation of the sample during handling (which also occurs in other nanoconfined hydrides), two major reasons could be responsible for the partial reversibility. Firstly, XRD and NMR measurements clearly show that elemental Na and $Na_2B_{12}H_{12}$ are the main dehydrogenation products of $NaBH_4$. The predicted high stability of $Na_2B_{12}H_{12}$ could prevent the rehydrogenation to $NaBH_4$, as recently postulated[47]. Secondly, since Na is liquid and has a relatively high vapour pressure at 500 °C, the loss of Na through evaporation during dehydrogenation of $NaBH_4$ is likely. In that case there will be insufficient Na to fully form $NaBH_4$ from the dehydrogenated boron compounds. To check if this latter assumption is true, extra Na was added to the melt infiltrated nanocomposites by heating a 20 wt% $NaBH_4$/C nanocomposite with 12.5 wt% NaH (95%, Aldrich). The overall composition of the mixture is 17.5, 70 and 12.5 wt% $NaBH_4$, C and NaH respectively (molar ratio Na:B = 2.1). It is expected that the Na formed after the dehydrogenation of the NaH will infiltrate the pores of the carbon as previously reported[50], thereby providing extra Na to the dehydrogenated nanocomposites. After dehydrogenation, the samples were rehydrogenated at 325 °C and 60 bar H_2 for 5 h.

Figure 5.10 shows the second hydrogen release run. The 20 wt% $NaBH_4$/carbon nanocomposite released approximately 0.7 wt% H_2/g sample (3.5 wt% H_2/g $NaBH_4$). The nanocomposite containing extra Na released 1.4 wt% H_2/g sample (8.0 wt% H_2/g $NaBH_4$), while 8.1 wt% H_2/g $NaBH_4$ is expected for fully reversible decomposition to $Na_2B_{12}H_{12}$. One has to consider that the additional Na could also have been rehydrogenated, and contribute to the hydrogen release. However, the additional NaH could contribute a maximum of 0.55 wt % H_2 per gram nanocomposite, and hence never fully account for the increase in reversibility. More importantly, ^{11}B NMR of the rehydrogenated sample (figure 5. 8) shows a large increase in the resonance due to $NaBH_4$ in the sample with extra Na, as well as fading of the resonance due to $Na_2B_{12}H_{12}$.

This

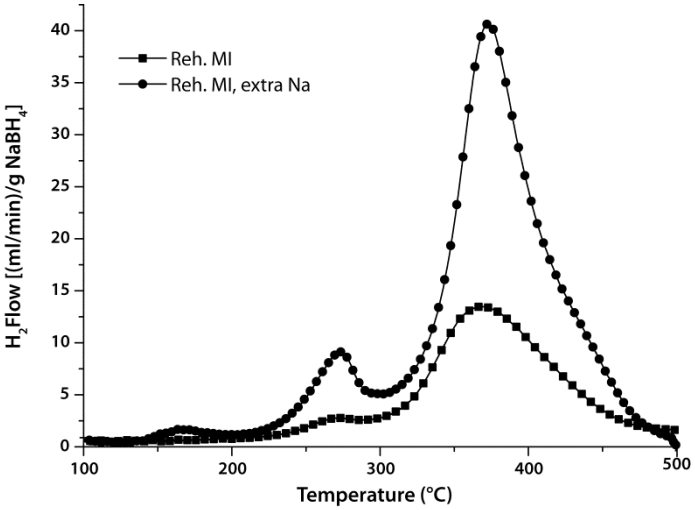

Figure 5.10: Hydrogen release from rehydrogenated sample of 20 wt% $NaBH_4$/C nanocomposites (Reh. MI) and a 20 wt% $NaBH_4$/C nanocomposite containing extra Na; molar ratio of Na: B = 2.1 (Rh. MI, extra Na)

proves that in these nanoconfined systems neither B nor $Na_2B_{12}H_{12}$ are intrinsically limiting factors for the reversibility of hydrogen sorption. Nearly full reversibility could be obtained by compensating for the loss of active Na from the system. Alternatively, loss of Na might be reduced by restricting operation temperatures and gas flow.

5.8 Stability

We also investigated the impact of nanoconfinement of $NaBH_4$ in carbon material on the equilibrium of the hydrogen release and uptake. Figure 5.11 shows the hydrogen release from bulk $NaBH_4$ and the nanocomposites under 1.1 bar H_2 in a magnetic suspension balance. No hydrogen was released in the bulk material upon heating to 400 °C, while for the nanocomposites, decomposition started already ~280 °C, well below ~ 539 °C reported for the equilibrium decomposition of $NaBH_4$ under 1 bar H_2[5]. The MI and SI nanocomposites released 0.5 and 1.3wt% H_2 per gram $NaBH_4$ respectively upon heating to 400 °C. This observation suggests that nanoconfinement in the

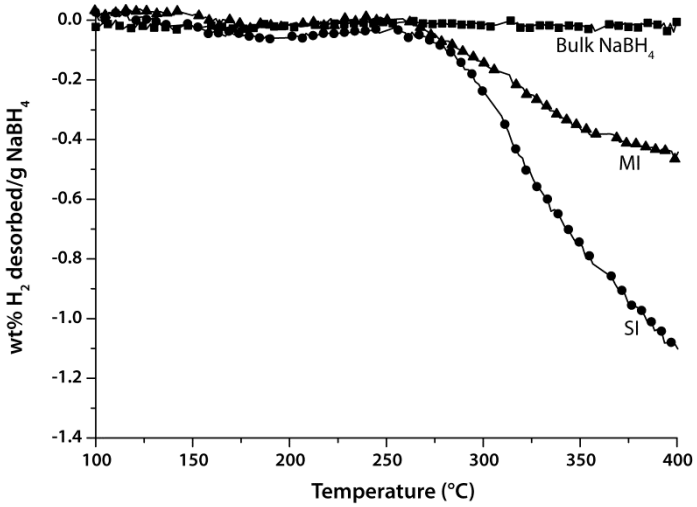

Figure 5.11: Hydrogen release from bulk $NaBH_4$, and MI (melt infiltrated) and SI (Solution impregnated) nanocomposites while heating under 1.1 bar H_2.

porous carbon material changed the stability or decomposition pathway of $NaBH_4$ as also observed in nanoconfined $LiBH_4$. Perhaps an intermediate product is formed during decomposition which is different in the nanoconfined and bulk $NaBH_4$. The difference in the amount of hydrogen released from the nanocomposites under 1.1 bar H_2 could be attributed to differences in the particle or domain sizes of $NaBH_4$ in the nanocomposites and/or different in reaction pathways as suggested by the NMR results.

5.9 General discussion

Most alkali metal borohydrides decompose to the metal hydride before further decomposition to the metal, although direct decomposition into the element is also possible. Thus for the dehydrogenation of $NaBH_4$ the following overall decomposition reaction equations can be written:

$$2\ NaBH_4 \rightarrow 2\ NaH + 2\ B + 3\ H_2 \qquad (5.1)$$

$$NaBH_4 \rightarrow\ \ Na + B + 2\ H_2 \qquad (5.2)$$

Decomposition according to equatio 5.1 releases 8.1 wt% H_2 while reaction 5.2

yields 10.8 wt% H_2. Experimentally, bulk $NaBH_4$ released ~8.1 wt% H_2 while the the melt infiltrated nanocomposite and the physically mixed sample released approximately 8.0 wt% H_2/(g $NaBH_4$) which would suggest that these samples decomposed according to reaction 1. However, the lower stability of NaH compared to $NaBH_4$ implies that NaH should already decompose at lower temperatures than required for the decomposition of $NaBH_4$[51, 52] especially in the presence of carbon[50]. Furthermore, the NMR results clearly show that the decomposition products of $NaBH_4$ are mostly $Na_2B_{12}H_{12}$ and Na. These observations suggest that only partial decomposition of $NaBH_4$ takes place according to the following overall reaction equation:

$$12\ NaBH_4 \rightarrow 10\ Na + Na_2B_{12}H_{12} + 18\ H_2 \qquad (5.3)$$

Interestingly, decomposition according to (5.3) is expected to yield 8.1 wt% H_2 which is in a good agreement with the amount of hydrogen released from the samples. The presence of two desorption steps in the bulk $NaBH_4$ and in all the rehydrogenated nanocomposites could be due to either an intermediate decomposition product, or heterogeneity of the $NaBH_4$. For the solution impregnated sample, formation of $NaBO_2$ is observed with both XRD and NMR. As NaOH is present, this can probably be explained by the following reaction:

$$NaBH_4 + 2\ NaOH \rightarrow NaBO_2 + 2\ Na + 3\ H_2 \qquad (5.4)$$

Since the molar ratio of $NaBH_4$ to NaOH in the aqueous $NaBH_4$ solution is 20:1, only about 2.5% of the $NaBH_4$ is consumed in this reaction (except if traces of water is still present in the sample). Unlike for the MI sample, no clear resonance due to $Na_2B_{12}H_{12}$ was observed with NMR after dehydrogenation. The reversibility seen in the SI sample shows that phases other than oxidation products must be present after dehydrogenation since $NaBO_2$ cannot be rehydrogenated to $NaBH_4$. Unfortunately, neither elemental B nor other boron compounds can clearly be identified with solid-state NMR due to possible overlap of these resonances with the broad $NaBO_2$ resonance. The microstructure and/or distribution of the $NaBH_4$ over the carbon depend on the

preparation method, as seen from NMR and nitrogen physisorption results. Also Figure 5. 3 shows different hydrogen release profiles for SI and the MI nanocomposites. However, at present we cannot identify which boron species are reversibly formed after dehydrogenation in the SI samples.

Remarkable is the reversible formation of $NaBH_4$ in these nanocomposites especially at such mild conditions as used in this study since for $NaBH_4$ reversible hydrogen sorption has not yet been reported. Reversibility in complex hydrides especially borohydrides is typically hampered by the formation of at least two crystalline or amorphous phases after desorption which are the metal or metal hydride phase and boron/boron species. Bulk $NaBH_4$ forms crystalline Na and amorphous $Na_2B_{12}H_{12}$ after desorption. Reversibility in such a system is difficult because of the slow solid state diffusion required for the recombination of these macroscopically segregated immobile phases. This is evidenced by the fact that after rehydrogenation, NaH and $Na_2B_{12}H_{12}$ were seen instead of $NaBH_4$. This suggests that NaH is first formed during rehydrogenation and since it is a solid at the rehydrogenation conditions, it did not react with the $Na_2B_{12}H_{12}$ to form $NaBH_4$. Furthermore, Caputo et al recently calculated that $Na_2B_{12}H_{12}$ is very stable (standard enthalpy of formation at 0 K = -1086 kJ/mol $Na_2B_{12}H_{12}$ or - 181 kJ/mol H_2) and cannot be rehydrogenated if formed during dehydrogenation of $NaBH_4$[47]. However, the results presented in this study clearly showed that nanoconfined $NaBH_4$ exhibits partial reversible hydrogen sorption and that full reversibility can be achieved if Na is not lost during dehydrogenation. Therefore the barrier to reversibility in bulk $NaBH_4$ is not due to the stability of $Na_2B_{12}H_{12}$ but rather due to the inability of NaH (formed during rehydrogenation) and $Na_2B_{12}H_{12}$ to react with H_2 to form $NaBH_4$ at moderate conditions because of phase separation and poor kinetics of solid-state diffusion required for their recombination. Furthermore, bulk $NaBH_4$ decomposes above 500 °C and Na loss through evaporation at this high temperatures (except when desorption is carried in a closed system) practically hinders the reversibility of the dehydrogenation reaction. Confining the $NaBH_4$ in nanoporous carbon reduces these problems. When confined, the dehydrogenated phases are all kept together in the pores of the carbon. Therefore the diffusion or recombination

distance between the Na and $Na_2B_{12}H_{12}$ is greatly reduced, enabling the reversible formation of $NaBH_4$ from its dehydrogenated products even at relatively mild conditions without a catalyst.

Our work clearly demonstrate how the kinetics of hydrogen release from $NaBH_4$ can be greatly enhanced and reversibility enabled by nanosizing and nanoconfinement in carbon. Preliminary investigations also indicate that under 1 bar H_2 pressure, part of the hydrogen is already released starting from 280 °C which is below the temperature at which the dehydrogenation reaction of $NaBH_4$ would be expected in equilibrium[12]. This indicates that the enthalpy and/or entropy for the decomposition reaction might be different for nanoconfined $NaBH_4$ compared to bulk material, or the presence of intermediate decomposition steps for $NaBH_4$ which is different when confined in nanoporous carbon but the details are outside the scope of the present work.

Despite the fact that the hydrogen release temperatures are lowered and reversibility observed when $NaBH_4$ is confined in nanoporous carbon, for practical application in fuel cell cars, further reduction in the desorption temperatures to about 150 °C is required in order to avoid Na loss. In addition, the $NaBH_4$ loading must be increased to above 60 wt% in order to increase the overall hydrogen content of the nanocomposite. The latter might be achieved by using nanoporous hosts with higher pore volume.

5.10 Conclusions

The thermal hydrogen sorption properties of $NaBH_4$ have been investigated. XRD, solid-state NMR and hydrogen release measurements revealed that $NaBH_4$ decomposes into elemental Na and $Na_2B_{12}H_{12}$ when heated to 600 °C, with a release of 8.1 wt % H_2. $NaBH_4$ was successfully confined into a nanoporous carbon material through impregnation with an aqueous $NaBH_4$ solution and also by melt infiltration under hydrogen pressure. Confining $NaBH_4$ in nanoporous carbon material lowers the desorption temperatures significantly, with most of the hydrogen released around 350 °C(in Ar flow) in the solution impregnated nanocomposites compared to 560 °C for the bulk material. Remarkably, reversible formation of $NaBH_4$ from its dehydrogenation products was demonstrated for the first time as the dehydrogenated $NaBH_4$/C

nanocomposites can be rehydrogenated to $NaBH_4$ at relatively mild conditions of 325 °C and 60 bar H_2 for 5h. Reversibility of the system is limited by loss of Na at high temperatures during hydrogen release. Compensation of Na loss by extra Na resulted in almost full rehydrogenation of the dehydrogenated products to $NaBH_4$. Although at the moment $NaBH_4$/C nanocomposites do not meet the requirements for onboard applications, our work demonstrate the strength of nanoconfinement in carbon materials as an approach towards reversible hydrogen storage materials.

Acknowledgement

We would like to thank M. van Zwienen, A. van der Eerden and A. Mens for their technical support. We thank Timcal Ltd. Switzerland for providing the high surface area graphite, and NWO-Vidi Netherlands, 016.072.316 for financial support. The Netherlands Organisation for Scientific Research (NWO) is acknowledged for its support of the solid-state NMR facility for advanced materials research at Radboud University. Finally we thank Prof. Arno Kentgens and Dr. Jan van Bentum of Radboud University, Nijmegen for their support regarding the NMR results.

References

1. H. I. Schlesinger, H. C. Brown, A. E. Finholt, J. R. Gilbreath, H. R. Hoekstra and E. K. Hyde, *J. Am. Chem. Soc.*, 1953, **75**, 215-219.
2. S. C. Amendola, P. Onnerud, M. T. Kelly, P. J. Petillo, S. L. Sharp-Goldman and M. Binder, *J. Power Sources*, 1999, **84**, 130-133.
3. U. B. Demirci, O. Akdim and P. Miele, *Int. J. Hydrogen Energy*, 2009, **34**, 2638-2645.
4. D. S. Stasinevich and G. A. Egorenko, *Russ. J. Inorg.Chem.*, 1968, **13**, 341–343.
5. P. Martelli, R. Caputo, A. Remhof, P. Mauron, A. Borgschulte and A. Züttel, *J. Phys. Chem. C*, 2010, **114**, 7173-7177.
6. J. Urgnani, F. J. Torres, M. Palumbo and M. Baricco, *Int. J. Hydrogen Energy*, 2008, **33**, 3111-3115.

7. W. Grochala and P. P. Edwards, *Chem. Rev*, 2004, **104**, 1283-1315.
8. *Handbook of Chemistry & Physics*, 2010-2011.
9. R. A. Varin, T. Czujko, C. Chiu, R. Pulz and Z. S. Wronski, *J. Alloys Compd.*, 2009, **483**, 252-255.
10. S. Orimo, Y. Nakamori and A. Züttel, *Mater. Sci. Eng., B*, 2004, **108**, 51-53.
11. M. Aoki, K. Miwa, T. Noritake, G. Kitahara, Y. Nakamori, S. Orimo and S. Towata, *Applied Physics A*, 2005, **80**, 1409-1412.
12. M. Au, A. R. Jurgensen, W. A. Spencer, D. L. Anton, F. E. Pinkerton, S. J. Hwang, C. Kim and R. C. Bowman, *J. Phys. Chem. C*, 2008, **112**, 18661-18671.
13. M. Au, W. Spencer, A. Jurgensen and C. Zeigler, *J. Alloys Compd.*, 2008, **462**, 303-309.
14. Z. Z. Fang, X. D. Kang, P. Wang and H. M. Cheng, *J. Phys. Chem. C*, 2008, **112**, 17023-17029.
15. A. F. Gross, J. J. Vajo, S. L. Van Atta and G. L. Olson, *J. Phys. Chem. C*, 2008, **112**, 5651-5657.
16. X. D. Kang, P. Wang, L. P. Ma and H. M. Cheng, *Applied Physics A*, 2007, **89**, 963-966.
17. J. J. Vajo and G. L. Olson, *Scr. Mater.*, 2007, **56**, 829-834.
18. J. J. Vajo, S. L. Skeith and F. Mertens, *J. Phys. Chem. B*, 2005, **109**, 3719-3722.
19. G. L. Xia, Y. H. Guo, Z. Wu and X. B. Yu, *J. Alloys Compd.*, 2009, **479**, 545-548.
20. J. Xu, X. B. Yu, Z. Q. Zou, Z. L. Li, Z. Wu, D. L. Akins and H. Yang, *Chem. Commun.*, 2008, 5740-5742.
21. S. Cahen, J. B. Eymery, R. Janot and J. M. Tarascon, *J. Power Sources*, 2009, **189**, 902-908.
22. P. Ngene, P. Adelhelm, A. M. Beale, K. P. de Jong and P. E. de Jongh, *J. Phys. Chem. C*, 2010, **114**, 6163-6168.
23. M. S. Wellons, P. A. Berseth and R. Zidan, *Nanotechnology*, 2009, **20**.
24. G. Barkhordarian, T. Klassen, M. Dornheim and R. Bormann, *J. Alloys Compd.*, 2007, **440**, L18-L21.

25. J. F. Mao, X. B. Yu, Z. P. Guo, H. K. Liu, Z. Wu and J. Ni, *J. Alloys Compd.*, 2009, **479**, 619-623.
26. S. Garroni, C. Milanese, A. Girella, A. Marini, G. Mulas, E. Menendez, C. Pistidda, M. Dornheim, S. Surinach and M. D. Baro, *Int. J. Hydrogen Energy*, 2010, **35**, 5434-5441.
27. S. Garroni, C. Pistidda, M. Brunelli, G. B. M. Vaughan, S. Surinach and M. D. Baro, *Scr. Mater.*, 2009, **60**, 1129-1132.
28. T. Czujko, R. A. Varin, Z. Wronski, Z. Zaranski and T. Durejko, *J. Alloys Compd.*, 2007, **427**, 291-299.
29. Z. Z. Fang, P. Wang, T. E. Rufford, X. D. Kang, G. Q. Lu and H. M. Cheng, *Acta Mater.*, 2008, **56**, 6257-6263.
30. J. Gao, P. Adelhelm, M. H. W. Verkuijlen, C. Rongeat, M. Herrich, P. J. M. Van Bentum, O. Gutfleisch, A. P. M. Kentgens, K. P. de Jong and P. E. de Jongh, *J. Phys. Chem. C*, 2010, **114**, 4675-4682.
31. R. D. Stephens, A. F. Gross, S. L. Van Atta, J. J. Vajo and F. E. Pinkerton, *Nanotechnology*, 2009, **20**.
32. W. Lohstroh, A. Roth, H. Hahn and M. Fichtner, *ChemPhysChem*, 2010, **11**, 789-792.
33. P. E. de Jongh and P. Adelhelm, *Chemsuschem*, 2010, **3**, 1332-1348.
34. C. P. Baldé, B. P. C. Hereijgers, J. H. Bitter and K. P. de Jong, *Angew. Chem., Int. Ed.*, 2006, **45**, 3501-3503.
35. R. W. P. Wagemans, J. H. Van Lenthe, P. E. de Jongh, A. J. Van Dillen and K. P. de Jong, *J. Am. Chem. Soc.*, 2005, **127**, 16675-16680.
36. A. Zaluska, L. Zaluski and J. O. Ström-Olsen, *Appl. Phys. A: Mater. Sci. Process.*, 2001, **72**, 157-165.
37. R. A. Varin and C. Chiu, *J. Alloys Compd.*, 2005, **397**, 276-281.
38. A. Ampoumogli, T. Steriotis, P. Trikalitis, D. Giasafaki, E. G. Bardaji, M. Fichtner and G. Charalambopoulou, *J. Alloys Compd.*, 2011, **509**, S705-S708.
39. M. Felderhoff, C. Weidenthaler, R. von Helmolt and U. Eberle, *Phys. Chem. Chem. Phys.*, 2007, **9**, 2643-2653.

40. P. Adelhelm, J. B. Gao, M. H. W. Verkuijlen, C. Rongeat, M. Herrich, P. J. M. van Bentum, O. Gutfleisch, A. P. M. Kentgens, K. P. de Jong and P. E. de Jongh, *Chem. Mater.*, 2010, **22**, 2233-2238.
41. M. H. W. Verkuijlen, J. B. Gao, P. Adelhelm, P. J. N. van Bentum, P. E. de Jongh and A. P. M. Kentgens, *J. Phys. Chem. C*, 2010, **114**, 4683-4692.
42. K. J. D. Mackenzie and M. E. Smith, *Multinuclear Solid-State NMR of Inorganic Materials. Pergamon*, 2002.
43. A. D. Irwin, J. S. Holmgren and J. Jonas, *J. Non-Cryst. Solids*, 1988, **101**, 249-254.
44. G. D. Soraru, N. Dallabona, C. Gervais and F. Babonneau, *Chem. Mater.*, 1999, **11**, 910-919.
45. S. J. Hwang, R. C. Bowman, J. W. Reiter, J. Rijssenbeek, G. L. Soloveichik, J. C. Zhao, H. Kabbour and C. C. Ahn, *J. Phys. Chem. C*, 2008, **112**, 3164-3169.
46. V. Stavila, J. H. Her, W. Zhou, S. J. Hwang, C. Kim, L. A. M. Ottley and T. J. Udovic, *J. Solid State Chem.*, 2010, **183**, 1133-1140.
47. R. Caputo, S. Garroni, D. Olid, F. Teixidor, S. Surinach and M. D. Baro, *Phys. Chem. Chem. Phys.*, 2010, **12**, 15093-15100.
48. N. Brun, R. Janot, C. Sanchez, H. Deleuze, C. Gervais, M. Morcrette and R. Backov, *Energy Environ. Sci*, 2010, **3**, 824-830.
49. P. Ngene, M. van Zwienen and P. E. de Jongh, *Chem. Commun.*, 2010, **46**, 8201-8203.
50. P. Adelhelm, K. P. de Jong and P. E. de Jongh, *Chem. Commun.*, 2009, 6261-6263.
51. X. Ke and I. Tanaka, *Phys. Rev. B: Condens. Matter*, 2005, **71**, 024117.
52. J. Šubrt and K. Tobola, *J. Therm. Anal. Calorim.*, 1976, **10**, 5-12.

Chapter 6

Summary and Outlook

Summary

The large-scale use of hydrogen for intermittent energy storage and as a fuel for cars can contribute to the realization of a more sustainable energy system in the future. However several technical challenges have to be addressed, of which compact, safe and cost effective hydrogen storage is a crucial one. A promising approach is the use of metal hydrides with high hydrogen content for reversible hydrogen storage. Alkali-metal borohydrides like $LiBH_4$ and $NaBH_4$ have high gravimetric and volumetric hydrogen densities. However hydrogen release occurs at elevated temperatures only, and is not readily reversible under practical conditions. This thesis describes a study on nanosizing and nanoconfinement of alkali-metal borohydrides using porous scaffolds to address these issues. The aim is to gain understanding of the effects of physical confinement at the nanoscale and interaction with the nanoporous host material on the hydrogen release and uptake in these complex-metal hydrides. We investigated $LiBH_4/SiO_2$, $LiBH_4/C$, $LiBH_4$(Ni)/C and $NaBH_4/C$ nanocomposites.

Chapter 2 describes the synthesis, structural characterization and hydrogen sorption properties of $LiBH_4$ confined in ordered mesoporous silica (SBA-15). Silica was initially reported to catalyze hydrogen desorption from $LiBH_4$. Our idea was to combine the catalytic effect with nanoconfinement in well defined pores, varying the pore size. $LiBH_4$/SBA-15 nanocomposites were synthesized by melt infiltration of $LiBH_4$. A high hydrogen pressure was applied to avoid the decomposition of $LiBH_4$ during melting. Structural characterization showed that the $LiBH_4$ was indeed confined in the pores (7-10 nm) of the SBA-15. Hydrogen was released at temperatures significantly lower than for bulk $LiBH_4$. However the hydrogen release was not reversible. The irreversibility was due to the formation of stable lithium silicates upon hydrogen release. The porous SiO_2 reacted with the decomposition product(s) of $LiBH_4$.

To avoid or limit irreversible reactions a less reactive nanoporous host is needed, hence in **Chapter 3** the use of nanoporous carbon materials for nanoconfinement of $LiBH_4$ is discussed. $LiBH_4/C$ nanocomposites with different $LiBH_4$ loading were prepared by melt infiltration, and the influence of loading on the structure and hydrogen sorption properties was investigated. The nanoconfined $LiBH_4$ released hydrogen in a single step at temperatures significantly lower than for the bulk

material. The activation energy for dehydrogenation was lower for the nanocomposites (110-140 kJ/mol) than for bulk $LiBH_4$ (169 ± 5 kJ/mol), and the pre-exponential factor for the nanocomposites increased with decreasing loading. Nanocomposites with more than half filled carbon pores released ~14 wt% $H_2/LiBH_4$ upon heating to 400 °C, while for lower loadings ~18.5 wt% H_2 was detected, corresponding to full decomposition to B, H_2 and either LiH or Li respectively. Confinement effects were clearly observed using high pressure DSC: the structural phase transition at 110 °C and melting of $LiBH_4$ at 280 °C shifted to temperatures lower by 10-50 °C, and could not be detected if less than 50 % of the carbon pores was filled. Decomposition of nanoconfined $LiBH_4$ started around 255 °C under 1 bar H_2, while the equilibrium decomposition temperature for bulk $LiBH_4$ under 1 bar H_2 is ~370 °C. Partial reversibility of the hydrogen release was observed only in the nanocomposites, and under relatively mild rehydrogenation conditions. Thus nanoconfinement of $LiBH_4$ in porous carbon materials led to changes in kinetics, reversibility and equilibria of the hydrogen uptake and release reactions depending on the loading and hence the average paricle or domain size of $LiBH_4$.

As a next step we explored the combination of nanoconfinement and additives as described in **Chapter 4**. First, Ni nanoparticles (average size 5 nm) were deposited into the nanoporous carbon material and subsequently $LiBH_4$ was melt infiltrated to form $LiBH_4$(Ni)/C nanocomposites. The addition of Ni to the nanoconfined $LiBH_4$ resulted in only a slight decrease in the initial hydrogen release temperature. More importantly, the presence of Ni increased the reversible capacity of the nanoconfined $LiBH_4$ from 6 wt% H_2 to 9.2 wt% H_2 at mild rehydrogenation conditions (320 °C, 40 bar H_2), and led to lower hydrogen release temperatures in subsequent desorption cycles. Structural studies were performed using EXAFS, TEM and NMR. The changes in hydrogen release and reversibility were related to the formation of nickel boride (Ni_xB) nanoparticles, which reversibly changed composition (x) during cycling. Their presence influenced the structure of the active phases, possibly acting as nucleation centres for the phase transformations.

Chapter 5 extends the investigation to $NaBH_4$ which is more stable than $LiBH_4$, and has hardly been investigated so far. $NaBH_4$ was successfully confined into a nanoporous carbon material via impregnation with an aqueous alkaline $NaBH_4$

solution, and also by melt infiltration under hydrogen pressure. Bulk $NaBH_4$ decomposed irreversibly into Na and $Na_2B_{12}H_{12}$ with a release of 8.1wt% H_2 upon heating to 600 °C under Ar. For nanoconfined $NaBH_4$ the decomposition was shifted to ~ 370 °C. The preparation method influenced the structure and hydrogen desorption temperatures of the nanocomposites. Unlike the bulk $NaBH_4$, the dehydrogenated nanocomposites could partially be rehydrogenated (3.4 wt% $H_2/NaBH_4$) to form $NaBH_4$ at 325 °C and 60 bar H_2. This is the first time that reversibility is reported for $NaBH_4$. It was shown that the loss of Na is a limiting factor for the reversibility in these nanocomposites. Compensation by adding extra Na resulted in almost full reversibility. The equilibrium decomposition temperature of $NaBH_4$ is ~540 °C in 1 bar H_2, however for the nanoconfined $NaBH_4$ hydrogen release started around 280 °C under 1.1 bar H_2. The improved hydrogen sorption properties and especially the reversible formation of $NaBH_4$ were attributed to the effect of physical confinement at the nanoscale which limits the macroscopic segregation of the immobile dehydrogenated phases.

Outlook

The studies described in this thesis show nanosizing and nanoconfinement in nanoporous carbon materials as a promising strategy towards reversible hydrogen storage. Although hydrogen release temperatures were lowered and reversibility was achieved in nanoconfined alkali borohydrides, the hydrogen densities of the nanocomposites discussed in this thesis are too low due to added weight of the carbon materials. For practical application, much more porous carbon materials with higher loadings would have to be used. Furthermore applications in combination with a PEM fuel cell will require even lower desorption temperatures, and stability upon cycling typically > 1000 times. However this work shows that we can fundamentally change the hydrogen release kinetics, reversibility and also the equilibria for hydrogen uptake and release in complex metal hydrides. Some general conclusions can be drawn and perspective for future investigations given.

Hydrogen release kinetics is strongly influenced by the nanoconfinement, as the specific surface areas increase, and diffusion distances decrease with nanosizing. Additionally an increase in nucleation site density might play a role. Also activation barriers might decrease due to a lower thermodynamic stability of the

complex metal hydride (see below). The use of carbon nanotubes and other nanoporous carbon materials with well defined pore sizes and geometry could help in elucidating the effects of particle or domain sizes of the metal hydride on hydrogen release and uptake kinetics. The reversibility of hydrogen desorption from nanocomposites shows that limiting the phase segregation of the dehydrogenated products is key to improve the hydrogen uptake kinetics. An additional increase in reversible capacity of nanoconfined $LiBH_4$ and $NaBH_4$ with the addition of Li and Na respectively is a strong indication that also the loss of one of the active components during cycling can limit reversibility. Use of additives that reversibly form a stable compound with one of the active phases limits grain growth, as demonstrated in chapter 4 with Ni in the case of nanoconfined $LiBH_4$.

Exciting are the thermodynamic effects observed in carbon-confined metal hydrides. A factor is possibly electronic interaction between the carbon and the complex metal hydride. Electron donation from graphite may reduce the positive charge of the Li^+ or Na^+, thus weakening the bond with the BH_4^- anion, and thereby destabilize the complex metal borohydride. The impact of such electronic interactions is strong for nanoconfined metal hydrides due to their close proximity to the carbon surface. Lithium intercalation in-between the graphene layers upon dehydrogenation of nanoconfined $LiBH_4$ also destabilizes the hydrided with respect to the dehydrogenated phase. Without doubt also particle size affects the thermodynamic stability of the phases, as reflected in changes in melting point and phase transition temperatures for $LiBH_4$. Also physical confinement/clamping is expected to play a role. Use of carbon materials with different surface properties could provide more insight into how interaction with the support and physical confinement /anchoring of the phases affects the stability of the nanoconfined metal hydride. With the present knowledge, it is difficult to deconvolute the impact of the different parameters, as they are not varied independently, and characterization of the local structure and electronic properties is a challenge for these light-element materials. The use of techniques such as synchrotron based in-situ X-ray Raman spectroscopy (XRS), in-situ NMR, and neutron scattering experiments could provide further information. Computational studies will be indispensible to provide further insight into the origin of such thermodynamic effects and the impact of the individual parameters.

In conclusion, the results discussed in this PhD thesis shows that nanoconfinement in porous carbon materials is an effective strategy to fundamentally change the kinetics, reversibility and the equilibrium of hydrogen uptake and release in metal hydrides. Our work established a new preparation technique for nanoconfined alkali borohydride, and combined nanoconfinement with additives (catalysts). Remarkable is the high reversibility achieved in these nanocomposites under moderate rehydrogenation conditions. Nanoconfinement is a relatively new approach, and full understanding of the effects needs further research: preparing model compounds, development of advanced characterization techniques, and computational studies. Nevertheless, our work has provided information on factors that influence the dehydrogenation and rehydrogenation rates, stability and most importantly on how to achieve full reversibility of the hydrogen release. It is expected that this approach will be relevant also for other fields in material science.

Samenvatting

Grootschalige toepassing van waterstof voor het opslaan van energie uit niet-continue bronnen (zoals wind- en zonne-energie) en als brandstof voor auto's kan bijdragen aan het introduceren van hernieuwbare energie in de samenleving. Om dit mogelijk te maken moeten echter een aantal technische uitdagingen worden opgelost. Eén daarvan is de compacte, veilige en goedkope opslag van waterstof. Een veelbelovende optie is het gebruik van metalen die een grote hoeveelheid waterstof reversibel binden. Alkalimetaalboorhydriden zoals $LiBH_4$ en $NaBH_4$ bevatten veel waterstof, zowel op basis van gewicht als van volume. Helaas is een hoge temperatuur nodig om de waterstof vrij te maken, en wordt het niet gemakkelijk weer opgenomen. Dit proefschrift beschrijft een onderzoek naar het verkleinen van de deeltjesgrootte tot enkele nanometers/het opsluiten van de alkalimetaalboorhydriden in poreuze matrices. Doel is om inzicht te krijgen in de invloed van fysieke opsluiting in nanoporiën en interactie met het matrix materiaal op de afgifte en opname van waterstof in deze complexe metaalhydriden. $LiBH_4/SiO_2$, $LiBH_4$/C, $LiBH_4$(Ni)/C en $NaBH_4$/C werden onderzocht.

Hoofdstuk 2 beschrijft de synthese, karakterisatie van de structuur, en de opname en afgifte van waterstof door $LiBH_4$ opgesloten in geordend mesoporeus silica (SBA-15). Eerder werd gerapporteerd dat silica een katalysator zou zijn voor de waterstofafgifte door $LiBH_4$. Ons plan was om dit katalytisch effect te combineren met het opsluiten in nanoporiën van verschillende grootten. Nanocomposieten bestaande uit $LiBH_4$ en SBA-15 werden bereid door middel van smeltinfiltratie van $LiBH_4$. Een hoge waterstofdruk (~ 100 bar) was nodig om ontleding van $LiBH_4$ tijdens het smelten tegen te gaan. Karakterisatie van de structuur liet zien dat het $LiBH_4$ inderdaad in de 7-10 nm poriën van het SBA-15 opgesloten was. Waterstof werd bij duidelijke lagere temperaturen afgegeven dan voor een "bulk" materiaal. Helaas was de afgifte van waterstof niet omkeerbaar. Dit was het gevolg van de vorming van stabiele Si-verbindingen tijdens het afgeven van de waterstof, doordat de poreuze SiO_2 matrix reageerde met de ontledingsprodukten van het $LiBH_4$.

Om onomkeerbare reacties te verminderen of geheel te vermijden is een minder reactieve matrix nodig. Daarom wordt in **Hoofdstuk 3** het gebruik van een nanoporeuze koolstof matrix besproken om $LiBH_4$ in op te sluiten. Nanocomposieten werden bereid door verschillende hoeveelheden $LiBH_4$ in de

poreuze structuur in te smelten, en gekeken werd naar de afgifte en daarop volgende opname van waterstof. De nanocomposieten van $LiBH_4$ met koolstof gaven alle waterstof in één keer af bij veel lagere temperaturen dan puur $LiBH_4$. Ook de activerings-energie voor waterstofafgifte was lager voor de nanocomposieten (110-140 kJ/mol) dan voor puur $LiBH_4$ (169 ± 5 kJ/mol), en de preëxponentiële factor nam toe met afnemende belading. Nanocomposieten met meer dan half gevulde poriën gaven ~14 gew% H_2/$LiBH_4$ af als ze werden opgewarmd naar 400 °C, terwijl voor lagere vulgraden ~18.5 gew% H_2 gemeten werd. Dit komt overeen met volledige ontleding in B, H_2 en LiH in het eerste geval, en in B, H_2 en Li in het tweede geval. Opsluitingseffecten werden duidelijk waargenomen met behulp van DSC-metingen: de structuurverandering bij 110 ^oC en het smelten bij 280 ^oC vonden bij 10-50 ^oC lagere temperaturen plaats voor nanocomposieten, en konden zelfs niet meer gedetecteerd worden als de vulgraad van de poriën kleiner was dan 50 vol%. Ontleding van het $LiBH_4$ in de nanocomposieten startte bij 255 ^oC onder 1 bar H_2, terwijl voor puur $LiBH_4$ de ontleding onder deze omstandigheden pas bij ~370 °C begon. Na afgifte van de waterstof werd alleen reabsorptie waargenomen voor de nanocomposieten, onder relatief milde omstandigheden. Het is duidelijk dat het opsluiten van $LiBH_4$ in de poriën van een koolstof matrix veranderingen geeft in zowel de kinetiek en reversibiliteit als ook in de evenwichtsligging van waterstofafgifte, afhankelijk van de belading (en daarmee samenhangend de deeltjesgrootte) van het $LiBH_4$.

Als volgende stap hebben we de combinatie van opsluitingseffecten met toevoeging van een katalysator bestudeerd, zoals beschreven in **Hoofdstuk 4.** Eerst werden Ni nanodeeltjes (met een grootte van 5 nm) afgezet in de poriën van de koolstof matrix. Vervolgens werd door insmelten $LiBH_4$ toegevoegd, waardoor $LiBH_4$(Ni)/C nanocomposieten gevormd werden. De toevoeging van het Ni leidde tot slechts een beperkte daling van de initiële temperatuur van waterstofafgifte. Interessanter was dat de aanwezigheid van Ni leidde tot een betere omkeerbaarheid van de waterstofafgifte; van 6 gew% H_2 naar 9.2 gew% H_2 opname onder milde omstandigheden (320 °C, 40 bar H_2). Tevens leidde dit tot afgifte van waterstof bij lagere temperaturen in de daaropvolgende cycli. De structuur van de nanocomposieten werd in detail bestudeerd met technieken zoals EXAFS, TEM en NMR. De veranderingen in waterstofafgifte en opname konden in verband

gebracht worden met de vorming van nikkel boride (Ni_xB) nanodeeltjes, die omkeerbaar hun nikkel-boor verhouding (x) aanpasten tijdens het cycleren. Hun aanwezigheid had invloed op de structuur van de actieve fase in de monsters, mogelijk dienden ze als nucleatie kernen voor het vormen van nieuwe fasen.

In **Hoofdstuk 5** wordt het onderzoek beschreven naar $NaBH_4$, een stof die nog stabieler is dan $LiBH_4$ en waar weinig over bekend is in de context van waterstofopslag. $NaBH_4$ werd aangebracht in een koolstof matrix door impregneren met een basische oplossing van $NaBH_4$ in water of door smelt infiltratie onder waterstofdruk. Puur $NaBH_4$ ontleedde bij verhitten tot 600 ^oC in een atmosfeer van argon onomkeerbaar in Na en $Na_2B_{12}H_{12}$ waarbij 8.1 gew% waterstof vrijkwam. Voor de nanocomposiet met koolstof verliep de ontleding al bij ~370 °C. De manier waarop de nanocomposiet werd gemaakt had invloed op de structuur en waterstofafgiftetemperatuur. Heel anders dan voor puur $NaBH_4$, konden de ontledingsproducten van de nanocomposiet wel waterstof opnemen (3.4 gew% $H_2/NaBH_4$) daarbij $NaBH_4$ vormend bij 325 °C en 60 bar H_2. Dit is de eerste keer dat omkeerbaarheid van de ontledingsreactie van $NaBH_4$ gerapporteerd wordt. Het verlies van Na is een beperkende factor voor het hervormen van $NaBH_4$. Nadat extra Na was toegevoegd, werd vrijwel volledige reversibiliteit gevonden. De evenwichtsontledingstemperatuur van $NaBH_4$ is ~540 °C in 1 bar waterstof. Voor de nanocomposiet met H_2 ving de afgifte van waterstof echter al bij 280 °C aan onder 1.1 bar H_2. De gewijzigde interactie met waterstof, in het bijzonder de mogelijkheid om $NaBH_4$ terug te vormen uit de ontledingsproducten, wordt toegeschreven aan de invloed van fysieke opsluiting van de actieve component in nanoporiën, waardoor macroscopische scheiding van de vaste ontledingsproducten tegen wordt gegaan.

Samenvattende opmerkingen en blik op de toekomst

Het in dit proefschrift beschreven onderzoek toont aan dat opsluiten in de nanoporiën van een poreus koolstof materiaal een veelbelovende aanpak is om tot reversibele waterstofopslag te komen. De opsluiting verlaagt de temperatuur waarbij waterstof wordt afgegeven en bewerkstelligt omkeerbaarheid van de ontledingsreacties van alkalimetaalboorhydriden. Echter, door toevoeging van de koolstofmatrix is de waterstofdichtheid in deze materialen te laag voor praktische

toepassing; dit zou koolstof materialen met een groter porievolume vereisen. Bovendien vraagt toepassing in combinatie met PEM-brandstofcellen ook lagere waterstofafgiftetemperaturen, en stabiele waterstofafgifte en opname tijdens meer dan 1000 keer cycleren. Belangrijk is echter dat met ons werk is aangetoond dat we de snelheid van waterstofafgifte, omkeerbaarheid van de reactie, en ook de evenwichtsliggingen voor deze complexe metaalhydriden kunnen beïnvloeden. We zullen onderstaand enkele algemene conclusies en suggesties voor toekomstig onderzoek op een rij zetten.

De snelheid waarmee waterstof kan worden afgegeven wordt sterk beïnvloed door opsluitingseffecten, omdat het specifiek oppervlak van het actief materiaal daardoor groter wordt en de relevante diffusieafstanden kleiner. Ook een toename in de dichtheid van het aantal nucleatiekernen kan een rol spelen. Het gebruik van zeer regelmatige koolstof matrices, met uniforme poriegrootten en –symmetrie, zou kunnen helpen om het effect van metaalhydridedeeltjesgrootte op de waterstofafgifte en opname snelheid te ontrafelen. De omkeerbaarheid van de waterstofafgifte in het geval van nanocomposieten toont aan dat de scheiding van de verschillende fasen die ontstaan door ontleding een essentiële factor is om de waterstofopnamesnelheid te verbeteren. De vergroting van de hoeveelheid door de ontledingsproducten opgenomen waterstof door middel van het toevoegen van Li (in het geval van $LiBH_4$) of Na (in het geval van $NaBH_4$) bewijst dat het verlies van deze componenten een factor is die de reversibiliteit beperkt. Het gebruik van toevoegingen die een verbinding kunnen aangaan met één van de actieve componenten in het systeem beperkt de korrelgroei, zoals we in hoofdstuk 4 lieten zien voor Ni, dat werd toegevoegd aan de $LiBH_4$ nanocomposiet.

Spannend zijn de verschuivingen in de fase-evenwichten in het geval van nanocomposietmaterialen. Mogelijkerwijs speelt elektronische interactie tussen de koolstof en het complex metaalhydride een rol. Overdracht van elektrondichtheid van de koolstof kan de positieve lading op Li^+ en Na^+ verminderen, en daardoor de binding met het BH_4^- anion verzwakken, wat lokaal leidt tot een lagere stabiliteit van het complex metaalboorhydride. Voor metaalhydriden opgesloten in de nanoporiën van een matrix kan dit effect groot zijn, omdat de afstand tussen metaalhydride en koolstof klein is. Intercalatie van lithiumatomen tussen de grafeenlagen tijdens waterstofafgifte door $LiBH_4$ verkleint ook de stabiliteit van

het hydride ten opzichte van de ontledingsproducten. Zonder twijfel spelen ook deeltjesgrootte-effecten een rol, zoals ook duidelijk wordt uit de veranderingen in smeltpunt en de temperatuur van de faseovergang van het $LiBH_4$. Ook verankering van de actieve fase zal waarschijnlijk bijdragen. Wanneer verschillende typen koolstofmatrices zouden worden gebruikt, met verschillende oppervlakte-eigenschappen, zou meer inzicht verkregen kunnen worden in hoe de interactie met de matrix en de verankering de stabiliteit van de hydridefasen beïnvloedt. Met de huidige kennis is het echter lastig de invloed van deze verschillende parameters te ontrafelen, omdat ze niet onafhankelijk van elkaar gevarieerd werden. Bovendien is het een uitdaging om de lokale structuur en elektronische eigenschappen van deze materialen goed te meten. Het gebruik van geavanceerde technieken zoals op deeltjesversneller gebaseerde in-situ Röntgenstraling Raman Spectroscopie (XRS) en nucleair magnetische resonantiemetingen (NMR) alsook neutronenverstrooiingsexperimenten zouden verdere informatie kunnen verschaffen. Om echt inzicht te krijgen in de oorsprong van de effecten op de stabiliteit, en de bijdrage van de verschillende parameters, zullen ook theoretische benaderingen van het probleem onontbeerlijk zijn.

Concluderend kunnen we stellen dat de resultaten in dit proefschrift aantonen dat het opsluiten van metaalhydriden in de nanoporiën van een koolstofmatrix een effectieve manier is om zowel de kinetiek alsook de reversibiliteit en evenwichtsliggingen van de waterstofafgifte en opnamen in deze materialen structureel te beïnvloeden. We hebben een nieuwe manier vastgesteld om nanocomposieten van alkalimetaalboorhydriden te maken, en om hier kleine hoeveelheden van een katalysator aan toe te voegen. Opmerkelijk is de grote reversibiliteit die bereikt kan worden in deze nanocomposieten onder milde omstandigheden.

Het maken van nanocomposieten is een relatief nieuwe aanpak en volledig begrip van de effecten die optreden vraagt om verder onderzoek: modelsystemen maken, het toepassen van geavanceerde karakterisatietechnieken en een combinatie met theoretisch onderzoek. Desalniettemin geeft ons werk veel informatie over de factoren die van invloed zijn op de snelheid waarmee waterstof kan worden afgegeven en opgenomen, de stabiliteit van de fasen en bovenal hoe het mogelijk is

om de waterstofafgifte reversibel te maken. Het is te verwachten dat deze aanpak ook van belang zal zijn voor ander onderzoek op het gebied van materialen.

List of Publications and Presentations

P.Ngene, R. van den Berg, M. H. W. Verkuijlen, K. P. de Jong and P. E. de Jongh. *Reversibility of the Hydrogen Desorption from $NaBH_4$ by Confinement in Nanoporous Carbon*. Energy Environ. Sci., 2011, 4, 4108–4115

P. Ngene, M. H. W. Verkuijlen, Q. Zheng, J. Kragten, P. J. M. van Bentum, J. H. Bitter and P. E. de Jongh. *The role of Ni in increasing the reversibility of the hydrogen release from nanoconfined $LiBH_4$*. Faraday Discuss., 2011, 151, 47-58.

P. Ngene, M. R. van Zwienen and P. E. de Jongh. *Reversibility of the hydrogen desorption from LiBH4: a synergetic effect of nanoconfinement and Ni addition.* Chem. Commun., 2010, 46, 8201–8203

P. Ngene, P. Adelhelm, A. M. Beale, K. P. de Jong, P. E. de Jongh. *$LiBH_4$/SBA-15 Nanocomposites Prepared by Melt Infiltration under Hydrogen pressure: Synthesis and Hydrogen Sorption Properties*. J. Phys. Chem. C 2010, 114, 6163–6168

P. Ngene, M. H. W. Verkuijlen, C. Barre, K. P. de Jong and P. E. de Jongh., *Impact of $LiBH_4$ loading on the hydrogen sorption properties of $LiBH_4$ confined in Nanoporous carbon materials*. In preparation

P. S. Miedema, P. Ngene, A. M. J. van der Eerden, T. Weng, D. Nordlund, D. Sokaras, R. A. Mori, A. Juhin, P. E. de Jongh and F. M. F. de Groot., *In-situ X-ray Raman spectroscopy of $LiBH_4$*. Submitted for publication.

M. H.W. Verkuijlen, P. Ngene, D. de Kort, P. Jan M. van Bentum, E. R. H. van Eck, P. E. de Jongh, and A. P. M. Kentgens., *A solid-state NMR study of nanoconfined $LiBH_4$ and the mobility of BH_4*. In preparation

J. Gao , P. Ngene, I. Lindemann, K. P. de Jong, and P. E. de Jongh., *How to control the reversibility of H_2 sorption in nanoconfined complex metal hydrides.* In Preparation

Oral Presentations

P. Ngene, K. P. de Jong and P. E. de Jongh. *Nanoconfined Alkali-metal borohydrides for reversible hydrogen storage*. Chemistry As Innovating Science (CHAINS), November 2011, Maarssen, Netherlands.

P. Ngene, R. van den Berg, K. P. de Jong and P. E. de Jongh. *Synergetic effect of nanoconfinement and catalyst addition on the de- and re-hydrogenation behavior of alkali borohydrides.* Gordon-Kenan Research Seminar (GRS), July, 2011, Easton, MA, USA.

P. Ngene, R. van den Berg, K. P. de Jong and P. E. de Jongh. *Confinement of $NaBH_4$ in nanoporous carbon: Impacts on Kinetics, thermodynamics and reversibility of the hydrogen sorption.* 22nd North American catalysis society meeting (NAM), June 2011, Detriot, USA.

P. Ngene, R. van den Berg, K. P. de Jong and P. E. de Jongh. *$NaBH_4$/C nanocomposites: Synthesis and effects of nanoconfinement on the kinetics, thermodynamics and reversibility of the hydrogen desorption from $NaBH_4$.* 2nd symposium "Advances in Dutch Hydrogen and Fuel Cell Research" March 2011, Eindhoven, the Netherlands.

P. Ngene, K. P. de Jong and P. E. de Jongh. *How nanoconfinement in porous carbon and Ni addition can be combined to improve the H_2 release and uptake behaviour of $LiBH_4$.* The 12th Netherlands' Catalysis and Chemistry Conference (NCCCXII), March 2011, Noordwijkerhout, the Netherlands.

P. Ngene, R. van den Berg, Q. Zheng and P. E. de Jongh. *Synergetic effect of nanoconfinement and catalyst addition on the hydrogen release and uptake behaviour of alkali borohydrides. 7th Sustainable hydrogen conference. January 2011, De Werelt, Lunteren, the Netherlands*.

P. Ngene, K. P. de Jong and P. E. de Jongh**.** *Combined effects of nanoconfinement and catalysis on the hydrogen sorption properties of $LiBH_4$.* International Symposium on Metal-Hydrogen Systems (MH2010), July 2010, Moscow, Russia

P. Ngene, P. Adelhelm, K. P. de Jong, Petra E. de Jongh. *Nanoconfined $LiBH_4$ prepared by melt infiltration: Synthesis and H_2 sorption properties*. Materials Reserach Society (MRS) Fall meeting. December 2009, Boston, MA, USA.

Poster Presentations

P. Ngene, K. P. de Jong and P. E. de Jongh. *Combined effect of nanoconfinement and Ni addition on the hydrogen sorption properties of $LiBH_4$*. Gordon-Kenan Research Conference (GRC), July 2011, Easton, MA, USA.

P. Ngene, K. P. de Jong and P. E. de Jongh. *Effects of Nanoconfinement and Ni addition on the Hydrogen Sorption Properties of Alkali borohydrides*. *NWO Scientific meeting on Chemistry related to Physics & Material Sciences / Dutch Polymer Days. 14 &15 March 2011*, Veldhoven, the Netherlands.

P. Ngene, K. P. de Jong and P. E. de Jongh. *Effects of Ni Nanoparticles on the Hydrogen Sorption Properties of Nanoconfined $LiBH_4$ Prepared via Melt infiltration*. The 11th Netherlands' Catalysis and Chemistry Conference (NCCCXI), March 2010, Noordwijkerhout, the Netherlands.

P. Ngene, K. P. de Jong, Petra E. de Jongh. *$LiBH_4$/SBA-15 Nanocomposites prepared by Melt infiltration: Synthesis and H_2 sorption properties*. 9th EuropaCat, August 2009, Salamanca, Spain

P. Ngene, P. Adelhelm, K. P. de Jong, Petra E. de Jongh. Hydrogen sorption properties of melt infiltrated $LiBH_4$/SBA-15 nanocomposites. 10th Netherlands' Catalysis and Chemistry Conference (NCCCX), March 2009, Noordwijkerhout, the Netherlands

P. Ngene, P. Adelhelm, K. P. de Jong, Petra E. de Jongh. *Hydrogen Storage in Nanoscaffolded boronhydrides*. 1st symposium "Advances in Dutch Hydrogen and Fuel Cell Research" March 2009, Petten, the Netherlands.

Acknowledgements

This PhD thesis would not have been possible without the help, support and encouragement of many to whom words are inadequate to express my gratitude and appreciations.

First of all, I would like to thank my advisors Petra de Jongh and Krijn de Jong who patiently guided me through the whole PhD. Working with you has been a pleasure. Petra, thanks for your quidance and supervision, gold is valuable only when refined, and you provided the refiners fire. Your enthusiasm, creativity, insight, passion for excellence and constant criticism challenged me and helped me tremendously in developing my scientific, writing and presentation skills. You also gave me opportunity to present my work at several national and international conferences. Krijn I remain grateful for your mentorship, encouragement and confidence in me which was of a great help, most especially at the end of my first year. You were always willing to listen and advice me, and I have benefited immensely from your broad scientific, industrial, teaching and mentorship experiences.

Philipp, working with you for 2 years was a great fun. The field of nanoconfiment was new when we started, nevertheless your good ideas and experience in nanoporous carbon materials was very helpful. You helped me quickly acquire some experience that was very useful in becoming an independ researcher. I am very grateful for your assistance both in research and personal perspectives.

Hirsa, you have been a wonderful colleaque and friend for the last four years. We have a lot in common, therefore there is always something to talk about and those conversations have been very fruitful in dealing with scientific and non scientific challenges. You were always there to listen, advice and willing to help when needed. Thanks for being a free consultant to me on “living and working in the Netherlands”. I wish you great success in finishing your thesis and getting your dream job.

My appreciation goes to present and former members of the Hydrogen team. Philipp, Rene, Sankara, Qiang, Jinbao, Rien, Yuen, Christina and Angeloclaudio. You provided a nice and friendly working atmosphere in the lab. Working with you guys was fun. The open discussion about each others work and genuine interest to

help one another was very instrumental for the scientific success achieved within the last four years. Rien your great technical experience was instrumental to the smooth running of the equipments from which the results described in this thesis were obtained, including our unique inexpensive reactor that enabled the synthesis of nanoconfined $NaBH_4$ discussed in chapter 5. Paul and Kess are also acknowledged for fruitful discussions and help at the beginning of the project.

It would have been impossible to study nanoconfined alkali-metal borohydrides without a useful technique like the solid state NMR. For this I would like to express my profound gratitude to Arno, Jan and Margriet (Radbound University Nijmegen) for a fruitful collaboration. Margriet, I really enjoyed working with you. Thanks for your enthusiasm and willingness to measure my samples which are often many, and for sharing your extensive knowledge on solid state NMR.

I would like to acknoweledge my former bachelor and master students: Roy, Joris, Christophe and Charlotte for their good work which contributed to the success of this thesis.

Frank thanks for advancing my knowledge in X-ray spectroscopy through your course and our combined work on X-ray Raman spectroscopy of nanoconfined $LiBH_4$. Piter M, it was very nice collaborating with you on this XRS studies and I am excited about the outcome. Similarly I want to thank Harry for the work we did together on EXAFS and for all the discussions especially during my first beam trip at HASY lab. Andy thanks for introducing me to Rietveld refinement and your contribution to the work described in chapter 2.

Ad E, you are greatly acknowledged for your technical assistance. Working with you was always relaxing and reassuring, and an opportunity to improve my Dutch language. From the start of my PhD you were there to help with setting up autoclaves for melt infiltration and even at the end, you are still there helping with special arrangements for successful synchrotron experiments in Standford. Similarly I will like to thank Ad M, Vincent, Marjan, Fouad, Fred and Hans for their assistance over the years. Dymph and Monique, thanks for being available and willing to provide the needed help in administrative matters during the course of the PhD.

I would like to thank Mariska and Gonzalo for sharing their knowledge and experience on mesoporous silica. I am also grateful to Evelien and Tamara for the

Nederlands samenvatting. Arjan, and Jovana, it was fun working together with you and Krijn during the ANO werkcolleges.
Arndt, although we met close to the end of my PhD, the collaboration we started on inelastic neutron scattering measurement of nanoconfined $LiBH_4$ is already yielding promising results. I wish you success as you continue on this project with my successor.
The last four years was shaped by nice and accommodating atmosphere provided by all my colleaques in the group. My former and present office mates: Marianne, Davide, Rob, Evelien, Dilek, Annelie, Upakul, Illona, Luis, Piter, Bart, Peter H, and Mustafa. Thanks you all for making my stay in the group pleasant. Clare, it was unfortunate we could not continue the cooking challenge with Eli, Philipp, Hike, Jinbao, Oge and Sankara. It was very exciting moments. Goodluck with finishing your thesis. Matti, I will miss the nice discussion we often have about scientific and non scientific issues. To all the members of the inorganic chemistry and catalysis group, thanks for making my stay in the department easier, pleasant and fruitful.
My appreciation goes to friends and acquitances that have made my stay and life outside PhD to be fun and fulfilling. Chidi Umeh- Ujubuonu thanks for your interest, support and constant encouragement. Austine, Sandra, Donatus Eze, Nnamdi, Amara, Chibuzo, Ify, Angelique, Chuks Osagie and Tony, *ndewonu*, *unu bu nwanne di na mba!* I am grateful to the Abarshi's family, the Adepoju's family, Farai, Orji, Berkely, Emeka Njoku, Barnabas Okeke, Kalu Uduma, Labake, Elizabeth, all the members of the POP parish Utrecht, and many more that I can not mention here. I also wish to express my gratitude to my colleaques at the Young Entrepreneurs for Africa (YEFA) for the excellent team work.
Words are inadequate to fully express my profound appreciation and gratitude to my family: my lovely and caring mum, sisters (Anthonia, Josephine and Rose), Ejike, Monday, Chuks, Friday and Ebuka for the love, support and care they have shown to me all the days of my life. Uncle Tony, thanks for making me realize my dreams. You are a God sent, *dalu, Chukwunna gozie gi.* To my darling and beloved sweetheart, big kiss and thanks for all your love, support, understanding and help. You have been a bowel of blessings to me and a pillar of support throughout this period. Armstrong Chukwudubem thanks for being a nice boy and understanding when papa needed time to study.

About the author

Peter Ngene was born on the 28th of August 1978 in Enugu, Nigeria. He completed the senior secondary school education in 1995 from Government special science school Ganye in Adadmawa state, Nigeria. In 1997, he gained admission into the Federal University of Technology Owerri (FUTO) and received a bachelor of engineering degree in Chemical Engineering in January 2002. After the one year mandatory national youth service, he worked as a process engineer at Dangote Sugar refinery, Lagos, from May 2003 to December 2005. In January 2006, he started a Master of Science degree program in MEMS (Microelectromechanical systems) Enginnering which was jointly organized by ESIEE Paris, France and Nanyang Technological University Singapore. Several design projects were carried out both in ESIEE and NTU. His master thesis, entitled "Synthesis of novel nanostructured complex hydrides for on-board hydrogen storage" was undertaken in the heterogeneous catalysis group, Institute for Chemical and Engineering Sciences (ICES), Singapore. In June 2007, he received a dual Master of Science (MSc.) degree in MEMS engineering from both universities, and in September that same year he joined the Inorganic Chemistry and Catalysis group at Utrecht University under the supervision of Dr. P.E. de Jongh and Prof. dr. ir. K.P de Jong. The results obtained during this period are described in this thesis and were presented at several (inter)national conferences. In 2010, He received the VIRAN award for the best poster presentated during the Netherlands Chemistry and Catalysis Conference in Noordwijkerhout. During his PhD studies, he was active in extracurricular activities including being a member of the PhD committee of the Debye institute for NanoMaterials Science and a founding member of the Young Entrepreneurs for Africa (YEFA).